Recent technological and methodological advances for the investigation of landslide dams

Xuanmei Fan[1], Anja Dufresne[2*], Jim Whiteley[3,4], Ali P. Yunus[1], Srikrishnan Siva Subramanian[1], Chukwueloka A.U. Okeke[5], Tomáš Pánek[6], Reginald Hermanns[7,8], Peng Ming[9], Alexander Strom[10], Hans-Balder Havenith[11], Stuart Dunning[12], Gonghui Wang[13], Carlo Tacconi Stefanelli[14]

*corresponding author

[1]State Key Laboratory of Geohazard Prevention and Geoenvironment Protection, Chengdu University of Technology, Chengdu, Sichuan, People's Republic of China

[2]Engineering Geology and Hydrogeology, RWTH-Aachen University, Lochnerstr. 4-20, 52066 Aachen, Germany

[3]School of Earth Sciences, University of Bristol, Wills Memorial Building, Queens Road, Bristol, BS8 1RJ, United Kingdom

[4] British Geological Survey, Environmental Science Centre, Nicker Hill, Keyworth, Nottingham, NG12 5GG, United Kingdom

[5]Department of Civil Engineering, College of Engineering, Covenant University Ota, Ogun State, Nigeria

[6]Department of Physical Geography and Geoecology, University of Ostrava, Chittussiho 10, Slezská Ostrava, Czech Republic

[7]Geohazards and Earth Observation, Geological Survey of Norway, Trondheim, N-7491, Norway

[8]Department of Geoscience and Petroleum, Norwegian University of Science and Technology, Norway

[9]Department of Geotechnical Engineering, Tongji University, Shanghai, China

[10]Geodynamics Research Centre LLC, 3rd Novomikhalkovsky passage, 9, 125008 Moscow, Russia

[11]Department of Geology, Université de Liège, Belgium

[12]School of Geography, Politics and Sociology, Newcastle University, Newcastle upon Tyne, NE1 7RU, UK

[13]Section of Mountain Hazards, Disaster Prevention Research Institute, Kyoto University, Kyoto, Japan

[14]Department of Earth Sciences, University of Firenze, Via La Pira, 4, Florence 50121, Italy

Keywords: landslide dam, sedimentology, embankment dam, hazard mitigation, geophysics, numerical modelling, remote sensing, dating, rockslide dam

Abstract

River-damming by landslides is a widespread phenomenon around the world. Recent advances in remote sensing technology and increased commercial availability of their products enable theassemblage of increasingly more complete inventories for size and distribution analysis, and improve monitoring efforts. On the ground, multi-method dating campaigns improve our understanding of the timelines of dam formation and failure. In comparison to single-dating methods, they reduce uncertainty by using different materials from the landslide deposit, facilitate the advantages of each method, and consider the deposit and the source area. They can pin dates on the time of lake drainage where backwater sediments are included in the dating campaign and thus inform about dam longevity. Geophysical methods provide non-invasive and rapid methods to investigate the properties and interior conditions of landslide dams. By identifying, e.g. evolving zones of weakness and saturation they can aid in the monitoring of a dam in addition to providing information on interior stratification for scientific research. To verify results from geophysical campaigns, add details of dam sedimentary characteristics and geotechnical properties, knowledge of landslide/dam sedimentology is essential. This is gathered at sections from breached dams, other (partially) eroded landslide deposits, and through laboratory testing of sampled material. Combining the knowledge gained from all these methods with insights from blast-fill and embankment dam construction, physical and numerical modelling in multi-disciplinary research projects is the way forward in landslide dam research. This review offers a broad, yet concise overview of the state-of-the-art in the aforementioned research fields. It completes the review of landslide dam research of Fan et al. (2020) on the formation and impact on landslide dams.

1. Introduction

Landslide dams are formed by various types of mass movements and are characterized by both complex and composite geomorphologic features and geotechnical properties. The challenges of landslide dam research lie in (i) understanding the dam failure mechanisms, (ii) analysing internal and external factors for the prediction of their formation and stability under diverse geo-environmental conditions, (iii) assessing their possible short- and long-term hazards and impacts, as well as (iv) risk reduction and management. The dam-lake-systems are complex, resulting from the interactions between the mass movement itself, topographic constraints, and the river and catchment dynamics. Their instantaneous formation and immediate hazards juxtapose the long-term effects they have on the landscape. In the time after immediate hazards are mitigated, any apparent stability of the dam, suggested by the presence of a lake, may distract from secondary or delayed hazards (such as collapse of seemingly stable dams centuries after their

formation). Hence, landslide dams form part of a process chain or hazard cascade. The long- and short-term impacts of large landslide dams can only be understood if their timeslines are known through dating their formation and failure (e.g. Ivy-Ochs et al., 2017; Ivy-Ochs et al., 2009). Furthermore, our improved knowledge of their global distribution of landslide dams and geomorphic characteristics provide a good basis for statistical analyses (cf. Fan et al., 2020) of their dimensions and longevities.

Technological developments have improved available data collection tools (e.g. satellites, unmanned aerial vehicles - UAVs) for landslide dams, which help identify the large numbers of landslide dams in the aftermath of single, large-scale triggering events, such as the 2008 Wenchuan earthquake (China), the 2015 Gorkha earthquake (Nepal), and the 2016 Kaikoura earthquake (New Zealand) (Casagli et al., 2016; Fan et al., 2012b; Guzzetti et al., 2012; Massey et al., 2018; Scaioni et al., 2014). New research on the interior structure and depositional facies of large landslides helps better understand the relationship of landslide sedimentology to dam stability, such as preferential seepage pathways or processes of overtopping failure. In particular, the failure stages as a function of grain size changes with depth within the deposit can be better understood by considering depositional facies characteristics and distribution (Dufresne et al., 2016; Dunning and Armitage, 2011; Weidinger et al., 2014). Recent studies bring together the experiences gained from geophysical investigations, identifying the opportunities and limitations of the different methods (Wang et al., 2016a; Wang et al., 2016c; Wang, 2008). Likewise, although small-scale field and laboratory models are mainly designed for artificial dams, a lot can be gleaned from their performance to better understand failure mechanisms of natural blockages. Finally, the increasing number of computer programs and numerical modelling tools that have become available in recent decades, ranging from simple to robust approaches, can increasingly handle the modelling of geomorphic processes starting from dam formation, its projected stability, breach, and potential breach-induced flooding (Fan et al., 2019a).

With these recent developments in laboratory-scale geotechnical testing systems, geological and geophysical investigation tools, remote sensing technology and availability, combinations of age-dating methods, and new numerical modelling techniques, scientists seek solutions to overcome the challenges involved in landslide dam assessment. This review is a continuation of our paper on the formation and impacts of landslide dams (Fan et al., 2020). Herein, we present the technological and methodological advances in landslide dam research over the past decades.

2. Recent Advances in Landslide Dam Investigations

This section is a review of the state-of-the-art in (2.1.) remote sensing, (2.2.) dating, (2.3.) geophysical methods, and (2.4.) sedimentology and geotechnical properties of landslide dam research. With remote sensing techniques, landslide deposits are identified on much larger scales than previously possible. Consequently, the number of identified landslide dams in inventories and databases increases, providing statistically significant data for analyses of spatial distribution and dam dimensions. Dating then sets the spatial data in a temporal context, and allows expanding frequency analyses of river-blocking events from historical inventories into the geological past. It can furthermore inform about the longevity of individual dams by including associated sediments into dating campaigns. Geophysical investigations deliver insights into the internal structure of intact dams, and sedimentological analyses of breached dams (or other, partially eroded landslide deposits) add knowledge on the associated geotechnical properties—both vital for understanding the processes involved and the properties relevant in dam stability analyses.

2.1. Remote sensing

Remote Sensing techniques and sensors have undergone considerable technological progress and have become powerful tools for many aspects of landslide (dam) identification and investigation in recent years (Ermini et al., 2006; Fan et al., 2013; Scaioni et al., 2014) as resolution, accuracy, acquisition time, logistics (sensor dimensions), and availability keep improving.

2.1.1 Landslide dam inventories

Historical aerial photographs and optical (Visible-NIR spectrum) remote sensing satellite images are typically employed for the creation of dam inventories (e.g. Emmer et al., 2016; Korup, 2005b). Recently, free web services, such as Google EarthPro® or Bing Maps™, which provide 3D models and image archives, are also used for landslide dam recognition and the creation of inventories (Strom and Abdrakhmatov, 2018; Tacconi Stefanelli et al., 2015; Tacconi Stefanelli et al., 2018). Optical image interpretation is particularly useful in post-event reconstruction (Fan et al., 2009; Yamazaki and Matsuoka, 2007), since the differences between mobilized material and the unaffected areas are usually evident. Most commonly, dam inventories are created through visual interpretation of landslide source and deposition zones by comparing pre- and post-event false-color composites or panchromatic images. For example, Fan et al. (2012b) created an inventory comprising 828 landslide dams induced by the 2008 Wenchuan earthquake in China

by visual interpretation of satellite and aerial images, including ASTER, ALOS AVNIR-2, ALOS PRISM, Cartosat-1, SPOT-5, and IKONOS data.

Older landslides are more difficult to identify from imagery. In such cases, dam inventory mapping may involve detecting the dammed lake instead (e.g. Emmer et al., 2016). This is because water bodies can be highlighted easily in remote sensing images using various spectral indices and transformations (Feyisa et al., 2014; McFeeters, 1996); Table 1. However, in the initial stage of dam formation, lake extents are difficult to distinguish unless the inflow is sufficiently high. Also, many landslide dams fail shortly after formation and the lakes are drained. Despite significant progress in automatic or semi-automatic detection of landslides (e.g. Smith et al., 2020), visual interpretation of landforms is still an efficient and reliable method for compiling regional inventories of landslide dams, as well as for inventories of large landslides themselves (e.g. (Strom and Abdrakhmatov (2018)). The most effective method is a combination of remote sensing data with site investigations, especially in forested areas and in areas with extremely narrow valleys where very steep slopes mask large parts of an image by shadows or disadvantageous satellite line-of-sight.

Table 1 Automated water extraction indices based on remote sensing that are used in lake (water) body identification.

Index	Formula	Reference
Normalized difference water index (NDWI)	$NDWI = \frac{Green - Near\ InfraRed}{Green + Near\ InfraRed}$	McFeeters (1996)
Modified normalized difference water index (MNDWI)	$MNDWI = \frac{Green - SWIR1}{Green + SWIR1}$	Han-Qiu (2005)
Automated water extraction index (AWEI)	$AWEI = 4 \times (Green - SWIR1) - (0.25 \times NIR + 2.75 \times SWIR2)$	Feyisa et al. (2014)
Tasseled Cap Wetness (TCW)	*TCW = 0.0315 Blue + 0.2021Green + 0.3102 Red + 0.1594 NIR - 0.6806SWIR1 - 0.6109 SWIR2*	Crist (1985)
Water Index (WI)	*WI= 1.7204 + 171Green + 3 Red - 70 NIR – 45 SWIR1 – 71SWIR2*	Fisher et al. (2016)

For locating breached dams, Safran et al. (2015) suggest (i) looking for landslide deposits on either side of the river, (ii) checking for highly constricted and/or laterally displaced river reaches, (iii) locating knickpoints/rapids, (iv) identifying terraces, since they suggest sediment accumulation within the impoundment, and (v) looking for outburst deposits in the river channel. Implementing these suggestions is possible with high-resolution images and digital elevation models, including Google Earth® imagery, aerial photos, and LiDAR (Light Detection and

Ranging - a surveying method that measures distances using a laser) digital elevation models (DEMs).

2.1.2 Dam and lake geometry mapping

Landsat, SPOT, and ASTER optical images have significant historical archives, and together with global DEMs, are the most utilized remote sensing data for estimating the geometry of landslide dams, water surface elevations, and lake areas and volumes (e.g. Delaney and Evans, 2015; Delaney and Evans, 2017; Parvaiz et al., 2012). Global coverage (1-3 arc-seconds) SRTM DEM, developed from single-pass interferometry of C-Band radar, and ASTER GDEM generated from stereo-pairs of optical images are available since the last 10-20 years. In terms of accuracy, these datasets can provide satisfactory first-order topographic characterization (Delaney and Evans, 2017) of larger features. The basic geometric characteristics measured from DEMs and imageries include dam height (H), transverse (cross-river) length (L), longitudinal (along-river) width (W), the volume of the landslide dam (V_d), area of the lake (A_l), perimeter of the lake (P_l), and the lake storage volume (V_l).

Since 2015, global SRTM DEM is available at 1-arc-second resolution, with only 3-arc-second data available prior to this (except in the United States). For historical cases, archived aerial photos are the best suited (Tacconi Stefanelli et al., 2018). Declassified Corona satellite imagery (US spy satellites 1960-1972) were also assessed in some historical cases (Shroder Jr and Weihs, 2010). Dimensions of individual landslide dams can also be determined by Unmanned Aerial Vehicle (UAV) platforms (Fan et al., 2019b; Wallace et al., 2012). UAV (also termed UAS – Unmanned Aerial Systems or simply drones) images and structure-from-motion (SfM) photogrammetric techniques for developing DEMs are gaining popularity owing to their low cost, high resolution, and rapid deployment (Figure 1).

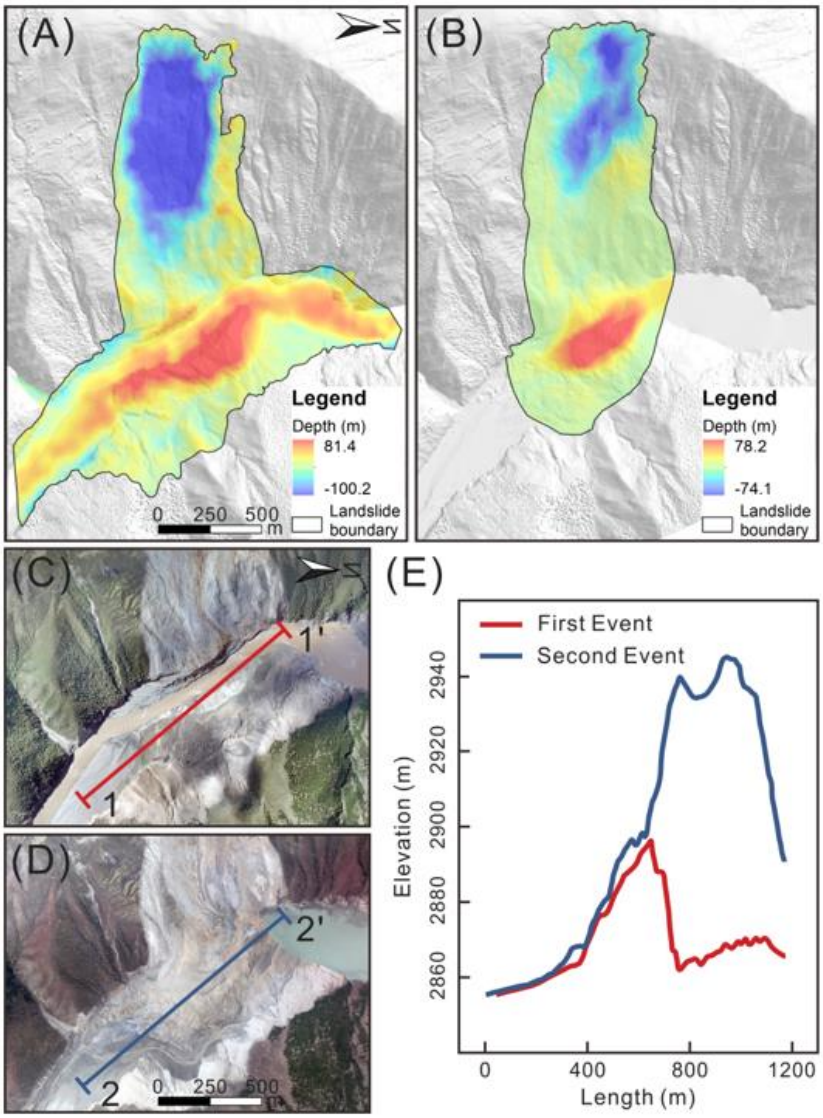

178

179 **Figure 1**. Multi-temporal digital elevation model and orthophotos of Jinsha landslide damming event of
180 2019 (modified after Fan et al. (2019b)). (A) and (B) shows the hill-shaded DEM and elevation changes of
181 two different dates (10-13-2018 and 11-03-2018), (C) and (D) are orthophotos of the same, and e shows
182 the long profile A-A' and B-B' given in (C) and (D).

183

184 Using SRTM data, Tacconi Stefanelli et al. (2018) detailed the geometry of 51 landslide dams in
185 the Cordillera Blanca, Peru. Delaney and Evans (2015) used optical images together with DEM
186 to determine the shoreline and lake volume formed by the 2000 Yigong rockslide-dammed lake,
187 Tibetan Plateau. They later developed a pixel-by-pixel technique following Leblanc et al. (2006)
188 and others (Dong et al., 2014; Dong et al., 2011a) to obtain mean pool height of the lake and
189 applied it to Lake Gojal, a 2010 rockslide-dammed lake formed in the Hunza River, Pakistan.
190 Where pre-slide topography is absent, the dam height can be estimated by creating a longitudinal
191 profile of the river extending far downstream and upstream to reconstruct the initial stream level
192 prior to damming, also providing estimates of the initial lake depth and volume. However, in

mountainous regions with extremely rugged terrain, spatial resolution of 1-3 arc seconds DEMs is insufficient for creating such profiles.

The technological advances in remote sensing instruments have improved the spatial resolution in topographic measurements through developments such as LiDAR sensors. The laser sensor can be placed on aerial (ALS - Airborne Laser Scannering) or ground platforms (TLS - Terrestrial Laser Scanning). ALS tends to cover a wide area at moderate resolution (1 m to 10 m), whereas TLS is better suited for local-scale surveys at higher resolution (about 1 cm to 1 m). Post-processing of LiDAR surveys can filter vegetation coverage and model the terrain surface in densely forested areas (e.g. Eeckhaut et al., 2007; Görüm, 2019; Jaboyedoff et al., 2012).

2.1.3 Monitoring dam deformation

Deformation analysis of landslide dams requires interpretation of co-registered optical images taken at different times in order to compare equivalent areas (Barazzetti et al., 2014). Multi-temporal photogrammetric techniques allow quantitative comparison of DEMs and the evaluation of volume changes (Lucieer et al., 2014; Peternel et al., 2017). UAV platforms are well-suited to this purpose as they can easily provide multi-temporal, high-resolution images at short time intervals. In general, landslide dam monitoring using optical images has two main drawbacks: the strong dependency on meteorological and light conditions, and the potential presence of vegetation that limit photogrammetric techniques.

In adverse climatic conditions, repeat pass satellite imagery utilizes Synthetic Aperture Radar (SAR), a powerful tool for measuring surface deformation of unstable slopes over large regions (Rott and Siegel, 1999; Tofani et al., 2010). SAR is an active radar sensor system (i.e. not affected by cloud coverage or light conditions) that can be installed on spaceborne, airborne and ground-based platforms. It registers the backscattered echo from the target surface in amplitude and phase image maps.

Interferometric Synthetic Aperture Radar (InSAR), which analyses the phase difference between two images of the same area at different times, has proved to be an extremely powerful tool for measuring terrain displacement (Massonnet and Feigl, 1998; Raspini et al., 2017; Walter et al., 2020). Several subsequent methodologies have been developed (e.g. DInSAR and Multi-Temporal Interferometry) in order to remove errors due to temporal and geometric decorrelation (Colesanti et al., 2003; Crosetto et al., 2005; Raspini et al., 2017; Rott and Siegel, 1999; Wasowski and Bovenga, 2014). Permanent Scatterer Interferometry (PSI) (Ferretti et al., 2001) measuring millimetric movements of natural reflectors with coherent backscatter over time (i.e. rock outcrops or infrastructure, but not vegetated areas), has become popular in landslide identification and monitoring (e.g. Tofani et al., 2010). Satellite or S-based InSAR is suitable for monitoring slow-moving landslides and apparently stable landslide dams, and could also be used

to detect precursory movements to sliding failure (Intrieri et al., 2018). The main drawbacks of these spaceborne techniques are related to the sensor (phase and temporal resolution) and the topography (visibility in steep mountain terrains). Ground-based SAR (GBSAR) overcomes many of the drawbacks of the satellite platform by drastically reducing the repeat time (up to few minutes) and allowing choice of the line-of-sight (LOS), although vegetation cover, and transport and logistics issues can still limit the method.

LiDAR sensors are also used in landslide monitoring and post-event analysis, providing multi-temporal high-resolution DEMs to obtain positive and negative volumetric changes between data sets (Corsini et al., 2009; Pesci et al., 2011). After the 2016 Kaikoura (New Zealand) earthquake, Massey et al. (2018) used airborne LiDAR data for site-specific landslide dam surveys and assessments.

2.1.4 Summary

Increases in spatial resolution (~ few meters), reductions in time revisit periods (up to one day) of the latest addition of satellites (e.g. SENTINEL-2, Pleiades-HR, PlanetScope constellations, etc.), and open cloud platforms (e.g. Google Earth Engine) make them increasingly useful for landslide inventory mapping. For example, PlanetScope constellations, with 120 satellites currently in orbit, offer a revisit time of one day and imageries at ~3 m resolution in four wavelengths (red, green, blue, and near-infrared), which is a game changer in rapid disaster mapping. Optical imageries, however suffer from dependency on meteorological factors (cloud cover) in adverse weather conditions, usually associated with rainfall-induced natural hazards. Although spaceborne microwave sensors overcome this issue, the data require significant preprocessing. Some of these microwave sensors are on-par with optical imageries in terms of spatial and temporal resolutions. For instance, the COSMO-SkyMed system, with a constellation of four satellites offers very high revisit frequency and resolution up to 1 m in spotlight mode.

In data-sparse regions, dam geometric mapping still relies upon SRTM DEM or ASTER GDEM. These two datasets have vertical accuracy of ~16 m and ~17 m, respectively (Farr et al., 2007; Tachikawa et al., 2011; Yunus et al., 2016). Promising improvements in terms of vertical accuracies by eliminating major error components from existing DEMs may be helpful in future studies. For example, the MERIT DEM was developed by removing multiple error components from SRTM3 v2.1 and AW3D-30m v1 (Yamazaki et al., 2017). This DEM represents the terrain elevations at 3-arc-second resolution and almost covers the entire globe. However, for data-rich regions, obtaining accurate geometrical parameters for landslides and landslide dams is relatively easy. For example, the Geospatial Authority of Japan provide nationwide 5-m airborne LiDAR digital elevation with vertical accuracy of ~ 1 m (Avtar et al., 2015).

A cheap alternative in data-sparse regions is thus employing optical photogrammetry using UAVs to obtain 3D models. The rapid advancement of UAV systems in terms of cost, miniaturization and flying time means they are becoming indispensable tools in landslide dam mapping. However, at present the flying time for a low-medium cost UAV (e.g., DJI Phantom 4) is limited to 20-30 minutes with a one- or two-battery power supply; and they can only fly to a limited height, restricting the coverage of large areas of interest. The development of professional drones for scientific use and the reductions of sensor dimensions promises the overcoming of current UAV limitations (Rossi et al., 2018). Commercially available TanDEM-X data (DEM at ~10 m resolution, ~4 m vertical accuracy) may be a viable alternative, but there exist gaps in spatial coverage, especially for steep mountainous terrains (e.g., Wenchuan, China). With more orbital passes in future, TanDEM-X missions are expected to overcome this limitation.

2.2. Dating timelines of dam formation and failure

In historical inventories, the spatial distribution, time of formation and, in cases with sufficiently long observation times, the years of stability are well-constrained (cf. Fan et al., 2020 for list of world-wide inventories). Whereas the same spatial analysis tools apply for pre-historic events, the timeline of dam formation and failure is poorly, or not at all, constrained. To date, only 220 landslide dams have been dated in the world (Figure 2A)., and yet the correct determination of a landslide dam's age is vital for understanding the longevity as well as the frequency of river damming. Therefore, we focus on this gap in knowledge, summarize available dating methods, and underline the value of better age constraints.

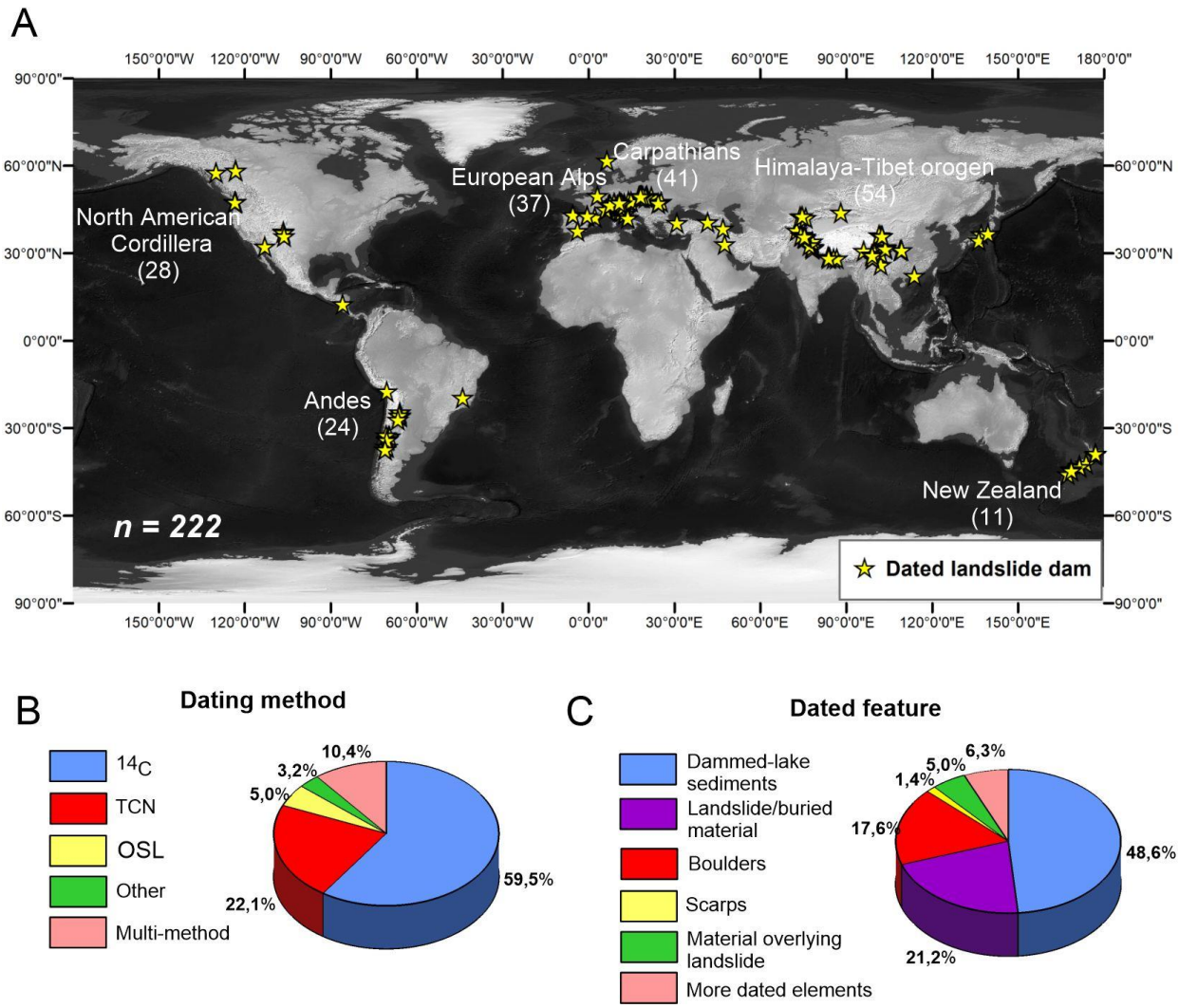

Figure 2 (a) Worldwide distribution of dated landslide dams (n=222). Numbers inside brackets are the total number of dated landslide dams in selected regions. (b) and (c) display the proportion of individual methods and landslide features respectively used for the landslide dam age determination.

Dating of landslides is a broad topic, and review papers exist that we recommend to the interested reader (Lang et al., 1999; Pánek, 2015). In the following, we focus on work done on dating landslide dams as well as new developments that are promising applications for this particular phenomenon. The methods of dating landslide dams are described in Table 2 and their application to specific datable landslide features is shown in Figure 3. Although a broad range of dating methods exists, only some of them have become widely used (Figure 2b), which we review in the following paragraphs.

Table 2 Methods applicable for dating of landslide dams.

Dating method	Useful time range	Dated landslide materials and features	Advantage	Limits	Examples of references

Radiocarbon ^{14}C	~0.2–50 ka	Organics incorporated or buried by landslide; dammed-lake deposits; trees drowned in dammed lakes	High precision of dating; abundance of organic material within dammed-lake deposits	Lack of organics incorporated within landslide material; risk of inaccurate dating results of dammed deposits due to hard water effects; does not date impoundment but lake phase that can last thousands of years.	Adams (1981); Geertsema and Clague (2006); Nicolussi et al. (2015); Reneau and Dethier (1996); Schuster et al. (1992)
TCN[1] (^{10}Be, ^{26}Al, ^{36}Cl, ^{21}Ne, ^{3}He)	0 – several Ma	Exposed landslide scarps or boulders	Relatively ubiquitous datable landslide features; target minerals common in rocks; dates the impoundment event.	Possible errors of dating related to unknown pre-exposure inheritance; rejuvenation of exposure ages due to erosion and tilting	Castleton et al. (2016); Delgado et al. (2020); Hermanns et al. (2015); Hermanns et al. (2004); Hermanns et al. (2017); Hewitt et al. (2011); Ivy-Ochs et al. (2017); Ivy-Ochs et al. (2009); Prager et al. (2009); Sanhueza-Pino et al. (2011); Schleier et al. (2017); Schleier et al. (2015)
Luminescence (OSL[2], TL[3], IRSL[4], TT-OSL[5])	<300 ka (up to 1 Ma in case of TT-OSL)	Dammed-lake deposits; alluvial or aeolian deposits on the surface of landslides or buried by landslide debris	Datable materials are ubiquitous; replaces ^{14}C in the absence of organics	Insufficient bleaching of grains during some types of transport (e.g. fluvial); lower precision of dating. Dates stratigraphically related sediments but not the impoundment.	Bao et al. (2020); Chen et al. (2018); Guerrero et al. (2018); Lee and Dai (2011); Zhang et al. (2019)
U-series ($^{234}U/^{230}Th$)	<350 ka	Secondary speleothems or calcite cement infilling voids within landslide material	Datable materials are ubiquitous in limestone terrains; might replaces ^{14}C in the absence of organics	Lack of datable materials in non-carbonate terrains; presence of detrital Th cause departure from closed-system behaviour and lead to inaccurate dating results; post-dates the impoundment.	Ostermann et al. (2017); Ostermann and Sanders (2017)
Short-lived radioactive isotopes (^{210}Pb, ^{137}Cs)	Several decades (~150 years in case of ^{210}Pb)	Dammed-lake deposits	High precision of dating	Extremely short time range	Pánek et al. (2013)
Tephrochronology, $^{40}Ar/^{39}Ar$	0 – several Ma	Tephras or lava flows overlying or underlying landslides; tephras accumulated in the dammed lakes, tephra in ponds on the landslide	Long time-range, possibility of tracing tephra layers over extensive areas	Absence of datable materials in non-volcanic terrains; dates stratigraphically related deposits or the lake phase that can last for thousands of years.	Beetham et al. (2002); Hermanns and Niedermann (2011); Hermanns and Schellenberger (2008); Thouret et al. (2017)

Dendrochronology – dead trees	0 – several ka (dependent on existing local master chronology	Tree trunks buried by landslide; trees drowned in dammed lakes etc.	High precision; possible wiggle-matching analysis with ^{14}C dated trunks; possibility of inferring climatic conditions during landslide origin	Lack of available opportunities for dating	Nicolussi et al. (2015); Yamada et al. (2018)
Dendrochronology – living trees	0 – several hundreds of years	Tree cohorts growing on landslide bodies	Datable material is ubiquitous	Short time range – applicable only for young dams in pristine landscapes (not controlled by forest management); only rough estimate of landslide dam minimum age	Not applied for damming landslides
Lichenometry	0 – several hundreds of years (up to ca. 1,000 years)	Lichens growing on landslide scarps or boulders within accumulations of landslides	High precision; datable material is ubiquitous	Short time range: could underestimate real age.	Belousov (1994); Nikonov and Shebalina (1979)
Varve chronology	Floating	Varved lake deposits	High precision	Dating of the length of the lake phase	Trauth et al. (2000); Trauth and Strecker (1999)

[1]Terrestrial Cosmogenic Nuclide dating; [2]Optically Stimulated Luminescence; [3]Thermoluminescence; [4]Infrared Stimulated Luminescence; [5]Thermally Transferred-Optically Stimulated Luminescence

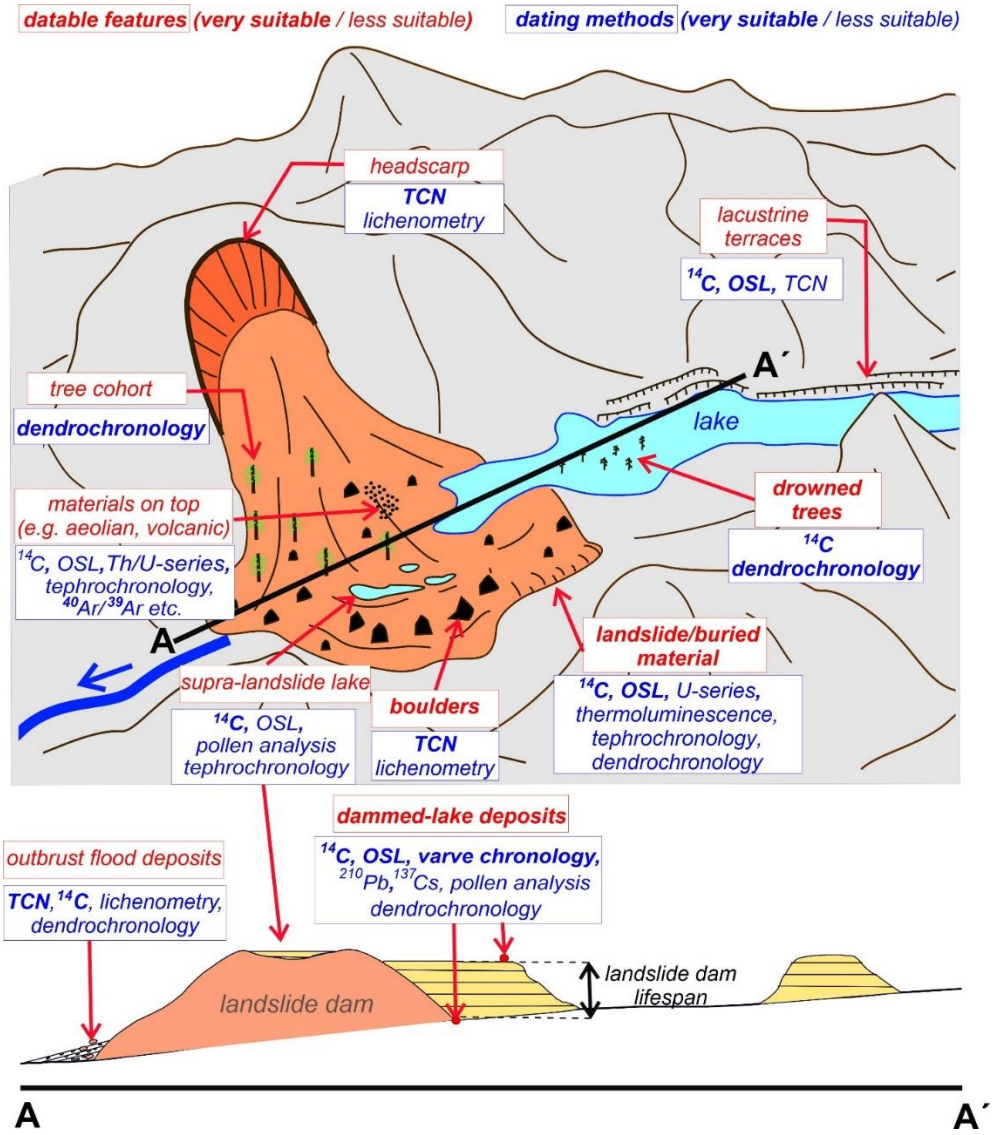

Figure 3 Datable features and materials with potential for the landslide dam age determination.

2.2.1 Indirect methods: dating lake sediments

Dating lacustrine sediments with ^{14}C has long been the most-used dating method to assign ages to landslide dams, accounting for ~50% of dated cases so far (e.g. Abele, 1974; Adams, 1981; Hermanns et al., 2012; Schuster et al., 1992; Trauth and Strecker, 1999). However, this method only provides minimum ages, as it dates sediments that were deposited after river damming by the landslide and ensuing sediment accumulation in the impoundment (with the exception of drowned trees within the lakes) (Schuster et al., 1992). The stratigraphic relations between the landslide sediments and the lake sediments are not always clear. Often, the only relation of the lake sediments to the landslide sediments is that they occur upriver of the dam; they may not even be in direct contact with the landslide body. This poorly-constrained relationship can further limit the use of ^{14}C dating. Multiple landslide phases forming a single dam are also rarely detectable. The method is also vulnerable to internal errors, such as the 'hard water effect' that

allows dead carbon from the substrate to be incorporated into the organic material that lived within the lake, introducing inaccuracies in dating the organic carbon.

Another technique for dating backwater lake sediments is Optically Stimulated Luminescence (OSL). This method determines the last time of daylight exposure of quartz or feldspar grains (cf. Preusser et al., 2008). Accurate dating results rely on the presumption that all grains are being 'reset' during pre-deposition material transport. This means that sufficient residence times in river waters from source to sink are needed to ensure sufficient exposure and resetting of the signal prior to burial in the lake sediments. As landslide material is not exposed to solar radiation for long periods, the method is limited to the backwater sediments, and has therefore not been used to date many landslide dams (~5% of dated cases; Figure 2B). Although the presumption that minerals experience sufficient exposure during transport might be problematic in high-energy (mountain) fluvial environments, the few attempts to date sediments deposited in lakes dammed by, or forming on, rock avalanche debris have delivered ages that are in excellent agreement with independent age control (e.g. Balescu et al., 2007; Castleton et al., 2016; Dong et al., 2014; Dufresne et al., 2018; Hamilton, 2014; Xu et al., 2015).

2.2.2 Dating dam material: the current challenge

A big step forward was achieved with the establishment of terrestrial cosmogenic nuclide dating (TCN) of landslide material (e.g. Ballantyne et al., 1998; Kubik et al., 1998; Hermanns et al., 2001). Using TCN, the landslide deposit can be dated directly, and the age revealed is thus independent of stratigraphic relationships. Hermanns et al. (2004) first used the TCN method to distinguish different generations of a landslide dam. Many rockslide dams (~22%) are dated using this method (e.g. Ivy-Ochs et al., 2017; Ivy-Ochs et al., 2009; Penna et al., 2011; Schleier et al., 2017; Yi et al., 2006). However, this method has to be used with some caution, as landslides often preserve their stratigraphy during emplacement; in particular large rockslides and rock avalanches (e.g. Abdrakhmatov and Strom, 2006; Charrière et al., 2015; Dufresne et al., 2016; Geertsema and Clague, 2006; Heim, 1932; Hewitt et al., 2008; Johnson, 1978; Weidinger et al., 2014; Yarnold and Lombard, 1989) leading to inheritance of nuclides produced on the slope prior to failure, which can lead to overestimations in deposition age (Hilger et al., 2019; Ivy-Ochs et al., 2009). One approach is to date the surface exposure of landslide scarps directly (Hermanns et al., 2004; Ivy-Ochs et al., 2009), but this is only applicable to scarps without post-failure erosion of the bedrock surfaces, which is uncommon. Furthermore, scarps might be rejuvenated by younger generations of mass movements, which are not related to the damming events (Delgado et al., 2020). In order to avoid uncertainties, it is recommended to combine dating of the landslide scarp and of the landslide dam material (Hermanns et al., 2004; Delgado et al., 2020).

Other absolute dating methods have seldom been applied to landslide dams, despite their applicability to the task. One such method is Th/U series dating of calcium precipitates that form within the rockslide body (Prager et al., 2009; Ostermann et al., 2017; Ostermann and Sanders, 2017). These precipitates postdate the failure event, and several samples can be dated within one precipitate, with the innermost sample being closest to the real age. Another very promising method is dendrochronology, which can yield seasonal precision under ideal conditions (Nicolussi et al., 2015; Yamada et al., 2018). For instance, the method of "wiggle matching analysis", which is a combination of tree-ring analysis of tree trunks found within the landslide body and multiple radiocarbon dating on the same sample material, allows precise dating to within a few years, even if the event is several thousand years old (Nicolussi et al., 2015). However, this approach relies on identifying a tree trunk that is preserved in the landslide mass, and exposed by erosional processes, or found in drill cores. Less-used dating methods include tephrochronology (Hermanns et al., 2011a), defining relationships to the marine limit (Hilger et al., 2018) or varve chronology (Trauth et al., 2000; 2001).

2.2.3 Summary

Dating landslide dams is often more complex than initially perceived, as dating requires detailed mapping of the morphology and stratigraphy of the landslide and its related sediments, the availability and precision of geochronological methods, and understanding of the landslide type forming the dam. Some types of mass movements, such as rock avalanches, volcanic mass movements, debris flows or landslides in unconsolidated sediments usually provide more dating opportunities (e.g. Delgado et al., 2020; Geertsema and Clague, 2006; Hermanns et al., 2004; Prager et al., 2009) in comparison to coherent rockslides (Beetham et al., 2002). Although recent progress in geochronological methods allows greater dating precision (i.e., a narrower range of dates) due to lowering of analytical uncertainties (Walker, 2005), the accuracy of dating (i.e. how close a result of dating is to the true age) is mostly limited by the availability of appropriate geological materials and datable landslide features (Lang et al., 1999). Therefore, reliable dating of landslide dams is still largely dependent on chance occurrence of ideal dating conditions. In such circumstances, yielding the most reliable time constraints for landslide dams is uncommon through multi-method dating, as shown by the relatively few successful multi-dating campaigns (e.g., Dong et al., 2014; Ostermann et al., 2017; Prager et al., 2009).

Besides the traditional use of ^{14}C dating on backwater sediments, recent progress has lead in particular to the direct dating of dam material. Furthermore, more and more multi-method dating campaigns have been applied around the globe to date landslides that caused river blockages (e.g. Dufresne et al., 2018; Hermanns et al., 2011b; 2004; Moreiras et al., 2015; Ostermann et

al., 2017), demonstrating one way in which the weaknesses of individual dating approaches can be overcome.

2.3. Geophysical methods

To better understand dam stability, the controlling factors need to be investigated, including the stratigraphy and physical properties of the deposited material (Wahl, 1997; Wahl, 2004). To this end, investigations of the interior of the dam itself are required. Due to the potential transient and unstable nature of dams, these investigations need to be rapid and non-invasive: geophysical methods are hence used routinely to characterise and monitor the internal condition of unstable slopes in analogous landslide environments (Jongmans and Garambois, 2007; McCann and Forster, 1990; Whiteley et al., 2019).

2.3.1 Overview of existing geophysical methods

To date, 19 geophysical investigations of 22 landslide dams are published in English-language ISI listed journals and English-language conference proceedings (Table 3). In just over half the cases, multiple methods (n=12) rather than a single method (n=10) were implemented. Seismic methods are most common (n=20), followed by geoelectric (n=15) and electromagnetic methods (n=4); Figure 4. In the following, we provide a background to these methods, and discuss the strengths and challenges in using geophysical methods to investigate landslide dams.

Table 3 A brief overview of the 19 geophysical investigations of 22 landslide dams exemplifying the efficacy of geophysical methods for landslide dam investigation.

Authors	Location	Trigger	Geophysical methods used[1]	Date of failure	Survey objective	Potential risk assessment / hazard mitigation purpose
Papyrin (2001)	Murgab River/ Usoi, Pamirs Mountains, Tajikistan	Co-seismic	VSP (see Ischuck, 2011) (plus ERT, gravity and magnetic surveys)[2]	1911 AD	Stratigraphic investigation	Stability assessment
Meric et al. (2005)	Romanche River/ Séchilienne, French Alps, France	Hydrological and co-seismic?	EM, ERT, SN, SP, SRT	Pre-failure	Geomorphological/ stratigraphic investigation	Volume estimation for modelling future landslide dam formation
Pánek et al. (2009)	Ropičanka River/ Mount Ropice, oravskoslezské Beskydy Mountains, Czech Republic	Fault induced rock weakening, possible co-seismic or hydrological	ERT, GPR	~1.5 ka BP (14C)	Geomorphological/ stratigraphic investigation	Understanding modes of landslide dam formation to assess future risks future risks

Delunel et al. (2010)	Vénéon River/ Lauvitel Valley, French Alps, France	Hydrological?	ERT	~4.7 ka BP (10Be)	Stratigraphic investigation, volume estimation	Understanding modes of landslide dam formation to assess future risks
Bianchi-Fasani et al. (2011)	Tasso River/ Scanno, Central Appennines, Italy	Co-seismic?	ERT, SRT, MASW, VES	12 - 2.3 ka BP (14C)	Stratigraphic investigation	Outburst flood risk assessment
Crosta et al. (2010)	Adda River/ Val Pola, Mount Zandila, Italian Alps, Italy	Hydrological?	SRT	1987 AD	Stratigraphic investigation	Outburst flood risk assessment / planning remedial engineering measures
Ischuk (2011)	Murgab River/ Usoi, Pamirs Mountains, Tajikistan	Co-seismic	Description of selected data described in Papyrin (2001)	1911 AD	Stratigraphic investigation	Outburst flood risk assessment
Plaza et al. (2011)	Paute River/ La Josefina, Parquiloma (Cerro Tamuga), Andes, Ecuador	Anthropogenic and hydrological	SRT	1993 AD	Stratigraphic investigation	Planning remedial engineering measures
Grandjean et al. (2011)	Doron-de-Pralognan River/ Ballandaz, Savoie, France	Hydrological?	EM, ERT, H/V, SASW, SRT	Pre-failure	Stratigraphic and hydrogeological investigation	Volume estimation for modelling future landslide dam formation
Niazi et al. (2010)	Jhelum River/ Hattian Bala, Azad Kashmir, Pakistan	Co-seismic	ERT	2005 AD	Stratigraphic investigation, seepage monitoring	Assessment of seepage or piping failure potential
Wang et al. (2013)	Tributary of Mianyuan River/ Tianchi, Sichuan Province, China	Co-seismic	MASW	2008 AD	Stratigraphic investigation	Assessment of seepage or piping failure potential / outburst flood risk assessment
Wang et al. (2014b)	Daduhe River/ Zhanggu, Guza,Sichuan Province, China	Co-seismic	MT	781 - 126 ka BP?	Stratigraphic investigation, identification of sliding surface	Understanding modes of landslide dam formation to assess future risks
Torgoev et al. (2013)	Unamed river/ Ak-kul, Minkush, Central Tien Shan, Kyrgyzstan	Co-seismic?	ERT, H/V	"Ancient"	Stratigraphic and hydrogeological investigation	Seismic stability assessment / seepage or piping failure assessment
Torgoev et al. (2014)	Naryn River/ Kambarata Hydroelectric Power Plant 2, Central Tien Shan, Kyrgyzstan	Anthropogenic	ERT	2009 AD	Seepage monitoring	Seepage or piping failure assessment
Wang et al. (2014a)	Qingzhu and Hongshi River/ Donghekou, Qingchuan County, Sichuan	Co-seismic	MASW	2008 AD	Stratigraphic investigation, identification of sliding surface	Outburst flood risk assessment / planning remedial engineering measures

	Province, China					
Wang et al. (2016a)	Imo River/ Higashi-Takezawa District, Niigata, Japan	Co-seismic	MASW	2004 AD	Stratigraphic investigation	Outburst flood risk assessment
Wang et al. (2018b)	Unamed river/ Akatani, Nara Prefecture, Japan	Hydrological	MTM, SP	2011 AD	Seepage identification	Seepage or piping failure assessment
	Unamned river/ Kuridaira, Nara Prefecture, Japan	Hydrological	MTM, SP	2011 AD		
	Imogawa River/ Terano, Niigata Prefecture, Japan	Co-seismic	MTM, SP	2004 AD		
	Kegeti River/ Kol-Tor, Kyrgyzstan			>0.2 ka BP		
Wang et al. (2018a)	Experimental setup, Eshima Island, Shimane Prefucture, Japan	Anthropogenic	SP	Recent	Precursory failure condition	Understanding modes of landslide dam formation to assess future risks / outburst flood risk assessment
Havenith et al. (2015)	Naryn River/ Kambarata Hydroelectric Power Plant 2, Central Tien Shan, Kyrgyzstan	Anthropogenic	ERT, H/V	2009 AD	Seepage monitoring, stratigraphic investigation	Seepage or piping failure assessment / seismic stability assessment
Havenith et al. (2018)	Vakhsh River/ Rogun Hydroelectric Power Plant, Tajikistan	Potentially seismically triggered	ERT, SRT, H/V	Pre-failure	Geomorphological/ stratigraphic investigation	Seepage or piping failure assessment / seismic stability assessment

[1]EM = Electromagnetic, ERT = Electrical resistivity tomography, GPR = Ground penetrating radar, H/V = Horizontal-to-vertical noise ratio, MASW = Multi-channel analysis of surface waves, MTM = Micro-tremor method, MT = Magnetotellurics, SASW = Spectral analysis of surface waves, SN = Seismic noise analysis, SP = Self-potential, SRT = Seismic refraction tomography, VES = Vertical electrode sounding, VSP = Vertical seismic profile. [2]ERT, gravity and magnetic survey results not accessed, VSP data described in part by Ischuck (2011).

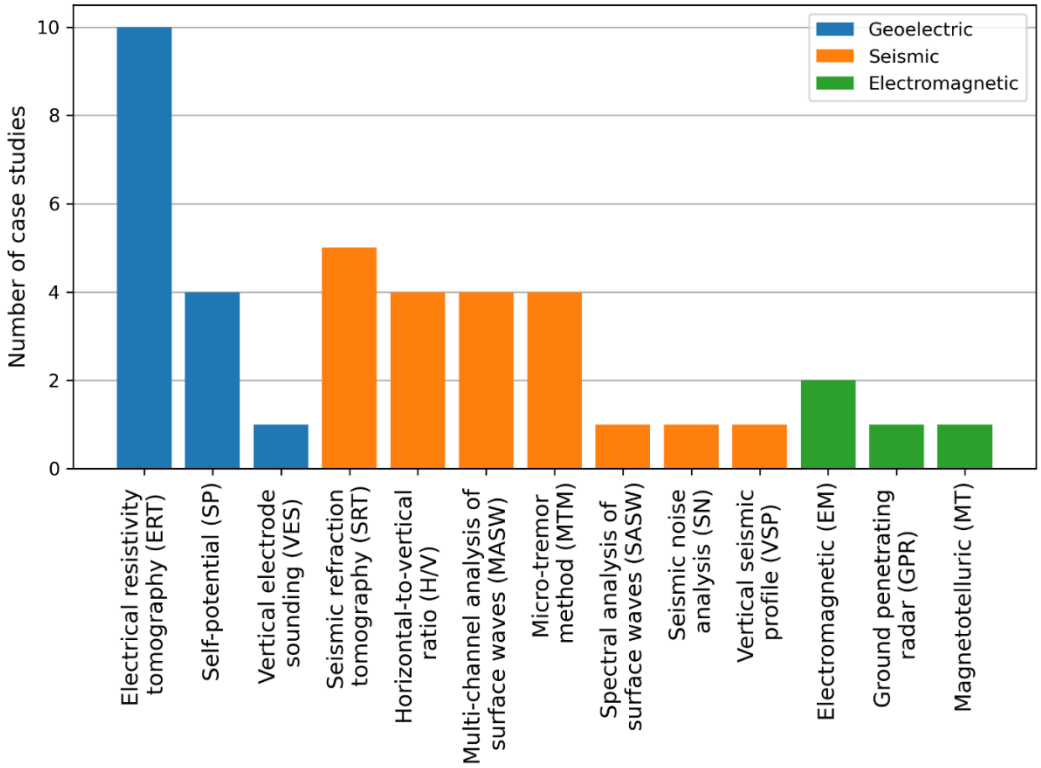

410

411 **Figure 4** The number of different geophysical survey methods used to investigate the internal structure
412 landslide dams from the data in Table 3.

413

414 ### *2.3.2 Electromagnetic surveys*

415 Three types of electromagnetic surveys are used to investigate landslide dams; active
416 electromagnetics (EM), ground penetrating radar (GPR), and magnetotellurics (MT). EM surveys
417 utilize diffuse electromagnetic signals in the tens of Hz (super-low EM) to tens of kHz (very-low
418 EM) frequency range (Tezkan, 1999), and measure profiles or surface maps of conductivity.
419 Spatial heterogeneities in conductivity may indicate differences in material composition, grain-
420 size or saturation (e.g. Santamarina et al., 2005).

421 GPR surveys generate wave-like signals at higher frequencies, typically a few MHz (high EM) to
422 a few GHz (super-high EM) range (Olhoeft, 2002). Frequency primarily controls depth of
423 penetration; larger wavelengths penetrate further, but cannot resolve small features. Conversely,
424 shorter wavelengths have lower depth penetration, but can resolve smaller features. GPR
425 measurements can assess the water content of materials (e.g. Garambois et al., 2002), but are
426 more commonly used to produce cross-sections identifying structural discontinuities, such as
427 depth to bedrock, stratigraphy and geomorphological features (e.g. Davis and Annan, 1989).

428 The MT method (Cagniard, 1953) is a passive technique, utilizing a range of frequencies from
429 <1Hz to tens of kHz (Strangway, 1983), with higher frequencies being typically used for shallow

investigations (Strangway et al., 1973). MT measures 1D soundings or 2D profiles of resistivity (the inverse of conductivity), and is sensitive to material composition, grain-size and saturation.

2.3.3 Geoelectric surveys

Two types of geoelectric survey are used in landslide dam investigations; electrical resistivity tomography (ERT) and self-potential (SP). In an ERT survey, a DC current is injected between a pair of electrodes, and the potential difference is measured between a separate pair (Griffiths and Barker, 1993). Expanding the spacing between the electrodes around a fixed mid-point increases the depth of the measurement, and produces a 1D vertical electrical sounding (VES) beneath the mid-point. The maximum depth of investigation is proportionally restricted to the available ground surface on which electrodes can be deployed. To acquire 2D or 3D ERT data, an array of electrodes is deployed and combinations of injection and potential electrodes at different positions and spacing produce cross-sections or volumes of resistivity (Loke et al., 2013). Inverted resistivity tomograms show variations in geology, hydrology, and engineering properties (e.g. Chambers et al., 2006; Perrone et al., 2014).

The SP method uses a single pair of electrodes to measure spontaneously occurring charges in the subsurface which arise from streaming potentials along with thermokinetic potentials and cultural activity (Patella, 1997). The method is primarily used to identify zones of fluid flow (e.g. Colangelo et al., 2006). The depth of investigation is related to the separation between the electrodes, with the measured self-potential field influenced by the subsurface features present between and beneath the electrodes.

2.3.4 Seismic surveys

Elastic waves can be artificially generated for 2D seismic profiling of the subsurface; compressional P-waves (measuring P-wave velocity) and transverse S-waves (measuring S- or shear-wave velocity) are used for seismic refraction tomography (SRT) surveys (Redpath, 1973). SRT measures the travel-time of elastic waves as they propagate from a source to seismic receivers (i.e., geophones) via refracted ray-paths in the subsurface. S-wave velocity is primarily controlled by changes in density, whereas P-waves are controlled by changes in both density and material incompressibility. The depth of investigation is related to the length of the geophone array deployment and amplitude of the source used. Geophones can be deployed in boreholes to measure the velocity of waves generated at the surface, a practice called vertical seismic profiling (VSP). SRT (and VSP) surveys are typically used to identify subsurface discontinuities and the elastic moduli of stratigraphic layers, which can provide information on the stratigraphic and hydrogeological state of subsurface materials (e.g. Whiteley et al., 2020). If only two seismic receivers are used, spectral analysis of surface waves (SASW) between simultaneously recorded wave fields can be used to provide an estimate of the vertical 1D profile of S-wave velocity and

shear modulus (Stokoe et al., 1994). More commonly, the multi-channel analysis of surface waves (MASW) technique measures the group of phase-velocity of surface (Rayleigh) waves (Park et al., 1999) to produce a 2D S-wave velocity profile. MASW surveys can be used to identify stratigraphic boundaries in the subsurface, as well as provide information on material stiffness (e.g. Donohue et al., 2011).

By recording naturally occurring, passive seismic signals (called 'ambient noise') and analyzing the corresponding horizontal-to-vertical spectral ratio (H/V), material stiffness can be estimated (Castellaro et al., 2005). If multiple seismic receivers are used, the micro-tremor method (MTM) can determine 2D subsurface structures (Okada and Suto, 2003). In addition, simply recording the seismic noise (SN) and analysing the spectral amplitude gives estimations of possible resonance phenomena that may occur in seismically unstable settings (Field and Jacob, 1993).

2.2.5 Examples of geophysical investigations of landslide dams

Geophysical surveys can be used to assess the volume of unstable slopes that may form future landslide dams. Meric et al. (2005) and Grandjean et al. (2011) used a combination of EM, ERT, SRT and SN methods to investigate the dimensions of two landslides that are at risk of damming rivers. More commonly, geophysical studies are used to investigate existing, recently formed landslide dams; for example, Wang et al. (2014a) used MASW surveys to demonstrate that bulk densities of the emplaced landslide dam material were similar to those of the pre-existing slope.

The sedimentology of historic landslide dams can be a target for geophysical investigations. A detailed reconstruction of late Holocene deep-seated gravitational slope deformation and toppling events at Ropice Mountain in the Czech Republic was aided by the use of ERT measurements and GPR profiles (Pánek et al., 2009). Additionally, geophysical surveys may be used to identify potential failure modes in seemingly stable dams; the Kol-Tor landslide dam in the Kyrgyz Republic was monitored using MTM and SP by Wang et al. (2018a), identifying seepage routes in the long-existing landslide dam, with the combined results from the separate surveys (Figure 5) improving the confidence of identified seepage zones. Geophysical surveys are also used to assist in the engineering of landslide dams. At the Karambata Hydro Power Plant 2 in Kyrgyz Republic, Havenith et al. (2015) and Torgoev et al. (2014) used ERT to assess compaction after the emplacement of a blast-fill dam. The ERT surveys showed high resistivity zones in the blast-fill material (about 75% of the dam volume), indicating good compaction; this blast-fill material was shown to be in better engineering condition than the earth-fill later introduced to cover the blast-fill materials.

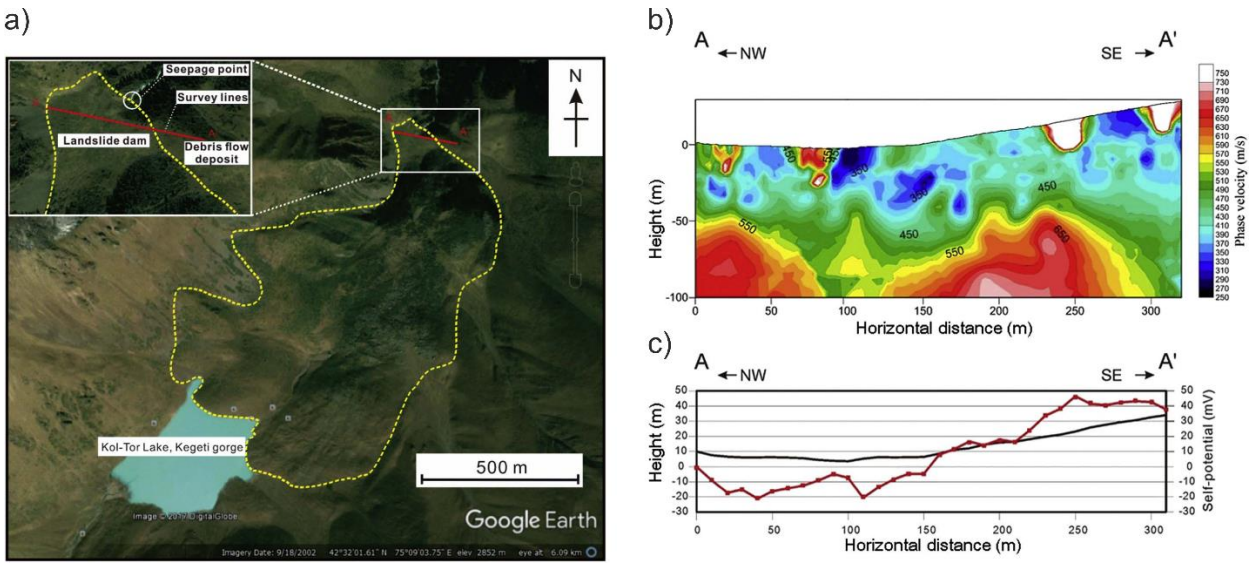

Figure 5 (A) The Kol-Tor lake and landslide dam in the Kyrgyz Republic showing the geophysical survey profile crossing the emplaced landslide dam (0 – 220 m horizontal distance) and debris flow deposit (220 – 310 m horizontal distance), (B) the results of the micro-tremor method survey, indicating areas of low-velocity ground associated with destabilization due to seepage at 80 m, 150 m and 170 m horizontal distance, and (C) the results of the self-potential from the same profile, with elevated readings in the landslide dam corresponding with the active seepage zone at 150m horizontal distance. Modified from Wang et al. (2018a).

2.3.6 Summary and outlook

Geophysical methods are increasingly used to investigate the properties and condition of landslide dams. These methods can characterize the total thickness, internal structure, and geotechnical properties of landslide dams in a rapid and non-invasive manner. Survey results can help assess dam stability by identifying material heterogeneities that indicate zones of weakness or fluid flow. Recent innovations in geophysical monitoring approaches can provide ongoing assessments of landslide dam stability, and identification of evolving zones of weakness which may lead to dam failure.

However, geophysical surveys provide indirect observations, with measurements acting as proxies for ground conditions, and they require careful interpretation supported by multi-technique surveys, and comparison with observed ground properties from laboratory or field observations. Where possible, data should be calibrated by measurements near geological outcrops or across known geological cross-sections that allow for extrapolations of results deeper in to dam structure.

2.4. Dam sedimentology and geotechnical properties

2.4.1 Landslide dam sedimentology

One approach to assess the type of landslide dam and its composition is to regard it simply as a landslide deposit. In their review of the Varnes (1978) classification of landslide types, Hungr et al. (2014, p.171) emphasize that "the goal of landslide classification systems is to stress the component that is the most important in determining the mechanical behavior of the landslide during and post-failure". The material classes in their classification span the full spectrum of soils (and their corresponding unified soil classes), rock, ice, and peat. Consequently, the different landslide types form deposits of very different sedimentology (composition, grain size distributions, etc.), structure (faults, layers, etc.), geotechnical (density, strength parameters, etc.) and hydrogeological properties (permeability, etc.). In addition, differences in river-blocking deposit volumes and thicknesses vary over several orders of magnitude depending on the source region and valley geometry, as well as on the proportion of the landslide actually blocking the river (e.g. Miller et al., 2018). This can make adjustments of existing classification schemes necessary when addressing landslide dam stability (cf. Fan et al., 2020). For example, the 2008 Wenchuan earthquake exemplified the diversity of landslides forming dams. In its aftermath, Fan et al. (2015) identified three types of landslide dams: (1) dams mainly composed of large boulders and blocks, (2) dams dominated by unconsolidated fine debris, and (3) layered dams with partly intact rock strata at the base overlain by larger boulders and blocks or soil with rock fragments (see also Fan et al., 2020).

Multi-layered deposits are common for large (>10^6 m^3) rockslides (RS) and rock avalanches (RA). For these landslide types, a three-part facies model of an upper coarse carapace, a heterogeneous body of highly fragmented debris, and a basal facies or mixed zone with incorporated substrates has become widely accepted (e.g. Davies and McSaveney, 2011; Dufresne et al., 2016; Dunning, 2006; Dunning and Armitage, 2011; Heim, 1932; Strom, 2006; Weidinger et al., 2014). The large boulders of the carapace may form a network dense enough to armor the deposit effectively against erosion by overtopping water flow similar to engineered rip-rap. The largest volume of RS/RA deposits, however, is made up by the body facies. This highly heterogeneous, fragmented interior consists of various sub-facies—some common across many deposits, others specific to individual deposits depending on source structures and emplacement conditions (Figure 6). Each sub-facies varies in spatial distribution and geotechnical properties. For example, facies-distribution within the carbonate Flims rockslide in Switzerland influenced the location of incision through the ~400-m-thick deposit (Wassmer et al., 2004). At Flims, the uppermost granular and intermediate facies have clast-in-matrix fabrics and spillways were found in two locations, with the more proximal one terminating at 1,060 m asl at the transition

from the intermediate to the 'structured facies' (the latter described as a 'thick layer of rock'). In a more distal location, this boundary is at around 900 m asl and the broad spillway within the upper intermediate facies narrows where it cuts through the more resistant structured facies (all descriptions from Wassmer et al. (2004)).

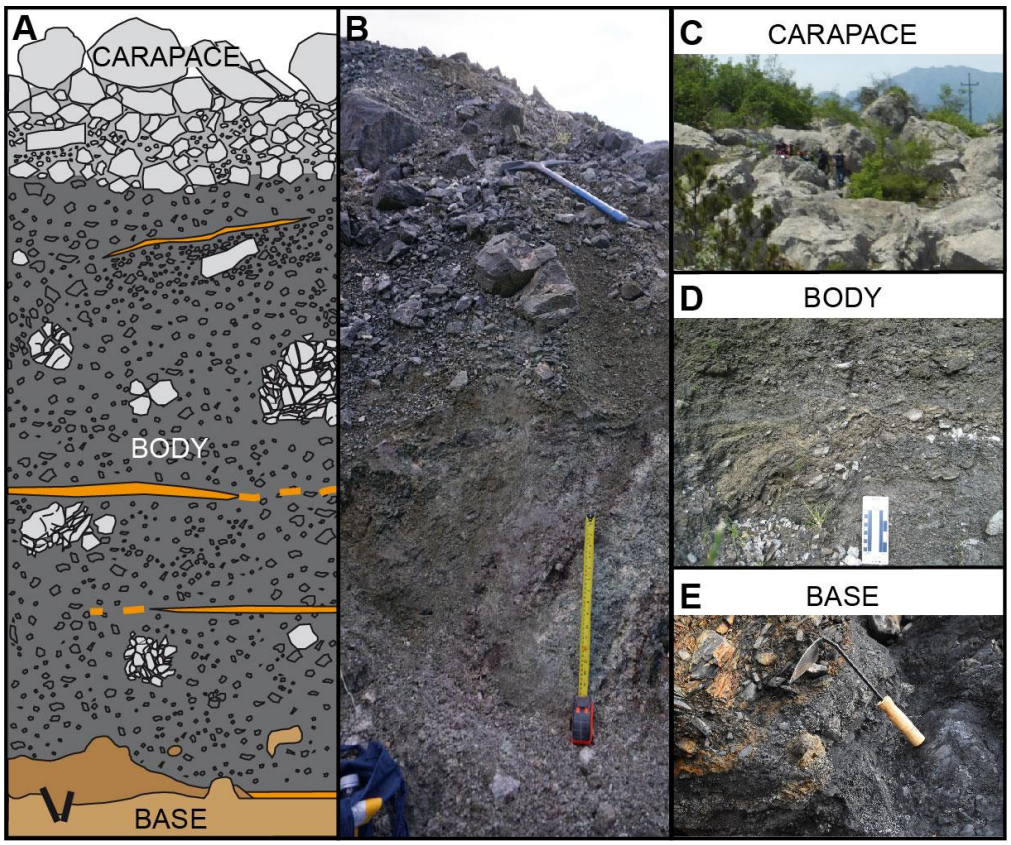

Figure 6 (A) Typical three-part facies model of an upper coarse carapace (light grey), a heterogeneous body facies (dark grey) with jigsaw-fractured and survivor clasts (larger light grey areas) and shear zones (orange), and the basal facies with a mixed zone (brown), basal shear (orange), faulting (black lines) and injection of in situ substrate (ochre). (B) Transition from carapace to body facies with intact stratigraphic succession near the 40-cm-long tapemeasure (Harold Price rock avalanche, British Columbia, Canada). (C) Prominent carapace at the Le Marocche rockslide in Italy (note people for scale). (D) Sheared but intact lithological succession in the mylonitic Round Top rock avalanche, New Zealand. (E) Example of a basal contact of the rockslide near the Longtangping village, Mianyang County, Sichuan, China.

The reviews of Weidinger et al. (2014) and Dufresne et al. (2016) show that any inverse grading in a RA or RS deposit is limited to the carapace-body transition (Figure 6B). Hence, reverse grading *sensu strictu* (i.e. a systematic change in grain size from one end to the other) does not apply to rockslide and rock avalanche deposits. Source stratigraphy is typically preserved in these deposits (e.g. Abdrakhmatov and Strom, 2006; Heim, 1932; Hewitt et al., 2008; Weidinger et al., 2014), and, depending on original bedding orientations and sliding geometry, results in specific horizontal or lateral distribution of lithologies (e.g. Hartvich, 2008; Strom, 2006; Strom, 2010) that influence where erosion and breach may occur preferentially.

Additionally, transitions in emplacement behavior of the landslide influence the degree of comminution and hence the deposit grain size distribution and erodibility. For example, a late-Pleistocene rockslide in the Betic Cordillera transformed from a proximal, well-stratified planar rockslide deposit into a highly comminuted rock avalanche, which resulted in several depositional facies (García-García et al., 2011). Further dynamic changes induced during landslide transport and emplacement include mixing with valley-fill sediments, water and/or ice as well as phase transition into debris avalanches and/or fully saturated debris flows (the 'complex' landslide type of Cruden and Varnes, 1996). Each of these transitions changes not only the dynamic behavior of the landslide, but also the thickness, morphology, and geotechnical properties of the resulting deposits.

Post-emplacement modifications, such as self-compaction under overburden, precipitation of minerals, inflow of fine sands and clays, or debris fan formation at the downstream face can alter dam permeability, erodibility, and overall material strength. Korchevskiy et al. (2011), for example, observed a decrease in seepage through the Burlykiya blast-fill dam during the first month after dam formation at constant lake level, and attributed this to the natural formation of reverse filters due to transfer of fine particles within the dam.

2.4.2 Landslide geotechnical properties

The presence (and distribution) or absence of an armoring carapace of large boulders that could protect from, or slow, downward erosion and spillway formation can reduce the risk of, or increase the time to, an overtopping failure. Even though the carapace is more permeable (as it is an openwork structure) and less dense than the lower levels, the larger clast sizes make it more resistant to mobilization/entrainment by water flows. Large boulders collapsing into a developing spillway can also re-stabilize the breach channel and stop or slow further downward erosion (e.g. Plaza et al., 2011) as well as create a hydrologically rougher, inefficient flow.

Permeability of the dam interior controls the formation of an upstream lake as well as the equilibration of inflow into the impoundment and seepage through or around the dam to keep the lake at a level below overtopping (e.g. at the Usoi dam of the Sarez Lake in Pamir; Hanisch and Söder, 2000; Ischuk, 2011). On the other hand, seepage may lead to internal erosion and consequent dam failure by piping (e.g. Dunning et al., 2006; see below). This failure type is, however, rare in landslide dams, highlighting their resistance to suffusion. Davies and McSaveney (2006) attribute the rarity of piping or slumping as a failure mechanism of landslide dams to the typically heterogeneous grain size distribution and very small average void size within the dams. Furthermore, the spatial distribution of different lithologies and depositional facies will have unique properties, such as permeability or critical erosive shear stress, affecting internal water flow.

Relatively few studies have detailed the geotechnical aspects of landslide dams. The data in Table 4 are variously based on field or laboratory tests of dam material, derived from numerical stability analyses or assumed through comparison with similar materials. Several studies report consistent changes in geotechnical properties with depth within the dam. Compressed rock density in a blast-fill dam increases from ~1.7 tons/m^3 near the surface to just over 2.0 tons/m^3 at depth (Korchevskiy et al., 2011). The Val Pola rockslide in Italy shows progressive decrease of hydraulic conductivity from 10^{-3} m/s near the top to 10^{-6} m/s at 70 m depth, though the data scatter at similar depths is around two orders of magnitude (Crosta et al., 2010).

Table 4 Geotechnical properties of selected landslides dams.

Higashi-Takezawa landslide (Japan): siltstone, sediments, 93% fine sand (Wang et al., 2016a)

V [10^6m^3]	Y [kN/m^3]		$\rho_{bulk,dry}$ [g/cm^3]	ρ_{rock} [g/cm^3]	W [%]	e	c [kN/m^2]	c' [kN/m^2]	θ [°]	κ [cm/s]	τ_c [Pa]
1.3	18	*Sliding plane:*					25.5		18.0		
		Head:	1.20	2.69	32.0	1.25				9.99×10^{-5}	
		Central:	1.38	2.63	21.4	0.92		19.8	35.6	1.41×10^{-2}	0.32
		Toe:	1.47	2.64	28.1	0.80		27.8	36.5	3.02×10^{-6}	

Hsiaolin colluvium slide (Taiwan), longevity: 84 minutes (Dong et al., 2011a)

V [10^6m^3]	D_{50} [mm]	D_{10} [mm]	Soil class	Y [kN/m^3]	GS	W [%]	c' [kN/m^2]	θ [°]	κ [cm/s]	LL [%]	PL [%]
25.2 (15.4)	0.24	0.005	SC	20.1	2.85	3.4	6	22	1×10^{-5}	24.1	7.5
	0.09	0.003	SM	20.6	2.56	1.7				23.1	3.6
	0.40	0.003	SC	21.3	2.80	1.8				25.6	7.7
	0.07	0.002	CL	21.7	2.71	1.8				29.5	7.8

Usoi rockslide (Tajikistan), 1911-today (Hanisch and Söder, 2000)

V [10^6m^3]	H [m]	freeboard [m]	discharge [m^3/s]	Y [kN/m^3]	c [kN/m^2]	θ [°]
2,000	600 (450)	50	45	22	neglected	25

Val Pola rockslide (Italy), July 1987 (Crosta et al., 2010)

V [10^6m^3]	κ [cm/s]	K [m/s]	d [m]	V_S [m/s]
	1×10^{-2} to 1×10^{-6}	2.7×10^{-3} to 1.4×10^{-4}	0-4	200-300
			4-15	600-1,000
			>15	1,700

La Josefina, 1993 (Plaza et al., 2011)

V [10^6m^3]	H [m]	D_{10} [mm]	D_{90}/D_{30}	Y [kN/m^3]	porosity [%]	c [kN/m^2]	θ [°]
20	100	100	30	27.6	15	5	45

Kambarata blast-fill dam, rockslide (Havenith et al., 2015)

V [10^6m^3]	H [m]		c [kN/m^2]	θ [°]	K [m/s]
0.78	25-30	Raised with gravel, sand, etc. to target height of 50m	200	38	4×10^{-3} (initial)
					3×10^{-5} (calibr.)

V: landslide volume (dam volume); γ: specific weight; ρ: density; W: water content; e: void ratio; c: cohesion; c': effective cohesion; θ: friction angle; κ: hydraulic conductivity; τ_c: critical erosive shear stress; GS: specific gravity; LL: liquid limit; PL: plastic limit; H: dam height (effective dam height); K: permeability; d: depth below dam surface; V_S: shear wave velocity

Other studies point to the influence of material characteristics on dam longevity from a purely empirical and observational perspective, stating that dams composed of coarser debris and those

637 that are grain-supported or made up of cohesive particles last longer (Costa and Schuster, 1988;
638 Ermini and Casagli, 2003; Weidinger et al., 2014; Shen et al., 2020). Comparing landslide type
639 and grain size distribution with dam longevity for 13 cases, Weidinger (2011) suggests that
640 rockslides (blocks; n=3) exceed rock avalanches (boulders; n=7), which in turn exceed landslides
641 composed of overall finer-grained debris (n=3) in structural longevity. Schuster (1986); (Schuster,
642 1995) conclude that dams formed from large boulders or cohesive clays are less likely to fail than
643 highly permeable or unconsolidated dams. They further state that the characteristics of volcanic
644 debris avalanche deposits (usually compact, poorly sorted, block-in-matrix fabrics with a high
645 proportion of sand-to-clay-sized particles) inhibit filtration, thereby promoting water accumulation
646 to the level of overtopping. Recently, Fan et al. (2020) compared longevity against the landslide
647 types forming the dam (based on data using 410 worldwide landslide dams). Their analysis shows
648 that 80% of complex, 65% of debris flows, and ~60% of dams in unconsolidated sediments have
649 a longevity of less than one year, whereas dams of rock/debris avalanches and rockslides last
650 longer. They further suggest that the influence of landslide or material type on the longevity of a
651 landslide dam decreases beyond the first year, and beyond 10 years about 30-40% of the dams
652 survived regardless of the landslide type.

653 Over time, weathering, mineralization and cementation influence the performance of dams.
654 Korchevskiy et al. (2011; p. 625) summarize that “siltstone, mudstone, sandstone and
655 conglomerate with clayey and carbonate-clayey cement and some varieties of shale and gneiss
656 undergo rapid and intense weathering”, which can lead to density heterogeneities and a high
657 infiltration gradient, and may increase the potential for piping and internal erosion. Prager et al.
658 (2009) and Weidinger et al. (2014) note the influence of secondary cementation after groundwater
659 and meteoric waters percolate through dam materials. Such cementation can significantly alter
660 water pathways over time. Dunning and Armitage (2011) modelled landslide dam stability
661 numerically (both with and without a carapace) through which phreatic tonguing occurred due to
662 the highly permeable openwork structure, which significantly decreased downstream face
663 stability. It is this mode of failure, with observed seepage front progression up the downstream
664 dam-face that caused the slumping failure of the Tsatichhu rock-avalanche dam in Bhutan
665 (Dunning et al., 2006). Xu et al. (2009) categorized failed landslide dams from the 2008
666 Wenchuan earthquake, classifying the main dam materials, but not their internal heterogeneity or
667 distribution of discrete facies.

668 Much can be learned from the study of artificial dams or from the construction and analysis of
669 blast-fill dams. In blast-fill dam design, the dams are essentially treated as deposits with two
670 zones of contrasting permeability: the upper carapace and the body (Adushkin, 2006; Adushkin,
671 2011; Korchevskiy et al., 2011). Reservoir levels are recommended to be kept below the facies
672 transition because “the abrupt difference between the permeability of the upper and lower parts

673 may lead to internal erosion if high discharge through the void spaces in the carapace directly
674 affects the underlying comminuted debris" (Korchevskiy et al., 2011; p. 633). The basal facies is
675 usually neglected, and coarse talus and trees in the emplacement area removed prior to blasting
676 to reduce permeability in the dam foundation. According to the same authors, the compressed
677 rock density of blast-fill and natural rockslide dams exceed that of embankment dams.
678 Korchevskiy et al. (2011) identified three blast-fill dams at which 70-80% of the increase in dam
679 body density occurred in the first year after emplacement. This suggests that if a dam survives
680 the first year, progressive changes in geotechnical properties may increase the likelihood of
681 continued future stability, which is in agreement with the empirical observations by Fan et al.
682 (2020) mentioned above.

683 At the Karambata Hydro Power Plant 2 in Kyrgyz Republic, Havenith et al. (2015) and Torgoev
684 et al. (2014) used ERT to assess compaction after the emplacement of a blast-fill dam. The ERT
685 surveys showed high resistivity zones in the blast-fill material (about 75% of the dam volume),
686 indicating good compaction; this blast-fill material was shown to be in better engineering condition
687 than the earth-fill later introduced to cover the blast-fill materials.

688 In contrast to rock-fill-dominated natural and artificial dams are those created by landslides in
689 unconsolidated sediments, and debris flows. Besides significant differences in the source
690 material, their deposits are more homogenous, since intensive fragmentation does not occur
691 (which results in the distinct three-facies structure typical of most of rock avalanche dams), and
692 many debris flows are turbulent, making the resultant bodies more uniform in grain-size
693 composition. The major factor influencing the sedimentology of unconsolidated natural dams is
694 the role of water in the formation and motion of the landslides, especially in debris flows. Water-
695 enriched debris has low internal friction angles and such dams are rarely as high as dams formed
696 by 'dry' rockslides or rock avalanches.

697 ### *2.4.3 Summary and outlook*

698 The data presented in this section is a collation from detailed sedimentological and geotechnical
699 analyses of landslide deposits, geophysical investigations of both, landslides and landslide dams,
700 and insights from artifical blast-fill dams. The way forward in landslide dam analyses is, in our
701 view, the continuation of such multidisciplinary investigations. They expand our knowledge of (a)
702 landslide composition, structure, and geotechnical properties, which can be transferred to dam
703 stability assessments, and (b) dam performance and changes in properties over time.

3. Recent Advances in Landslide Dam Analyses

In this section, we take a closer look at dam failure modes and the processes involved therein, and review the recent insights from physical analogue modelling and data from well-documented failures of embankment dams. This is followed by an overview of how potential hazard cascades (or individual processes therein) can be assessed through numerical modelling.

3.1. Dam failure modes and insights from analogue models

Landslide dams, and artificial water-retaining structures such as earth- or rockfill (embankment) dams, can fail by overtopping, piping or slope failure (Korup, 2002; Schuster et al., 1992). The majority of landslide dams that formed and rapidly failed in historic times breached through overtopping (Costa and Schuster, 1988; Peng and Zhang, 2012d). This is a process of fluvial erosion wherein erosion starts at the downstream side of the dam and progressively moves upstream and downward into the dam body (Figure 7A, E). Failure due to piping, on the other hand, plays a larger role in embankment dams than in landslide dams. Two definitions of this phenomenon exist. One defines it as seepage through the dam body (Figure 7B), which eventually develops into an erosive flow and can lead to dam failure—where the erosive flow starts is not specified. The other definition, usually applied in an engineering context, addresses 'piping' as an erosive flow in the foundation below a dam body (Figure 7C). For natural dams, however, erosive flow below the dam (i.e. through the underlying sediments) has never been reported since water typically finds pathways through the dam body itself, and therefore we use the term 'piping' to refer to seepage through a dam body only. Failure initiated by the collapse of the downstream slope (Figure 7D) is rare in natural dams.

In a review of 11,192 published cases of embankment dam failures, Foster et al. (2000) report that overtopping accounts for 48.4% and piping for 46.1% of the total number of failures (Figure 7E). Zhang et al. (2009a) reviewed 593 cases of earthfill dam failures and found that 36.4% of the dams failed by overtopping, whereas dam quality problems (piping, sliding, spillway defects, etc.) comprised 42.5% of the dominant causes of dam failure. Of these dam quality problems, 58.3 and 18.3% of the dam failures were caused by piping and sliding, respectively. Similarly, Peng and Zhang (2012d), analysing 144 cases of landslide and 176 cases of embankment dam failures found that 1%, 8%, and 91% cases of landslide dam failures were caused by slope failure, piping, and overtopping, respectively. On the other hand, slope failure, piping, and overtopping accounted for 5%, 37%, and 58% cases of failures for embankment dams.

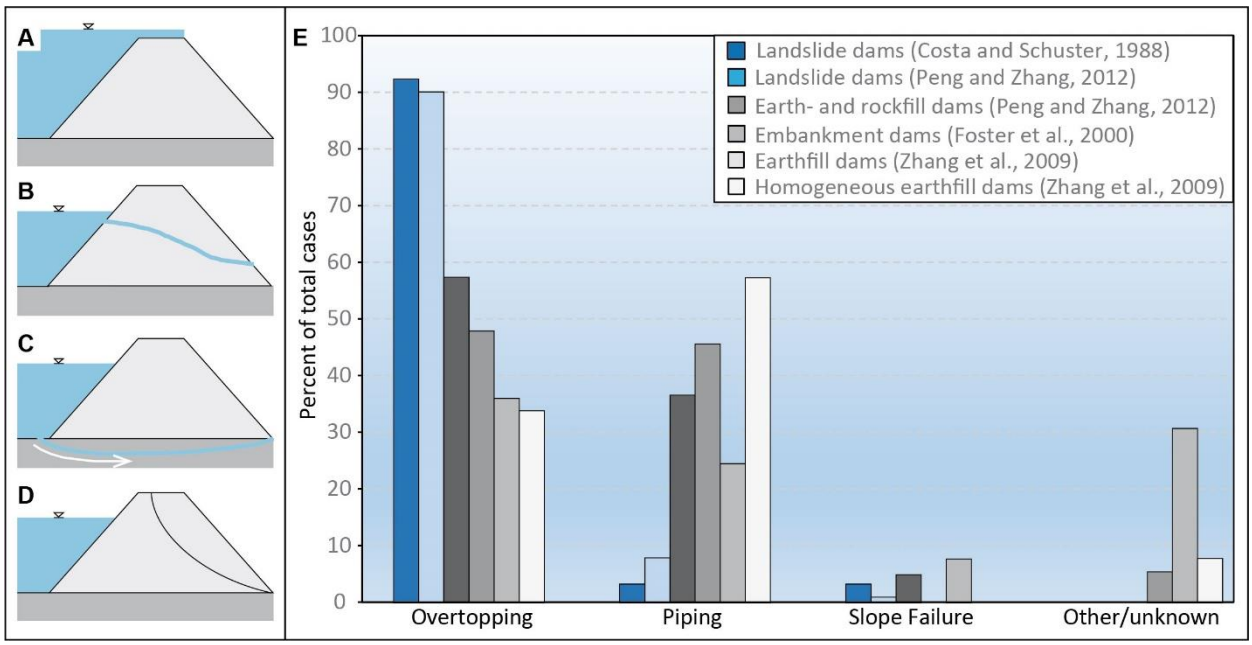

Figure 7 Failure modes of dams: (A) overtopping, (B) seepage/piping through the dam, (C) piping through the dam foundation (observed only in artificial dams), and (D) slope failure. (E) Distribution of failure modes from published datases (number of cases in parenthesis): Costa and Schuster (1988) (60); Peng and Zhang (2012c) (144 landslide, 176 earth- and rockfill dams); Foster et al. (2000) (11,192); Zhang et al. (2009b) (593, thereof 38 homogeneous earthfill dams).

Shen et al. (2020) statistically analyzed the longevity of landslide dams based on a database with 1,737 landslide dam cases, among which 352 cases were well recorded with longevity information and overtopping failure. According to the interaction between landslide dams and lake water, the longevity of landslide dams can be divided into three stages: infilling, overflowing and breaching. Their three-stage regression model shows better accuracy than that of the full longevity regression model because it considers the influencing factors of each stage.

Given the sparse research to date on the engineering behaviour and failure mechanisms of natural river blockages, physical modelling provides a solid means for understanding dam breach mechanisms, including the breach initiation process, breach parameters, breaching time, outflow hydrographs, and potential flood risk areas. However, the complexities associated with the failure of landslide dams have made the development of physical models very difficult. Notwithstanding, scientists and hydraulic engineers often prefer physical modelling over the development of numerical models due to the following reasons: (1) physical modelling allows for a better observation of the failure mechanisms of dams, under given space and time conditions; and (2) it allows for the inclusion of previously unknown parameters that could influence the stability of dams (Peakall et al., 1996; Young and Warburton, 1996).

To date, the focus of laboratory-scale modelling (and also of numerical modelling; cf. Section 3.2) has been on homogeneous earthfill dams. According to Singh (2013), the failure of earthfill dams

761 is commonly induced by erosion of the dam material by transient water flow either over or through
762 the dam. The former results in the overtopping of the dam, whereas the latter leads to seepage
763 and internal erosion (piping). Several physical modelling approaches investigated piping and
764 overtopping failures of earthfill dams and other river blockages, whereas few studies concentrated
765 on the sliding mechanism of dam failures. For instance, Okeke et al. (2017) and Wang et al.
766 (2018a) performed a series of large-scale physical (outdoor) experiments to investigate the
767 precursory factors leading to piping-induced failure. Their results show that the high turbidity of
768 the effluent seepage coincided with a decrease in self-potential values, together with several
769 internal displacements and dam crest settlement. They concluded that the failure of the dam
770 models comprises a four-phase process that includes: the discharge of hyperconcentrated flow
771 from the downstream toe, evolution of cracks on the dam crest, dam-crest settlement, and
772 undercutting of the downstream toe. To study the failure mechanisms of landslide dams due to
773 overtopping, Cao et al. (2011) used an 80-m long by 1.2-m wide by 0.8-m deep flume tank with
774 and without an initial notch on the dam crest, where the notch simulates an initial overtopping
775 breach. They found that the peak discharge of the outflow hydrograph was higher in the dams
776 built without an initial notch compared to dams with an initial notch.

777 ### *3.1.1 Overtopping failure*

778 The breaching of earthfill dams by overtopping is usually triggered by inadequate flood design
779 that arises from excessive rainfall (Singh, 2013). In natural dams, overtopping-induced failure is
780 commonly influenced by the volume and rate of discharge into the upstream lake, the size and
781 geometry of the impoundment, and the geotechnical properties of the dam materials. The failure
782 mechanism of dams by overtopping begins once water flows over the dam through its lowest level
783 (depression). The flow of water over the downstream slope generates excessive shear stress,
784 which initiates the erosion process. According to Singh (2013) and Schmocker and Hager (2009),
785 particle mobilization and transport commence once the shear stress generated by the flow of
786 water exceeds the critical shear stress of the dam material. Wang et al. (2016b) summarize
787 empirical equations that were developed to determine the critical erosive shear stress needing to
788 be exceeded for flow-induced erosion to take effect. The rate of erosion is mainly enhanced by
789 the formation of an initial breach or notch, which further leads to the development of localized
790 shear stress that intensifies the enlargement of the initial breach. The development of the breach
791 under continuous hydraulic action is directly proportional to the rate of erosion of the dam
792 materials. This is consistent with the pioneering works of Simmler and Samet (1982), who
793 concluded that during the overtopping of a dam, erosion of the downstream slope is initiated once
794 the flow rate over the dam reaches a critical value. This value is a function of several factors,
795 which include the downstream slope angle, the degree of compaction, and grain size.

Most physical models of overtopping failure of earthfill and landslide dams have been carried out using different sized rectangular flume tanks (see Table 5) (Awal et al., 2008a; Cao et al., 2011; Hancox et al., 2005; Macchione and Sirangelo, 1988; Schmocker and Hager, 2012; Simmler and Samet, 1982). A review of the literature on physical modelling of dams shows that the most significant parameters contributing to the overtopping failure of dams are: the degree of compaction, grain size distribution, and antecedent moisture content (Cao et al., 2011; Cestero et al., 2015; Chen et al., 2015; Hunt et al., 2005; Zhang et al., 2009a). Simmler and Samet (1982) performed a series of physical model tests to investigate overtopping-induced failure of earthfill dams. The authors report that the erosion process is influenced by the geometry and type of the material composing the dam, including the reservoir volume and the location of the impervious material. Hunt et al. (2005) performed a series of large-scale (outdoor) physical experiments to evaluate the rate of breach widening in dams constructed of cohesive homogeneous materials. The authors observed that the rate of breach widening decreased with an increase in compaction water content.

Similarly, Hanson et al. (2005) investigated the mechanisms of breach formation during overtopping-induced failure of dams constructed of cohesive materials. The authors found that several physical properties of the soil (clay content, compaction energy, compaction water content, and plasticity index) had a significant effect on the peak discharge, breach widening rate and headcut migration rate. Zhang et al. (2009a) and Cestero et al. (2015) came to similar conclusions.

Table 5 Summary of selected literature on physical modelling of overtopping failure of earthfill and landslide dams.

Material(s)	Simulated Failure Mechanism(s)	Experimental Apparatus	Major Findings	Reference
Sand and gravel	Overtopping*	Rectangular flume tank	The primary erosion mechanisms of the non-cohesive homogeneous embankments comprise tractive shear and turbulence. The erosion process was mostly vertical to lateral, with an hourglass-shaped breach channel.	Coleman et al. (2002)
Sand-clay mixtures	Overtopping	Rectangular flume tank	Peak outflow has a positive correlation with breach deformation time.	Chinnarasri et al. (2004)
Cohesive homogeneous material	Overtopping*	Large-scale (out-door) flume	Observed a four-phase breaching process of cohesive embankments. Headcut migration rate and breach widening rate significantly influenced the breach parameters and the peak discharge.	Hanson et al. (2005)
Cohesive homogeneous material	Overtopping*	Large-scale (out-door) flume	Breach widening process in cohesive embankments is controlled by the compaction characteristics of the soil.	Hunt et al. (2005)
Gravel and sand-gravel mixtures	Overtopping	Rectangular flume tank	Determined the peak discharge for a prototype dam. Used similarity rule to compute peak discharge.	Dupont et al. (2007)
Soil	Overtopping	Rectangular flume tank	The development of the breach channel depends on the upstream lake discharge, riverbed morphology, and grain size distribution.	Yan et al. (2009)

Uniform noncohesive sediment	Overtopping and sliding	Rectangular flume tank	Overtopping-induced breach development occurred with an increase in inflow discharge and decrease in dam height. Sliding was dominant in dams comprised of coarse material due to an increase in dam saturation.	Schmocker and Hager (2012)
Cohesive soils	Overtopping	Large-scale (out-door) flume	The breach evolution process, including the peak discharge and the final breach geometry depends on the shear strength properties of the dam material.	Zhang et al. (2009a)
Gravel	Overtopping/headcutting/sliding	Rectangular flume tank	Observed three (3) dominant typologies of dam failure (overtopping, headcutting and a combination of instability and headcutting), which mostly depends on the dam material, downstream slope and bed slope angles.	Gregoretti et al. (2010)
Sand-clay-gravel mixtures	Overtopping*	Rectangular flume tank	Initial notch, inflow discharge and soil properties influenced the dam breaching process.	Cao et al. (2011)
Sand-silt-clay mixtures	Overtopping	Rectangular flume tank	Headcut erosion plays a significant role in the breaching process of dams comprised of cohesive materials. The rate of erosion was controlled by the percentage of clay in the soil mixtures.	(Zhu et al., 2011)
Sand and coal	Overtopping*	Rectangular flume tank	The evolution of breach channel depends on the reservoir water level, discharge and physical properties of the dam materials.	Yu et al. (2013)
Commercial sand and kaolin clay	Overtopping	Rectangular flume tank	Soil properties have a major effect on the evolution of the breach parameters and migration of the headcut.	Cestero et al. (2015)
Homogeneous soil	Overtopping	Large-scale (out-door) flume	Identified four (4) stages of overtopping-induced breaching of levees.	Kakinuma and Shimizu (2014)
Heterogeneous sand mixtures	Overtopping and sliding	Rectangular flume tank	The longevity of the dams was influenced by the riverbed morphology, hydraulic conductivity and antecedent moisture content.	Chen et al. (2015)
Beach sand	Overtopping*	Rectangular flume tank	Peak discharge varied linearly with initial dam height.	Walder et al. (2015)
Noncohesive uniform sand	Overtopping*	Rectangular flume tank	The evolution of the breach profiles depends on the inflow discharge and the downstream boundary conditions.	Rifai et al. (2017)
Fairly uniform sand	Overtopping	Rectangular flume tank	The temporal evolution of the embankments was controlled by two major processes: wave-induced sediment transport and bank collapse under drawdown condition.	Cristo et al. (2017)
Copper tailings	Overtopping	Rectangular flume tank	The evolution of the breach profile was controlled by the number of reinforcement layers in the dam.	Jing et al. (2019)
Tailings material	Overtopping	Centrifuge model test	Dam breach occurred by a combination of continuous downcutting and lateral expansion of the breach channel.	Deng et al. (2019)

Overtopping* = overtopping with an initial breach (or notch) on the dam crest

Little is known about the influence of initial breach geometry on breach development and peak discharge. According to Singh (2013), the initial breach is generally V-shaped (triangular). However, some researchers have investigated overtopping failure of dams by using rectangular or triangular notches of diverse geometries to initiate the breaching process (Rifai et al., 2017; Walder et al., 2015; Yu et al., 2013). For instance, Coleman et al. (2002) found that the primary erosion mechanisms of the dams (constructed of non-cohesive, homogeneous materials) were by tractive shear and turbulence. Cao et al. (2011) used a trapezoidal notch of varying depths to

investigate the overtopping erosion of natural dams comprised of non-cohesive sand, sand and cohesive clay, and a mixture of sand and gravel. They found that lower peak discharge occurred and that floods in the downstream arrived sooner in dams with than in those without an initial breach. However, changes in initial breach geometry, as well as in grain size distribution, make a direct comparison between these studies challenging.

3.1.2 Internal Erosion, Seepage and Piping

Internal erosion involves the movement of water through a continuous crack or defect within a compacted fill, foundation, or at the contact between a fill and a foundation. According to Dunne (1990) and Bryan and Jones (1997), the three major conditions governing the occurrence of seepage and internal erosion in soils are: (1) the evolution of pore-water pressure and its effects on the shear strength of the soil, (2) the development of sufficient drag force that entrains materials in water seeping through and out of a porous medium, resulting in liquefaction or Coulomb failure, and (3) the gradual evolution of macro-pores. The formation of a piping hole at the exit face of a dam has been attributed to hydraulic gradients high enough to cause internal instability in the soil. This development accentuates subsequent entrainment and erosion of the soil at the periphery of the piping hole, leading to its enlargement (Fell and Fry, 2013; Okeke and Wang, 2016b). The erodibility of soils is an important parameter for evaluating the stability of dams. Field and laboratory investigations conducted by Wan and Fell (2004), Hanson et al. (2010), and Chang et al. (2011) found that the erodibility coefficient was inversely proportional to the degree of compaction, in addition to other factors such as plasticity index, clay content, degree of saturation, moisture content, and dispersivity. Soil erosion parameters are commonly evaluated using the hole erosion test (HET), and the slot erosion test (SET). Benahmed and Bonelli (2012) performed HET tests on cohesive soils to determine the critical shear stress and the erodibility coefficient of the soil mixtures. The authors found that critical shear stress increased with an increase in dry density and clay content, but decreased as water content increased.

In contrast to experiments on overtopping primarily utilizing flume tanks, research of internal erosion and piping use a wider range of experimental devices, including triaxial erodimeter, rigid-wall permeameter, rectangular flume tank, stress-controlled permeameter, laboratory pinhole test, and mini-JET apparatus (Table 6). One of the most notable contributions to the understanding of internal erosion and piping failure of earthfill dams was the intermediate report of the European Working Group on Internal Erosion in Embankment Dams (EWGIE). Many of the studies from this working group (Fell and Fry, 2013) provide detailed experimental approaches and discussions on the hydraulic criteria for internal erosion and piping in dams comprised of cohesive and non-cohesive materials. The critical hydraulic gradient and the critical seepage velocity for the initiation of internal erosion and piping are two essential criteria for evaluating dam

863 stability. Laboratory evaluations of these hydraulic parameters in soils have been achieved by
864 measuring one-dimensional seepage flow using a rigid-wall cylindrical permeameter (Ke and
865 Takahashi, 2012a; Kokusho and Fujikura, 2008). A major disadvantage of using the rigid-wall
866 permeameter is the inability to evaluate the stress states of soils subjected to internal erosion.
867 Consequently, several researchers (Bendahmane et al., 2008; Ke and Takahashi, 2012b; Moffat
868 and Fannin, 2011) developed new experimental techniques that comprise either a modified rigid-
869 wall permeameter cell with axial loading systems or a stress-controlled testing apparatus (triaxial
870 erodimeter). For instance, Chang and Zhang (2013) used a stress-controlled internal erosion
871 testing apparatus to investigate the initiation mechanism of internal erosion in gap-graded soils
872 under complex stress states. The authors defined three critical hydraulic gradients based on four
873 stages of internal erosion. They concluded that the pore system of the soil influenced the initiation
874 hydraulic gradient, whereas the soil shear strength, seepage pressure, and the initial stress
875 conditions control the failure hydraulic gradient.

876

877 **Table 6** Selected literature on experimental study of dam failure by internal erosion, seepage and piping

Material(s)	Simulated Failure Mechanism(s)	Experimental Apparatus	Major Findings	Reference
Glass beads	Piping	Rigid-wall permeameter	Susceptibility of a soil-filter system to piping is mostly dependent on the grain-size ratio.	Tomlinson and Vaid (2000)
Embankment material	Internal erosion	Pinhole test and miniature resistivity array	High resistivity values correlate with the development of piping hole.	Burns et al. (2006)
Sand – Coir fiber mixtures	Seepage and piping	Rigid-wall permeameter	Piping resistance increased with an increased fiber content.	Sivakumar Babu and Vasudevan (2008)
Uniform fine poorly-graded sand	Piping	True triaxial piping test apparatus (TTPTA)	Developed a new experimental apparatus which can measure seepage flow in either vertical or horizontal directions.	Richards and Reddy (2010)
Fly ash and geofiber	Piping	Rigid-wall permeameter	Optimum improvement in piping resistance was achieved with fiber content of 0.05% and fiber length of 50 mm.	Das et al. (2009)
Loess-derived soil horizon	Piping	Laboratory pinhole test	Pipeflow discharge and sediment discharge increased with an increase in hydraulic head.	Nadal-Romero et al. (2011)
Earthfill materials	Internal erosion	Rigid-wall permeameter	Suffusion is characterized by the episodic migration of fines. The onset of internal instability is controlled by hydraulic gradient and effective stress.	Moffat et al. (2011)
Commercial sand and crushed granite	Internal erosion	Stress-controlled erosion apparatus	Proposed three critical hydraulic gradients: initiation, skeletal-deformation and failure.	Chang and Zhang (2013)
Silica sand mixtures	Internal erosion	Rigid-wall permeameter	Critical hydraulic gradients for internal erosion have a positive correlation with fines content and relative density.	Ke and Takahashi (2012a)
Cohesionless sand	Piping	Stress-controlled erosion apparatus	Resistance to piping was affected by soil gradation, particle angularity and specific gravity.	Fleshman and Rice (2014)

Dry Creek and Cow Creek soils	Internal erosion and piping	Flume box and laboratory mini-JET	The physical properties of the soil (e.g., dry density, clay content, plasticity, moisture content, etc.) have a major influence on the development of internal erosion and piping.	Fox et al. (2013)
Sand-clay and sand-gravel mixtures	Suffusion	Triaxial erodimeter	Global backward erosion which is linked with a decrease in the specimen diameter.	Marot et al. (2016)
Silica sand mixtures	Seepage and piping	Rectangular flume tank	Identified five breach evolution processes: pipe evolution, pipe enlargement, crest settlement, hydraulic fracturing, and sloughing.	Okeke and Wang (2016b)
Silica sands and gravel mixtures	Seepage	Rectangular flume tank	Critical seepage velocity for dam failure has a positive correlation with dam height, dam crest width, pore geometry, upstream discharge and antecedent moisture content.	Okeke and Wang (2016a)
Sand-gravel mixture	Piping	Rectangular flume tank	Critical hydraulic gradient for piping depends on the thickness of the overlying clay layer.	Wang et al. (2016c)
Yangtze River beach sand	Piping	Stress-controlled permeameter	The critical hydraulic gradient for piping is positively correlated with the effective mean stress and the deviatoric stress.	Liang et al. (2017)
Sand-gravel mixtures	Suffusion	Triaxial erodimeter	Concluded that the critical hydraulic gradient for suffusion is controlled by the hydraulic loading history.	Rochim et al. (2017)
Fu-Long beach sand and uniform quartz sand	Piping	Stress-controlled permeameter	Observed that the average critical hydraulic gradients (0.98 and 1.01) of the soils were close to that of Terzaghi's theoretical value.	Yang and Wang (2017)
Landslide material	Seepage and piping	Large-scale (out-door) flume	Found a linear relationship between the turbidity of the effluent seepage and settlement of the dam crest.	Wang et al. (2018a)
Silica sand mixtures	Seepage	Rectangular flume tank	Soil properties played an influential role on the breaching process of the landslide dams. Sliding was the major failure mode of the dam models under steady state seepage loading.	Xiong et al. (2018)

3.1.3. Summary and outlook

One of the major challenges of physical modelling of earthfill and landslide dam failures is the adoption of a representative scale that can reproduce the forms and processes in the model. The reliability of the results obtained from physical modelling depends on the accuracy of the model in accordance with the laws of hydraulic similarity. The three factors which are usually considered in the physical modelling of fluvial processes are: (1) the type of material (shape, particle density and diameter, and grading), (2) fluid characteristics (density and viscosity), and (3) the kind of flow (flow depth, bed slope, and acceleration due to gravity) (Young and Warburton, 1996). Future research would benefit from systematic parameter studies and from studies that systematically increase the complexity of the dam materials. Combined numerical-physical approaches (including 3D numerical models) would add valuable insights and synergies.

3.2. Numerical modelling

In recent decades, numerical-modelling-based computer simulation tools were widely developed and used to predict the behaviour of natural geological processes. Numerical modelling of landslide dams relies heavily on the input data of the landslide geometry, and internal structure and properties of landslide bodies, obtained from remote sensing, geophysical techniques, and geotechnical assessment (discussed above). Herein, we provide an overview of recent studies that use numerical models to (1) reconstruct landslide dams in 2D and 3D, (2) investigate stability criteria of landslide dams, (3) model dam-breach, and (4) model dam-breach-induced flooding.

3.2.1 Modelling landslide dam formation and predicting dam geometry

The first application of numerical modelling for landslide dam studies is simulating the formation of the dam itself. There are two aims in this approach: firstly, to model the probability of landslide dam formation, and secondly, to reconstruct the geometry of landslide dams in 2D and 3D. Most of the numerical modelling programs that can model landslide runout (Rickenmann, 2005) can be used to predict/estimate whether or not a landslide will reach a nearby river and therefore form a dam. There are diverse numerical methods and programs for this purpose (Beguería et al., 2009; Crosta et al., 2006; Crosta et al., 2010; Crosta et al., 2009; Crosta et al., 2003; Hungr, 1995; Sassa et al., 2010; Takahashi, 1988; Van Asch et al., 2014; Van Tien et al., 2018). A recent comprehensive review of landslide runout modelling by (Fan et al., 2019a) details these approaches.

Hungr (2011) examined the possibility of predicting landslide dam geometry using empirical, 2D and 3D dynamic analyses of landslide runout. Using several example cases of landslides, the authors demonstrated the applicability of dynamic motion of landslides to analyzse the formation of landslide dams. As an example, the 1987 Val Pola rockslide in Northern Italy was simulated using both 2D and 3D models by DAN and DAN3D, respectively (Hungr, 2011). Using Bingham, Voellmy, and Frictional rheologies in the 2D DAN model, the runout distance and height of the landslide dam were successfully predicted. Frictional rheology was used in the DAN3D model, and agreeable results were obtained. This study is so far the only comparative study on the use of landslide runout models to predict landslide dam geometries. Recently, Van Tien et al. (2018) analysed the formation process of two massive dams following rainfall-induced deep-seated rapid landslide failures in the Kii Peninsula of Japan using an integrated model to simulate the initiation and motion of landslides (LS-RAPID) proposed by Sassa et al. (2010).

3.2.2 Modelling and prediction of landslide dam stability

The stability of a landslide dam is unknown until breach and subsequent failure. Numerical modelling can aid in predicting these events in situations where practical engineering judgments need to be made. Another aspect of modelling landslide dam stability is analysing the stability of adjacent slopes of a landslide dam (Awal, 2008; Awal et al., 2007; Awal et al., 2008b; Awal et al., 2009). In such cases, half of the landslide dam (slope body) will lie underwater, and the remainder will lie above water level, and there are few studies modelling both the unsaturated and saturated areas of landslide dams simultaneously (Regmi et al., 2013; Regmi et al., 2010).

Chen et al. (2015) presented a dam breaching/stability model, DB-IWHR, in which the adjacent slope failure during dam breaching is considered by the simplified Bishop method. Cao et al. (2011) presented a coupled 2D mathematical model based on shallow water hydrodynamic equations to simulate landslide dam failure. The dam breaching process is simulated as the interaction of sediment transport and slope failure. The model was tested against laboratory analysis of uniform model dams. However, the models for artificial dams do not normally consider the highly heterogeneous distribution of soil materials, which leads to dynamically varied erosion rates during dam breaching, and therefore these models are not directly applicable to landslide dams.

3.2.3 Modelling the breach: erosion and overtopping of landslide dams

Numerous models are available for simulating dam breaching of embankment dams (ASCE/EWRI, 2012; Zhang et al., 2016), and the majority of numerical models available for modelling landslide dam failure processes focus on this aspect (Braun et al., 2018; Breaching, 2011; Capart, 2013; Coleman et al., 2002; Dong et al., 2011; Fan et al., 2012a, 2012b; Fread, 1988, 1996; Jinchi, 2008; Konogai and Sattar, 2012; Larocque et al., 2013; Liu et al., 2012, Peng and Zhang, 2012b; Shi et al., 2015; Wu, 2013; Zhang et al., 2019; Zhi-xian and Jun, 2008). One of the most widelt used is BREACH developed by Fread (1984, 1988, 1996, 2014). The BREACH model was used to estimate dam-breach probability of many landslide dam cases, i.e. the Hsiaolin village landslide dam (Li et al., 2011) and the Tangjiashan landslide dam (Fan et al., 2012a, Konagai and Sattar, 2012; Li et al., 2011; Liu et al., 2012; Shi et al., 2015; Zhi-xian and Jun, 2008).

Another common and widely used dam-breach model is DABA, a physically-based numerical simulation tool (Chang and Zhang, 2010). The model can consider breach evolution, sediment erosion, variation of soil properties with depth, and can predict the outflowing flood hydrograph. The seepage flow of lake water through the dam is simulated by the hydrodynamic model using the broad-crested weir flow equation. It is assumed that the cross-section of the landslide dam is trapezoidal and the overall slope is changing at a constant rate. The key parameters, including

final dam-breach dimensions, the timing of the breach and peak flow are the typical model outputs. DABA also considers the variation of soil erodibility with depth. Several studies used the DABA model to simulate dam-breach; examples include the Tangjiashan landslide dam and Xiaogangjian landslide dam cases caused by the Wenchuan earthquake, in which the results were in good agreement with observed measurements (Peng and Zhang, 2012b; Peng et al., 2014; Shi et al., 2015). Shi et al. (2015) improved the DABA model to simulate the cascading breaching of several landslide dams in a series with some modifications on the time-related inflow rates and simultaneous erosion both in breach and on dam crest. With the improved DABA model, the cascading breaching of the Tangjiashan landslide dam and two smaller downstream landslide dams were simulated, and the critical condition for the overlapping effects of cascading dam breaching were identified. Recently, Chen and Zhang (2015) developed a two-dimensional numerical model, EDDA, to simulate the erosion and deposition of soil materials during landslide dam breaching and debris flow evolution. The heterogeneity of soil properties in two dimensions can be considered in cell-based regions.

3.2.4 Dam-breach-induced flood modelling

The final process in the disaster chain of landslides is modelling dam-breach-induced flooding. For these events, directly coupled models that can model both the initial breach and resulting floods are not yet available (although there do exist coupled hazard models which can model landslides and floods within a catchment simultaneously (Awal et al., 2008b; Bout and Jetten, 2018; Bout et al., 2018a; Bout et al., 2018b). In most cases, the breach is modeled separately, and the flood is modeled using the value of peak discharge from the breach model (Fan et al., 2012a; Fan et al., 2019b). The flood modelling package the Hydrologic Engineering Center River Analysis System (HEC-RAS) is used for this purpose (Brunner, 1995; Brunner, 2002). HEC-RAS, a one-dimensional predictive model is one of the most simplest dam-break program. It only requires the terrain cross-sections perpendicular to the direction of flow for computing the average water depth and flow velocity. Several studies have also modeled the dam-breach-induced flood using traditional flood routing models (Cao et al., 2011; Capart, 2013; Davies et al., 2007; De Roo et al., 2000; Fan et al., 2012a; Fread, 1984; Fread, 1996; Glancy and Bell, 2000; Hewitt, 1982; Manville, 2001; Morche and Schmidt, 2012; Peng and Zhang, 2012b; Risley et al., 2006; Sandrp, 2018; Satofuka et al., 2010; Sun et al., 2014; Tabata, 2001; Van Der Knijff et al., 2010; Walder and O'Connor, 1997; Xu et al., 2012; Yan et al., 2009; Zhu et al., 2012).

3.2.5 Numerical modelling of other landslide dam-related phenomena

In addition to the landslide runout, dam-stability, dam-breach, and dam-breach-induced flood modelling, other geomorphic processes exist where numerical modelling can be applied. Modelling the impact of landslide into a landslide dam reservoir and impulsive surges and their effects on dam stability are also common. This kind of modelling is similar to river-water tsunami

993 simulation, and few studies report their significance and processes for landslide dam studies
994 (Assier-Rzadkieaicz et al., 2000; Hermanns et al., 2013; Ward and Day, 2011). Studies that deal
995 with river water tsunami in an artificially dammed river are more common than landslide-dammed
996 rivers (Bardet et al., 2003). Different types of modelling are performed for debris flows induced
997 by a landslide dam breach (Chen et al., 2004; Cui et al., 2013).

998 ### *3.2.6 Summary and outlook*

999 Each numerical model has particular advantages and disadvantages. Starting from the landslide
1000 runout and resulting deposit/dam thickness (Figure 8) to the dam-breach-induced flood modelling,
1001 the scarcities in the input parameters for the numerical models are the primary disadvantage
1002 where material characterization is paramount. Both, the strength and the limitation of numerical
1003 models arise from the availability of data, such as rock mass strength parameters, runout
1004 parameters, landslide dam material parameters etc. If sufficient characterization of the soil/rock
1005 or dam parameters is available, all the numerical methods summarized in Table 7 can provide
1006 meaningful results.

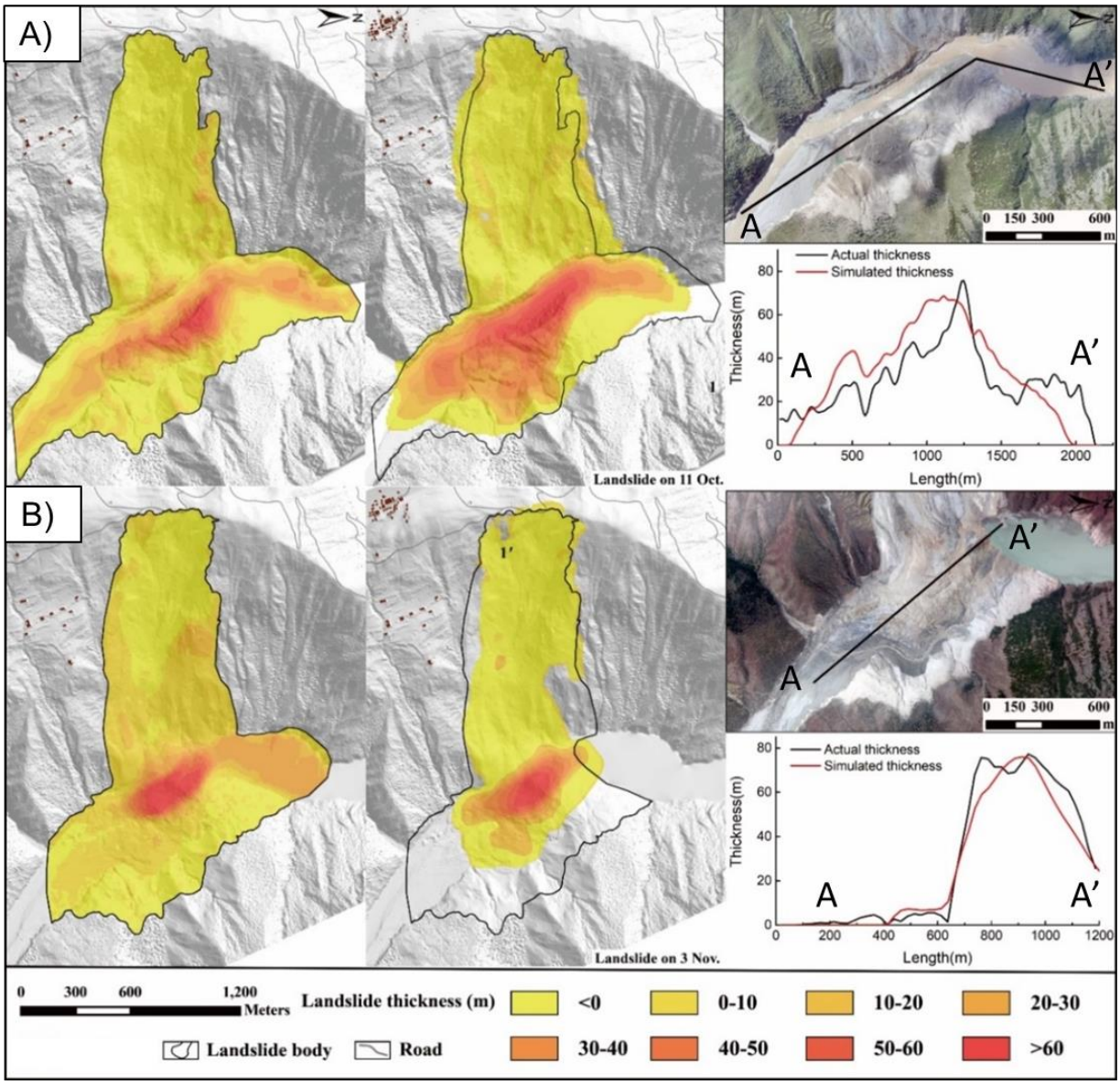

Figure 8 Example of simulating landslide dam geometry (thickness) using an integrated numerical simulation approach (modified from Fan et al. 2019c): comparisons between measured landslide thickness and numerically simulated landslide thickness for Baige landslide dams occurred on (A) October 11 and (B) November 3. Left: the measured landslide thickness; middle: predicted landslide thickness; and right: comparison of landslide accumulation thickness along the Jinsha River

Table 7 Compilation of different numerical modelling approaches used in landslide dam studies

Purpose	Methods	Details	Advantages	Disadvantages
Landslide runout	Continuum	Models simulate the moving mass as a two-dimensional or sometimes three-dimensional approximation in which the material is assumed incompressible, and the properties and kinematics are depth-averaged following the Saint-Venant approach. Several models have been proposed, and implemented in various software environments. See, for instance, the works of van Asch et al.,	Runout process simulated through physically-based laws. The shape of the deposit can be simulated.	Generally, not specific to landslide dam studies; usually ignore the multiphasic nature of the moving mass and the water body of the river; only the most advanced models can account for the

		(2014),Beguería et al., (2009), Hungr, (1995), Takahashi et al., (1992), Sassa et al. 2010, Van Tien et al. (2018), Crosta et al. (2003) and their proposed models.		landslide-bed and river interactions.
	Discontinuum	These approaches (both 2D and 3D) simulate the landslide mass as an assembly of (such as the discrete element method DEM, and the DDA, discontinuous deformation analysis). Several models have been proposed. See, e.g., Cundall and Strack, (1979), Liu et al. (2013), Poisel et al., (2008). More references are given in the text.	Runout process simulated through physically-based laws treating the landslide materials as individual shapes of masses with distinguished properties.	Generally, not specific to landslide dam studies; several (microscopic) model parameters without clear physical meaning; calibration of a large number of parameters are required; only the most advanced models can account for solid-fluid coupling.
Landslide deposits / dam geometry	Continuum	Both two-dimensional and three-dimensional models, i.e. DAN and DAN3D, respectively (Hungr, 2011), can be used. Using Bingham, Voellmy, and Frictional rheologies are possible.	Runout process simulated through physically-based laws similar to the landslide runout models. The only model of this kind.	Usually, ignore the multiphasic nature of the moving mass and the water body of the river; only the most advanced models can account for the landslide-bed and river interactions.
	Discontinuum	So far, no studies have attempted.	-	-
Dam-stability	Continuum	Very few studies are reporting a thorough geotechnical investigation of landslide dam stability.	Simple and explicit.	Does not account for breaching and erosion mechanisms.
	Discontinuum	So far, no studies have attempted.	-	-
Dam-breach	Continuum	Few highly cited numerical modelling approaches to model landslide dam breach	Mostly combined with empirical methods. Erodibility can be defined.	Heterogeneity of the landslide dam materials is not accounted.
	Discontinuum	So far no studies have attempted	-	-
Dam-breach flood	Continuum	HEC-RAS, Mikeflood, iRIC etc.	Simple, explicit and diverse models.	Does not account for breaching mechanisms.

Some of the reviewed models for dam-breach (e.g. BREACH) were used to simulate the breach of both artificial and landslide dams. However, Peng and Zhang (2012) argue that the direct application of the breaching models developed for embankment dams to landslide dams is inappropriate since the two types of dams are different in dam geometry and structure, and possess different material properties and implement different flood control measures. The authors note that the breach size and the peak outflow rate of the landslide dams would be overestimated, and the corresponding breaching time would be largely underestimated.

Despite some important advances in modelling landslide dam breaching, some problems remain unsolved:

(1) The heterogeneity of soil property distribution is not sufficiently considered. Landslide dams form by the quick deposition of landslides. A three-dimensional dam model incorporating spatial heterogeneity is needed to effectively simulate the complex breaching process of landslide dams.

(2) Both erosion and deposition need to be considered. Eroded soil and rock materials deposited regularly along the river close to landslide dams can have a large influence the hydrogeological environment. Whilst much attention is given to erosion processes, similar importance to deposition processes should also be given.

(3) The influence of seepage and internal erosion on erodibility of dam materials. Loss of fines due to internal erosion and variations in water content due to seepage have a significant effect on permeability and erodibility of dam materials. Consideration of these effects are required.

(4) The influence of boulders on the breaching of landslide dams. Boulders are frequently observed on top of, and sometimes inside of, landslide dams. Modelling the complex interactions between water flows at different scales between small soil particles and large boulder remains an outstanding challenge.

Landsliding into a river creates a disaster chain inducing individual hazards, i.e. dam-breach, river-tsunami, dam-breach-induced floods, and debris flows. Present models consider these hazards separately and can only model them as individual hazards and until recently, the idea of numerically modelling an entire disaster chain has not been considered. Studies aiming to numerically model entire landslide-induced disaster chains are gaining traction in recent years (Bout and Jetten, 2018; Bout et al., 2018a; Bout et al., 2018b; Fan et al., 2019c). A single numerical model to model the entire disaster chain is still an outstanding goal of future numerical modelling approaches.

4. Discussion

The formation of potentially unstable landslide dams is part of a hazard cascade starting with the landslide itself, flooding upstream of the blockage, and potentially catastrophic outburst floods downstream. This paper is a contribution towards understanding these phenomena by providing a comprehensive review of the state-of-the-art in dam investigation and analyses—ranging from remote sensing, dating, geophysical methods, sedimentology and geotechnical properties to laboratory analogue and numerical modeling. We conclude our review with examples of combined applications of the presented methods.

4.1 Dam dimensions, distributions, and timelines (*remote sensing, geophysics, dating, sedimentology*)

Advances in remote sensing technology and increased commercial availability of their products has lead to more widespread identification of landslide dams in recent decades. These provide a good basis for robust statistical analyses of dam distribution and dimensions. The first inventory studies utilizing remote sensing, i.e. historical aerial photographs were conducted by Korup (2005a, b). Since then, satellite image interpretations were used for landslide dam recognition and for the creation of inventories (Tacconi Stefanelli et al., 2015, 2016, 2018). Often, dam inventories are created through visual interpretation of landslide source and deposition zones by comparing pre- and post-triggering event false-color composites or panchromatic images. For example, Fan et al. (2012b) created an inventory comprising 828 landslide dams induced by the 2008 Wenchuan earthquake in China by visual interpretation of satellite and aerial images, including ASTER, ALOS AVNIR-2, ALOS PRISM, Cartosat-1, SPOT-5, and IKONOS data. Investigations on the regional scale typically involve inventory mapping for spatio-temporal studies. These maps can be event-based, which provide the most accurate data in terms of total number of dams identified, good control on geomorphic parameters (such as dam volume from pre- and post-event DEMs), and exact knowledge on the time of dam formation. Very recently, a worldwide inventory and database of 410 landslide dams >1 million m^3 in volume that were formed since 1900 since was compiled by Fan et al. (2020a).

Adding geophysical studies and dating campaigns to the outcome of remote sensing studies provides information on, e.g. (i) more exact dam dimensions in 3D, (ii) how often a region or a single site has been affected by river-damming landslides or (iii) whether multiple catastrophic failures with downstream flooding of the same dam have occurred and should be considered in hazard analyses. For example, successful reconstruction of the dimensions of still existing dams were achieved using geophysical methods; e.g. ERT, VES, MASW and SRT surveys at the Scanno Lake landslide dam (Italy; Bianchi-Fasani et al., 2011). At the Lauvitel landslide dam in France, ERT surveys revealed that the dam was part of a much larger rockslide deposit, emplaced over successively smaller rockslide events (Delunel et al., 2010) potentially signifying repeated damming. The Las Conchas valley in the Argentinian Andes (NW Argentina) was blocked several times by deposits from the same slope, with two major events dated to ~13.5 ka and ~4.8 ka BP, coinciding with local wet periods. ^{10}Be surface exposure dating of both the rock avalanche deposits and the scarps, and correlation of the obtained ages with the stratigraphy and chronology of adjacent dammed-lake deposits revealed this relationship (Hermanns et al., 2004). The study demonstrates that even dams dating back several thousands of years might be susceptible to failure by overtopping, driven by emplacement of landslide bodies into the dammed

lakes, and that other than seismicity, climatic factors can also control the failure of rock avalanche dams in arid regions.

The longevity of a landslide dam, and its respective lake, is best assessed using multi-method dating to yield the most reliable time constraints, although this approach is still uncommon, mainly because dating is limited by the availability of appropriate geological materials and datable landslide features (Lang et al., 1999). Consequently, relatively few successful multi-dating campaigns exist (e.g. Dong et al., 2014; Ostermann et al., 2017; Prager et al., 2009). One example, the Tschirgant rock avalanche deposit in Austria, was initially dated using a suit of ^{14}C ages and interpreted as being the result of two successive failures at ~3.75 and 3.15 ka (Patzelt, 2012). Adding ^{36}Cl and Th/U dating narrowed the possible time interval of the rock avalanche emplacement to 3.4 – 2.4 ka BP (Ostermann et al., 2017), with a most probable single-event age of 3.01±0.1 ka BP. Later IRSL (Infrared Stimulated Luminescence) dating of feldspar in uppermost lacustrine deposits upstream of the dam site returned an age of 2.31±0.13 ka, suggesting that the landslide-dammed lake existed for a few hundred years (Dufresne et al., 2018). Sedimentological and morphological analysis of the up- and downstream landscape can shed light on whether lake drainage was gradual or catastrophic.

4.2 Dam structures and properties (geophysics, sedimentology, laboratory analogue modeling)

The internal structure and composition of landslide dams is complex compared to relatively homogeneous engineered embankment dams. In these artificial dams, the hydrogeological (e.g. seepage flow and fluid pressure) and mechanical characteristics (strength and deformability) of the materials used, as well as the hydrological conditions (e.g. maximum flood level) are well-constrained, allowing for reliable stability prediction (factor of safety) and lifetime performance of the dam in the design stage. This is commonly assessed using analytical and numerical coupled hydro-mechanical methods. By contrast, landslide dams are typically highly heterogeneous in their internal composition—information that is unknown at formation.

Determining the internal structure of landslide dams, however, plays a key part in the assessment, planning and design of remedial engineering works. To this end, the study of (ancient) breached dams provides insights into the relationships between breach location, dam morphology and properties, albeit in their final, perhaps compacted and altered form, and therefore with a bias toward stable dams. Observations of facies-dependent incision behavior, like those of Wassmer et al. (2004), should be viewed in combination with descriptions of the overall debris distribution

(i.e., location of the lowest passages and freeboard; e.g. Usoi, (Hanisch and Söder, 2000)), the relationship between surface morphology and facies (e.g. Dunning et al., 2005) as well as lithological distribution. Debris distribution both, along-valley (Dunning et al., 2005) and across-valley (e.g. Korchevskiy et al., 2011; Strom, 1996; Strom and Korup, 2006), warrants adjustments in dam classifications since it determines the location of lowest freeboard. Likewise, lithological distribution in combination with facies distribution determines erodibility of the dam material. For example, at the giant Köfels and Flims rockslides, the initial spillways were abandoned upon encounter of a larger boulder (Dufresne et al., 2019), marking the transition to a more erosion-resistant facies (Wassmer et al., 2004).

Such transitions are expected in dams formed by rock avalanches or rockslides since they typically form a three-facies, layered deposit with an upper coarse carapace above a heterogeneous body, underlain by a (mixed) basal facies (Dunning and Armitage, 2012, Weidinger et al., 2014, Dufresne et al., 2016 for reviews). A few case studies highlight this; Crosta et al. (2010) collected SRT measurements at the Val Pola rock avalanche dam in Italy identifying three layers in the landslide dam, and providing the shear-wave velocities to estimate material density. Plaza et al. (2011) described how SRT surveys identified horizontal layers in the La Josefina landslide dam, Ecuador, later confirmed during excavations. Wang et al. (2014b) used MT soundings to determine the internal structure of the 781 - 126 ka Zhanggu landslide dam in Sichuan province, China, identifying a e 300-m-deep slip surface. Torgoev et al. (2013) used ERT and H/V measurements on the 'ancient' Ak-kul landslide dam in Kyrgyz Republic to identify zones of saturation and potential weakness within the dam structure (Figure 9). Wang et al. (2013) used MASW surveys and identified low-velocity zones in landslide dam layers. By combining MASW and MTM methods, Wang et al. (2016a) showed that the internal structure of a landslide dam was relatively undisturbed, but that weathered materials had low resistance to potential dam overtopping.

Hanisch and Söder (2000) hint at a change in dam properties about 140 m below the level of Lake Sarez behind the Usoi rockslide dam in Tajikistan (see also Strom, 2006; Strom, 2014). The occurrence of springs at this level indicates that the lower part of the dam has very low permeability, whereas the upper part is highly permeable, maintaining an average seepage discharge of 45 m^3/s (Hanisch and Söder, 2000). Data of 1D seismic structure determined by VSP surveys (from survey in 1975-1977, summarised by Papyrin, 2011), partly assisted the assessment by Ischuk (2011) that the Usoi dam is stable due to its large size.

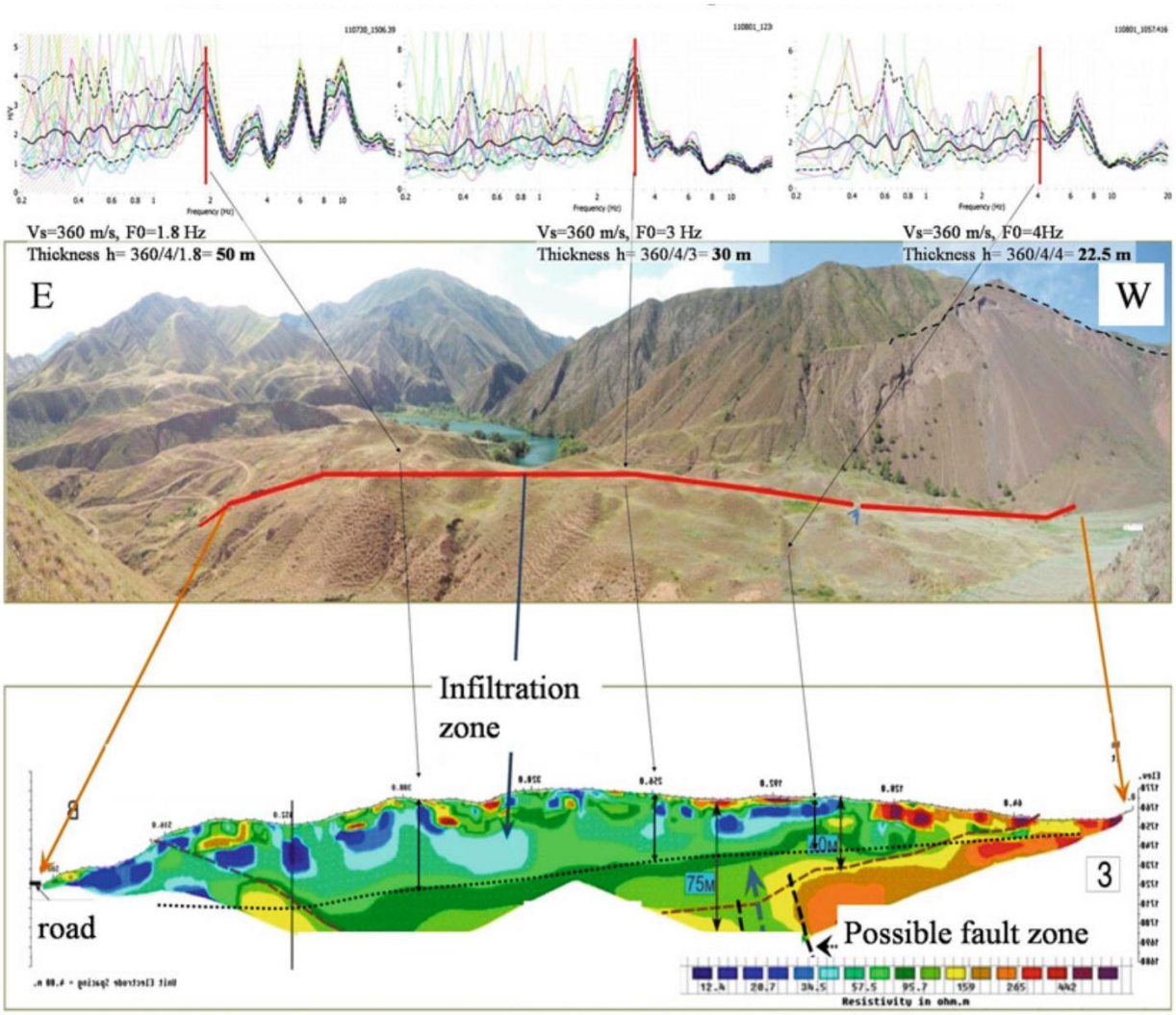

Figure 9 The results from an integrated H/V and ERT survey at the Ak-kul landslide dam in the Kyrgyz Republic. The zone of lower resistivity, indicating potentially saturated areas, combined with low resonance frequencies and high seismic impedance, indicating zones of weak material, suggests the landslide dam may be at risk of failure in the future. Reproduced from Torgoev et al. (2013).

4.3 Assessment and monitoring (numerical modeling, geophysics, geotechnical properties)

Estimating whether a given landslide can form a dam can be based on empirical data and the formulation of thresholds or indices in bi- or multi-variate analyses (cf. Fan et al., 2020 for review) or assessed by numerical modelling. Hungr (2011) examined the possibility of predicting landslide dam geometry using empirical, as well as 2D and 3D dynamic analyses of landslide runout. Based on several example cases, the authors demonstrated the applicability of dynamic motion of landslides to analyzse the formation of landslide dams. As an example, the 1987 Val Pola

rockslide in Northern Italy was simulated using both 2D and 3D models, DAN and DAN3D, respectively (Hungr, 2011). Using Bingham, Voellmy, and Frictional rheologies in the 2D DAN model, the runout distance and height of the landslide dam were successfully predicted. Frictional rheology was used in the DAN3D model, and agreeable results were obtained. This study is so far the only comparative study on the use of landslide runout models to predict landslide dam geometries. Recently, Van Tien et al. (2018) analysed the formation process of two massive dams following rainfall-induced deep-seated rapid landslide failures in the Kii Peninsula of Japan using an integrated model to simulate the initiation and motion of landslides (LS-RAPID) proposed by Sassa et al. (2010).

Very few numerical models account for stability assessment of adjacent slopes of the landslide dams (Awal, 2008; Awal et al., 2007; Awal et al., 2008b; Awal et al., 2008c; Awal et al., 2009; Awal et al., 2011; Chen et al., 2015b; Regmi et al., 2013; Regmi et al., 2010; Wang et al., 2016b). Wang et al. (2016b) are one of the studies which successfully modelled the lateral enlargement during breach for the Yigong landslide dam using slope stability analysis based on circular slip surface. Further, for landslide dam breach analysis, each numerical model i.e, BREACH, DABA, EDDA, EMBREA has particular advantages and disadvantages. Though all the above models have been used to successfully predict the dam breach of major landslide dams—i.e. the Tangjiashan landslide dam, the Xiaogangjian landslide dam, Hsiaolin village landslide dam—all the models have their limitations inherent to the modelling mechanisms and input data (Dong et al., 2011a; Li et al., 2011; Liu et al., 2012; Liu et al., 2009; Shi et al., 2015; Wang et al., 2015). The same applies to models predicting landslide dam-breach-induced flooding (Dai et al., 2005; Davies et al., 2007; Fread, 1984; Morche and Schmidt, 2012; Sun et al., 2014; Xu et al., 2012; Zhu et al., 2012). In addition to the general limitations inherent to the model and data, most of the previous studies on landslides, landslide dams, and dam-breach-induced floods mostly focused only on a single type of geomorphic hazard, though in reality all these hazards are inter-connected. The perspective was that the interactions between the different types of hazards are quasi-independent and hence were ignored (Yutao and Shengxie, 2009). To date, Fan et al. (2019c) of the 2018 Baige landslide is the only study that successfully modelled the landslide-induced hazardcascade, i.e. landslide runout, river damming, dam-breach, and dam-breach-induced flooding as a single continuum event. The key advantage of such a modelling approach is the adaptability for diverse input boundary conditions, allowing the interlinking of one numerical model with another, which allowed the successful stability assessment, monitoring and early warning of future hazards during the 2018 Baige landslide event (Fan et al., 2019b; Fan et al., 2019c).

Several geophysical campaigns have monitored seemingly stable, non-remediated landslide dams. Wang et al. (2018a) used combined MTM and SP monitoring to identify seepage zones in landslide dams in Japan and the Kyrgyz Republic, identifying zones of internal piping. Wang et

al. (2018b) also conducted SP monitoring on large-scale artificial dams, and identified artificially induced zones of fluid seepage. Niazi et al. (2010) used ERT to both characterize and monitor the structure of the Hattia Bala landslide dam in Kashmir, identifying low resistivity zones indicating lower density, high permeability material prone to seepage. Decreasing resistivity in these zones over time indicated increased seepage through the landslide dam.

Landslide dam hazard assessment and mitigation comprises two approaches: (1) rapid engineering measures to prevent catastrophic failure, and (2) engineering measures to improve long-term stability. The technique adopted in either of the two approaches could be geotechnical, geological, hydrological, and geophysical, or preferably a combination of two or more of these methods. Indeed, geophysical methods, such as multichannel analysis of surface waves (MASW), microtremor survey, and self-potential (SP) methods have proven to be two important methods that could be used to perform rapid hazard assessment in newly formed landslide dams (see Wang et al., 2013; Wang et al., 2018b). The fact that newly formed landslide dams are poorly compacted, heterogeneous and highly susceptible to failure justifies the use of a range of engineering geophysical and geotechnical methods to characterise their internal structure and material properties. Interestingly, recent research by Wang et al. (2018b) in select landslide dams in Japan and Kyrgyzstan observed that zones of low phase velocity profiles correspond to the areas that are susceptible to internal erosion, given their low degree of compaction, and thus their high erodibility coefficients. The results obtained from the application of these geophysical and geotechnical investigations would definitely aid in the design and construction of resilient engineering infrastructure against the occurrence of outburst floods from the collapse of landslide dams. Furthermore, the results are also applicable in the development of early warning systems against outburst floods.

Therefore, feasible mitigative measures against landslide dam failures and outburst floods from dam failures require the application of all the preventive actions enumerated by Schuster and Evans (2011) and methods in this paper.

Acknowledgements

This research is financially supported by the Funds for Creative Research Groups of China (Grant No. 41521002), the National Science Fund for Outstanding Young Scholars of China (Grant No. 41622206), the Funds for the State Key Laboratory of Geo-hazard Prevention and Geoenvironment Protection Independent Research Project (SKLGP2019Z002), National Key R&D Program of China (No. 2017YFC1501002). Tomáš Pánek acknowledges kind support from Czech Science Foundation project no. 19-16013S. Sincere thanks to the editor, Prof. Chris Fielding, for the kind acceptance of our proposal and encouragement to submit this research

work. Many thanks also go to editorial assistant Mr Tim Horscroft for the kind support. Lanxin Dai is thanked for improving Figures 1 and 3.

Reference

Abdrakhmatov, K. and Strom, A., 2006. Dissected rockslide and rock avalanche deposits; Tien Shan, Kyrgyzstan, Landslides from Massive Rock Slope Failure. Springer, pp. 551-570.

Abele, G., 1974. Bergsturze in den Alpen. Ihre Verbreitung, Morphologie und Folgeerscheinungen. Wiss. Alpenvereinshefte, 25.

Adams, J., 1981. Earthquake-dammed lakes in New Zealand. Geology, 9(5): 215-219.

Adushkin, V.V., 2006. Mobility of rock avalanches triggered by underground nuclear explosions, Landslides from Massive Rock Slope Failure. Springer, pp. 267–284.

Adushkin, V.V., 2011. Russian experience with blast-fill Dam construction, Natural and artificial rockslide dams. Springer, pp. 595–616.

Assier-Rzadkieaicz, S., Heinrich, P., Sabatier, P.C., Savoye, B. and Bourillet, J.F., 2000. Numerical modelling of a landslide-generated tsunami: the 1979 Nice event. Pure and Applied Geophysics, 157(10): 1707-1727.

Avtar, R., Yunus, A.P., Kraines, S. and Yamamuro, M., 2015. Evaluation of DEM generation based on Interferometric SAR using TanDEM-X data in Tokyo. Physics and Chemistry of the Earth, Parts A/B/C, 83: 166-177.

Awal, R., 2008. Study on landslide dam failure due to sliding and overtopping.

Awal, R., Nakagawa, H., Baba, Y., Sharma, R.H. and Ito, N., 2007. Study on landslide dam failure by sliding.

Awal, R., Nakagawa, H., Kawaike, K., Baba, Y. and Zhang, H., 2008. An integrated approach to predict outflow hydrograph due to landslide dam failure by overtopping and sliding. Proceedings of Hydraulic Enginnering, 52: 151–156.

Awal, R., Nakagawa, H., Kawaike, K., Baba, Y. and Zhang, H., 2009. Three dimensional transient seepage and slope stability analysis of landslide dam.

Balescu, S., Ritz, J.-F., Lamothe, M., Auclair, M. and Todbileg, M., 2007. Luminescence dating of a gigantic palaeolandslide in the Gobi-Altay mountains, Mongolia. Quaternary Geochronology, 2(1-4): 290–295.

Balica, S. and Wright, N.G., 2010. Reducing the complexity of the flood vulnerability index. Environmental Hazards, 9(4): 321–339.

Ballantyne, C.K., Stone, J.O. and Fifield, L.K., 1998. Cosmogenic Cl-36 dating of postglacial landsliding at the Storr, Isle of Skye, Scotland. The Holocene, 8(3): 347–351.

Bao, Y., Zhai, S., Chen, J., Xu, P., Sun, X., Zhan, J., Zhang, W. and Zhou, X., 2020. The evolution of the Samaoding paleolandslide river blocking event at the upstream reaches of the Jinsha River, Tibetan Plateau. Geomorphology, 351: 106970.

Barazzetti, L., Brumana, R., Oreni, D., Previtali, M. and Roncoroni, F., 2014. True-orthophoto generation from UAV images: implementation of a combined photogrammetric and computer vision approach. ISPRS Annals of Photogrammetry, Remote Sensing & Spatial Information Sciences, 2(5).

Bardet, J.P., Synolakis, C.E., Davies, H.L., Imamura, F. and Okal, E.A., 2003. Landslide tsunamis: Recent findings and research directions, Landslide tsunamis: recent findings and research directions. Springer, pp. 1793-1809.

Beetham, R.D., McSaveney, M.J. and Read, S.A.L., 2002. Four extremely large landslides in New Zealand. Landslides: 97–102.

Beguería, S., Van Asch, T.W.J., Malet, J.P. and Gröndahl, S., 2009. A GIS-based numerical model for simulating the kinematics of mud and debris flows over complex terrain. Natural Hazards and Earth System Sciences, 9(6): 1897-1909.

Belousov, T.P., 1994. On estimation of the recurrence period of Strong earthquakes in the Central Tien Shan. Journal of Earthquake prediction research, 3: 226–236.
Benahmed, N. and Bonelli, S., 2012. Investigating concentrated leak erosion behaviour of cohesive soils by performing hole erosion tests. European Journal of Environmental and Civil Engineering, 16(1): 43–58.
Bendahmane, F., Marot, D. and Alexis, A., 2008. Experimental parametric study of suffusion and backward erosion. Journal of geotechnical and geoenvironmental engineering, 134(1): 57–67.
Bianchi-Fasani, G., Esposito, C., Petitta, M., Scarascia-Mugnozza, G., Barbieri, M., Cardarelli, E., Cercato, M. and Di Filippo, G., 2011. The Importance of Geological Models in Understanding and Predicting the Life Span of Rockslide Dams: The Case of Scanno Lake, Central Italy, Natural and Artificial Rockslide Dams. Springer, pp. 323–345.
Bonnard, C., 2006. Technical and human aspects of historic rockslide dammed lakes and landslide dam breaches. Italian Journal of Engineering Geology and Environment(Special Issue 1): 21-30.
Bout, B. and Jetten, V.G., 2018. The validity of flow approximations when simulating catchment-integrated flash floods. Journal of hydrology, 556: 674-688.
Bout, B., Lombardo, L., van Westen, C. and Jetten, V., 2018a. A new model for integrated multi-hazard modelling of flooding and mass movements in mountainous watersheds, pp. 9172.
Bout, B., Lombardo, L., van Westen, C.J. and Jetten, V.G., 2018b. Integration of two-phase solid fluid equations in a catchment model for flashfloods, debris flows and shallow slope failures. Environmental Modelling & Software, 105: 1-16.
Brown, C.A. and Graham, W.J., 1988. Assessing the threat of life from dam failure. Journal of the American Water Resources Association, 24(6): 1303–1309.
Brunner, G.W., 1995. HEC-RAS River Analysis System. Hydraulic Reference Manual. Version 1.0, Hydrologic Engineering Center Davis CA.
Brunner, G.W., 2002. Hec-ras (river analysis system). ASCE, pp. 3782-3787.
Bryan, R.B. and Jones, J.A.A., 1997. The significance of soil piping processes: inventory and prospect. Geomorphology, 20(3-4): 209–218 https://doi.org/10.1016%2Fs0169-555x%2897%2900024-x.
Burns, B., Barker, R. and Ghataora, G.S., 2006. Investigating internal erosion using a miniature resistivity array. NDT & E International, 39(2): 169–174 https://doi.org/10.1016%2Fj.ndteint.2004.12.009.
Cagniard, L., 1953. Basic theory of the magneto-telluric method of gephysical prospecting. Geophysics, 18(3): 605 – 635 https://doi.org/10.1190%2F1.1437915.
Cao, Z., Yue, Z. and Pender, G., 2011. Landslide dam failure and flood hydraulics. Part II: coupled mathematical modelling. Natural Hazards, 59(2): 1021-1045.
Capart, H., 2013. Analytical solutions for gradual dam breaching and downstream river flooding. Water Resources Research, 49(4): 1968-1987.
Casagli, N., Cigna, F., Bianchini, S., Hölbling, D., Füreder, P., Righini, G., Del Conte, S., Friedl, B., Schneiderbauer, S. and Iasio, C., 2016. Landslide mapping and monitoring by using radar and optical remote sensing: Examples from the EC-FP7 project SAFER. Remote sensing applications: society and environment, 4: 92-108.
Castellaro, S., Mulargia, F. and Bianconi, L., 2005. Passive seismic stratigraphy: a new efficient, fast and economic technique. Geologia tecnica e ambientale, 3: 76-102.
Castleton, J.J., Moore, J.R., Aaron, J., Christl, M. and Ivy-Ochs, S., 2016. Dynamics and legacy of 4.8 ka rock avalanche that dammed Zion Canyon, Utah, USA. GSA Today, 26(06): 4–9 https://doi.org/10.1130%2Fgsatg269a.1.
Cestero, J.A.F., Imran, J. and Chaudhry, M.H., 2015. Experimental Investigation of the Effects of Soil Properties on Levee Breach by Overtopping. Journal of Hydraulic Engineering, 141(4): 04014085 https://doi.org/10.1061%2F%28asce%29hy.1943-7900.0000964.
Chambers, J.E., Kuras, O., Meldrum, P.I., Ogilvy, R.D. and Hollands, J., 2006. Electrical resistivity tomography applied to geologic, hydrogeologic, and engineering investigations at a former waste-disposal site. Geophysics, 71(6): B231–B239 https://doi.org/10.1190%2F1.2360184.

Chang, D.S. and Zhang, L.M., 2013. Critical Hydraulic Gradients of Internal Erosion under Complex Stress States. Journal of Geotechnical and Geoenvironmental Engineering, 139(9): 1454–1467 https://doi.org/10.1061%2F%28asce%29gt.1943-5606.0000871.

Chang, D.S., Zhang, L.M., Xu, Y. and Huang, R.Q., 2011. Field testing of erodibility of two landslide dams triggered by the 12 May Wenchuan earthquake. Landslides, 8(3): 321–332 https://doi.org/10.1007%2Fs10346-011-0256-x.

Charrière, M., Humair, F., Froese, C., Jaboyedoff, M., Pedrazzini, A. and Longchamp, C., 2015. From the source area to the deposit: Collapse, fragmentation, and propagation of the Frank Slide. Geological Society of America Bulletin: B31243.1 https://doi.org/10.1130%2Fb31243.1.

Chen, C.-Y., Chen, T.-C., Yu, F.-C. and Hung, F.-Y., 2004. A landslide dam breach induced debris flow–a case study on downstream hazard areas delineation. Environmental Geology, 47(1): 91-101.

Chen, J., Zhou, W., Cui, Z., Li, W., Wu, S. and Ma, J., 2018. Formation process of a large paleolandslide-dammed lake at Xuelongnang in the upper Jinsha River, SE Tibetan Plateau: constraints from OSL and 14C dating. Landslides, 15(12): 2399–2412 https://doi.org/10.1007%2Fs10346-018-1056-3.

Chen, S.-C., Lin, T.-W. and Chen, C.-Y., 2015. Modeling of natural dam failure modes and downstream riverbed morphological changes with different dam materials in a flume test. Engineering Geology, 188: 148–158 https://doi.org/10.1016%2Fj.enggeo.2015.01.016.

Chen, S.C., Hsu, C.L., Wu, T.Y., Chou, H.T. and Cui, P., 2011a. Landslide dams induced by typhoon Morakot and risk assessment, pp. 653–660.

Chen, X., Cui, P., You, Y., Cheng, Z., Khan, A., Ye, C. and Zhang, S., 2016. Dam-break risk analysis of the Attabad landslide dam in Pakistan and emergency countermeasures. Landslides, 14(2): 675–683 https://doi.org/10.1007%2Fs10346-016-0721-7.

Chen, X.Q., Zhao, W.Y., Gao, Q., Jia, S.T. and Zhu, X.H., 2011b. Experimental research on effect of man-made structure controlling dam-break flood. Chinese Journal of Mountain Science, 29(2): 217–225.

Chinnarasri, C., Jirakitlerd, S. and Wongwises, S., 2004. Embankment dam breach and its outflow characteristics. Civil Engineering and Environmental Systems, 21(4): 247–264 https://doi.org/10.1080%2F10286600412331328622.

Colangelo, G., Lapenna, V., Perrone, A., Piscitelli, S. and Telesca, L., 2006. 2D self-potential tomographies for studying groundwater flows in the Varco d'Izzo landslide (Basilicata, southern Italy). Engineering Geology, 88(3-4): 274–286.

Coleman, S.E., Andrews, D.P. and Webby, M.G., 2002. Overtopping breaching of noncohesive homogeneous embankments. Journal of Hydraulic Engineering, 128(9): 829-838.

Colesanti, C., De Zan, F., Ferretti, A., Prati, C. and Rocca, F., 2003. Generation of DEM with sub-metric vertical accuracy from 30'ERS-ENVISAT pairs, Proc. of FRINGE 2003 Workshop, Frascati, Italy, pp. 1–5.

Corsini, A., Cervi, F., Daehne, A., Ronchetti, F. and Borgatti, L., 2009. Coupling geomorphic field observation and LIDAR derivatives to map complex landslides, Landslides processes—from geomorphologic mapping to dynamic modeling, proceedings of the landslide processes conference, pp. 6–7.

Costa, J.E. and Schuster, R.L., 1988. The formation and failure of natural dams. Geological Society of America Bulletin, 100(7): 1054–1068.

Crist, E.P., 1985. A TM Tasseled Cap equivalent transformation for reflectance factor data. Remote Sensing of Environment, 17(3): 301–306 https://doi.org/10.1016%2F0034-4257%2885%2990102-6.

Cristo, C.D., Evangelista, S., Greco, M., Iervolino, M., Leopardi, A. and Vacca, A., 2017. Dam-break waves over an erodible embankment: experiments and simulations. Journal of Hydraulic Research, 56(2): 196–210 https://doi.org/10.1080%2F00221686.2017.1313322.

Crosetto, M., Crippa, B. and Biescas, E., 2005. Early detection and in-depth analysis of deformation phenomena by radar interferometry. Engineering Geology, 79(1-2): 81–91 https://doi.org/10.1016%2Fj.enggeo.2004.10.016.

1397 Crosta, G.B., Frattini, P., Fusi, N. and Sosio, R., 2006. Formation, characterization and modelling
1398 of the 1987 Val Pola rock-avalanche dam (Italy). Italian J. Eng. Geol. Envir., Special Issue I:
1399 145-150.
1400 Crosta, G.B., Frattini, P., Fusi, N. and Sosio, R., 2010. Formation, Characterisation and Modeling
1401 of the Val Pola Rock-Avalanche Dam (Italy), Natural and Artificial Rockslide Dams. Springer
1402 Berlin Heidelberg, pp. 347–368 https://doi.org/10.1007%2F978-3-642-04764-0_12.
1403 Crosta, G.B., Imposimato, S. and Roddeman, D., 2009. Numerical modelling of
1404 entrainment/deposition in rock and debris-avalanches. Engineering Geology, 109(1): 135-145.
1405 Crosta, G.B., Imposimato, S. and Roddeman, D.G., 2003. Numerical modelling of large landslides
1406 stability and runout. Nat. Hazards Earth Syst. Sci., 3(6): 523-538.
1407 Cruden, D.M. and Varnes, D.J., 1996. Landslides: investigation and mitigation. Chapter 3-
1408 Landslide types and processes. Transportation research board special report(247).
1409 Cui, P., Zhou, G.G.D., Zhu, X.H. and Zhang, J.Q., 2013. Scale amplification of natural debris
1410 flows caused by cascading landslide dam failures. Geomorphology, 182: 173-189.
1411 Cui, P., Zhu, Y.-y., Han, Y.-s., Chen, X.-q. and Zhuang, J.-q., 2009. The 12 May Wenchuan
1412 earthquake-induced landslide lakes: distribution and preliminary risk evaluation. Landslides,
1413 6(3): 209-223.
1414 Das, A., Jayashree, C. and Viswanadham, B.V.S., 2009. Effect of randomly distributed geofibers
1415 on the piping behaviour of embankments constructed with fly ash as a fill material. Geotextiles
1416 and Geomembranes, 27(5): 341–349 https://doi.org/10.1016%2Fj.geotexmem.2009.02.004.
1417 Davies, T. and McSaveney, M., 2006. Mobility of long-runout rock avalanches. In: J.J. Clague
1418 and D. Stead (Editors), Landslides. Cambridge University Press, pp. 50–58
1419 https://doi.org/10.1017%2Fcbo9780511740367.006.
1420 Davies, T.R., Manville, V., Kunz, M. and Donadini, L., 2007. Modeling landslide dambreak flood
1421 magnitudes: Case study. Journal of Hydraulic Engineering, 133(7): 713-720.
1422 Davies, T.R. and McSaveney, M.J., 2011. Rock-avalanche size and runout–implications for
1423 landslide dams, Natural and Artificial Rockslide Dams. Springer, pp. 441–462.
1424 Davis, J.L. and Annan, A.P., 1989. Ground-penetrating radar for high-resolution mapping of soil
1425 and rock stratigraphy 1. Geophysical prospecting, 37(5): 531–551.
1426 De Roo, A.P.J., Wesseling, C.G. and Van Deursen, W.P.A., 2000. Physically based river basin
1427 modelling within a GIS: the LISFLOOD model. Hydrological Processes, 14(11‐12): 1981-
1428 1992.
1429 DeKay, M.L. and McClelland, G.H., 1993. Predicting loss of life in cases of dam failure and flash
1430 flood. Insurance: Mathematics and Economics, 13(2): 165 https://doi.org/10.1016%2F0167-
1431 6687%2893%2990920-k.
1432 Delaney, K.B. and Evans, S.G., 2015. The 2000 Yigong landslide (Tibetan Plateau), rockslide-
1433 dammed lake and outburst flood: review, remote sensing analysis, and process modelling.
1434 Geomorphology, 246: 377-393.
1435 Delaney, K.B. and Evans, S.G., 2017. The evolution (2010–2015) and engineering mitigation of
1436 a rockslide-dammed lake (Hunza River, Pakistan); characterisation by analytical remote
1437 sensing. Engineering Geology, 220: 65–75 https://doi.org/10.1016%2Fj.enggeo.2017.01.003.
1438 Delgado, F., Zerathe, S., Audin, L., Schwartz, S., Benavente, C., Carcaillet, J., Bourlès, D.L. and
1439 Team, A., 2020. Giant landslide triggerings and paleoprecipitations in the Central Western
1440 Andes: The aricota rockslide dam (South Peru). Geomorphology, 350: 106932
1441 https://doi.org/10.1016%2Fj.geomorph.2019.106932.
1442 Delunel, R., Hantz, D., Braucher, R., Bourlès, D.L., Schoeneich, P. and Deparis, J., 2010. Surface
1443 exposure dating and geophysical prospecting of the Holocene Lauvitel rock slide (French
1444 Alps). Landslides, 7(4): 393–400 https://doi.org/10.1007%2Fs10346-010-0221-0.
1445 Deng, Z., Wu, S., Fan, Z., Yan, Z. and Wu, J., 2019. Research on the Overtopping-Induced
1446 Breaching Mechanism of Tailings Dam and Its Numerical Simulation. Advances in Civil
1447 Engineering, 2019: 1–10 https://doi.org/10.1155%2F2019%2F3264342.
1448 Dong, G., Zhang, F., Ma, M., Fan, Y., Zhang, J., Wang, Z. and Chen, F., 2014. Ancient landslide-
1449 dam events in the Jishi Gorge, upper Yellow River valley, China. Quaternary Research, 81(3):
1450 445–451 https://doi.org/10.1016%2Fj.yqres.2013.09.003.

Dong, J.-J., Li, Y.-S., Kuo, C.-Y., Sung, R.-T., Li, M.-H., Lee, C.-T., Chen, C.-C. and Lee, W.-R., 2011a. The formation and breach of a short-lived landslide dam at Hsiaolin village, Taiwan — part I: Post-event reconstruction of dam geometry. Engineering Geology, 123(1-2): 40–59 https://doi.org/10.1016%2Fj.enggeo.2011.04.001.

Dong, J.-J., Tung, Y.-H., Chen, C.-C., Liao, J.-J. and Pan, Y.-W., 2011b. Logistic regression model for predicting the failure probability of a landslide dam. Engineering Geology, 117(1-2): 52-61.

Donohue, S., Gavin, K., Long, M., Tolooiyan, A. and Trafford, A., 2011. Understanding Irish landslides using geophysics, Geophysical Association of Ireland Seminar on Engineering Geophysics.

Dufresne, A., Bösmeier, A. and Prager, C., 2016. Sedimentology of rock avalanche deposits – Case study and review. Earth-Science Reviews, 163: 234–259 https://doi.org/10.1016%2Fj.earscirev.2016.10.002.

Dufresne, A. and Dunning, S.A., 2017. Process dependence of grain size distributions in rock avalanche deposits. Landslides, 14(5): 1555–1563 https://doi.org/10.1007%2Fs10346-017-0806-y.

Dufresne, A., Ostermann, M. and Preusser, F., 2018. River-damming, late-Quaternary rockslides in the Ötz Valley region (Tyrol, Austria). Geomorphology, 310: 153-167.

Dufresne, A., Wolken, G., Hibert, C., Bessette-Kirton, E., Coe, J.A., Geertsema, M. and Ekström, G., 2019. The 2016 Lamplugh rock avalanche, Alaska: deposit structures and emplacement dynamics. Landslides, 16(12): 2301-2319.

Dunne, T., 1990. Chapter 1. Hydrology mechanics, and geomorphic implications of erosion by subsurface flow, Groundwater Geomorphology; The Role of Subsurface Water in Earth-Surface Processes and Landforms. Geological Society of America, pp. 1–28 https://doi.org/10.1130%2Fspe252-p1.

Dunning, S.A., 2006. The grain size distribution of rock-avalanche deposits in valley-confined settings. Italian Journal of Engineering Geology and Environment, 1: 117–121.

Dunning, S.A. and Armitage, P.J., 2011. The grain-size distribution of rock-avalanche deposits: implications for natural dam stability, Natural and artificial rockslide dams. Springer, pp. 479-498.

Dunning, S.A., Petley, D.N., Rosser, N.J. and Strom, A.L., 2005. The morphology and sedimentology of valley confined rock-avalanche deposits and their effect on potential dam hazard, pp. 691–701.

Dunning, S.A., Rosser, N.J., Petley, D.N. and Massey, C.R., 2006. Formation and failure of the Tsatichhu landslide dam, Bhutan. Landslides, 3(2): 107-113.

Dupont, E., Dewals, B., Archambeau, P., Erpicum, S. and Pirotton, M., 2007. Experimental and numerical study of the breaching of an embankment dam, Proceedings of the 32nd IAHR Biennial Congress-Harmonizing the demands from art and nature. Di Silvio, Giampolo.

Eeckhaut, M.V.D., Poesen, J., Verstraeten, G., Vanacker, V., Nyssen, J., Moeyersons, J., Beek, L.P.H.v. and Vandekerckhove, L., 2007. Use of LIDAR-derived images for mapping old landslides under forest. Earth Surface Processes and Landforms, 32(5): 754–769.

Emmer, A., Klimeš, J., Mergili, M., Vilímek, V. and Cochachin, A., 2016. 882 lakes of the Cordillera Blanca: An inventory, classification, evolution and assessment of susceptibility to outburst floods. CATENA, 147: 269–279 https://doi.org/10.1016%2Fj.catena.2016.07.032.

Ermini, L. and Casagli, N., 2003. Prediction of the behaviour of landslide dams using a geomorphological dimensionless index. Earth Surface Processes and Landforms: The Journal of the British Geomorphological Research Group, 28(1): 31-47.

Ermini, L., Casagli, N. and Farina, P., 2006. Landslide dams: analysis of case histories and new perspectives from the application of remote sensing monitoring techniques to hazard and risk assessment. Italian Journal of Engineering Geology and Environment, Special(1): 45–52.

Evans, S.G., Hermanns, R.L., Strom, A. and Scarascia-Mugnozza, G., 2011. Natural and artificial rockslide dams, 133. Springer Science & Business Media.

Evans, S.G., Hu, X.Q. and Enegren, E.G., 1996. The 1973 Attachie slide, Peace River Valley, near Fort St. John, British Columbia, Canada: a landslide with a high-velocity flowslide component in Pleistocene sediments, pp. 715–720.

1506 Fan, X., Dufresne, A., Subramanian, S.S., Strom, A., Hermanns, R., Stefanelli, C.T., Hewitt, K.,
1507 Yunus, A.P., Dunning, S., Capra, L. and others, 2020. The formation and impact of landslide
1508 dams–State of the art. Earth-Science Reviews: 103116.
1509 Fan, X., Gorum, T., van Westen, C.J., Xu, Q., Tang, C. and Huang, R., 2009. Distribution of large
1510 landslides and landslide dams triggered by the Wenchuan earthquake, Sichuan, China, pp.
1511 2863.
1512 Fan, X., Scaringi, G., Korup, O., West, A.J., van Westen, C.J., Tanyas, H., Hovius, N., Hales,
1513 T.C., Jibson, R.W., Allstadt, K.E., Zhang, L., Evans, S.G., Xu, C., Li, G., Pei, X., Xu, Q. and
1514 Huang, R., 2019a. Earthquake-Induced Chains of Geologic Hazards: Patterns, Mechanisms,
1515 and Impacts. Reviews of Geophysics, 57(2): 421-503.
1516 Fan, X., Tang, C.X., Van Westen, C.J. and Alkema, D., 2012a. Simulating dam-breach flood
1517 scenarios of the Tangjiashan landslide dam induced by the Wenchuan Earthquake. Natural
1518 hazards and earth system sciences, 12(10): 3031.
1519 Fan, X., van Westen, C.J., Tang, C., Xu, Q., Huang, R. and Wang, G., 2015. The Classification
1520 of Damming Landslides and Landslide Dams Induced by the Wenchuan Earthquake. In: G.
1521 Lollino, D. Giordan, G.B. Crosta, J. Corominas, R. Azzam, J. Wasowski and N. Sciarra
1522 (Editors), Engineering Geology for Society and Territory - Volume 2. Springer International
1523 Publishing, Cham, pp. 1143-1147.
1524 Fan, X., van Westen, C.J., Xu, Q., Gorum, T. and Dai, F., 2012b. Analysis of landslide dams
1525 induced by the 2008 Wenchuan earthquake. Journal of Asian Earth Sciences, 57: 25-37.
1526 Fan, X., van Westen, C.J., Xu, Q., Gorum, T., Dai, F., Wang, G. and Huang, R., 2013. Spatial
1527 Distribution of Landslide Dams Triggered by the 2008 Wenchuan Earthquake. In: C. Margottini,
1528 P. Canuti and K. Sassa (Editors), Landslide Science and Practice. Springer Berlin Heidelberg,
1529 Berlin, Heidelberg, pp. 279–285.
1530 Fan, X., Xu, Q., Alonso-Rodriguez, A., Siva Subramanian, S., Li, W., Zheng, G., Dong, X. and
1531 Huang, R., 2019b. Successive landsliding and damming of the Jinsha River in eastern Tibet,
1532 China: prime investigation, early warning, and emergency response. Landslides, 16(5): 1003-
1533 1020.
1534 Fan, X., Yang, F., Siva Subramanian, S., Xu, Q., Feng, Z., Mavrouli, O., Peng, M., Ouyang, C.,
1535 Jansen, J.D. and Huang, R., 2019c. Prediction of a multi-hazard chain by an integrated
1536 numerical simulation approach: the Baige landslide, Jinsha River, China. Landslides.
1537 Farr, T.G., Rosen, P.A., Caro, E., Crippen, R., Duren, R., Hensley, S., Kobrick, M., Paller, M.,
1538 Rodriguez, E., Roth, L. and others, 2007. The shuttle radar topography mission. Reviews of
1539 geophysics, 45(2).
1540 Fedorenko, V., 1988. Rockslides and rockfalls and their prediction. . Moscow State University
1541 Publishing House, Moscow (in Russian).
1542 Fell, R. and Fry, J.-J., 2013. State of The Art on the Likelihood of Internal Erosion of Dams and
1543 Levees by Means of Testing, Erosion in Geomechanics Applied to Dams and Levees. John
1544 Wiley & Sons, Inc., pp. 1–99 https://doi.org/10.1002%2F9781118577165.ch1.
1545 FEMA, 2004. Federal guidelines for dam safety: Hazard potential classification system for dams.
1546 FEMA Washington, DC.
1547 Ferretti, A., Prati, C. and Rocca, F., 2001. Permanent scatterers in SAR interferometry. IEEE
1548 Transactions on geoscience and remote sensing, 39(1): 8–20.
1549 Feyisa, G.L., Meilby, H., Fensholt, R. and Proud, S.R., 2014. Automated Water Extraction Index:
1550 A new technique for surface water mapping using Landsat imagery. Remote Sensing of
1551 Environment, 140: 23–35 https://doi.org/10.1016%2Fj.rse.2013.08.029.
1552 Field, E. and Jacob, K., 1993. The theoretical response of sedimentary layers to ambient seismic
1553 noise. Geophysical research letters, 20(24): 2925-2928.
1554 Fisher, A., Flood, N. and Danaher, T., 2016. Comparing Landsat water index methods for
1555 automated water classification in eastern Australia. Remote Sensing of Environment, 175:
1556 167–182 https://doi.org/10.1016%2Fj.rse.2015.12.055.
1557 Fleshman, M.S. and Rice, J.D., 2014. Laboratory Modeling of the Mechanisms of Piping Erosion
1558 Initiation. Journal of Geotechnical and Geoenvironmental Engineering, 140(6): 04014017
1559 https://doi.org/10.1061%2F%28asce%29gt.1943-5606.0001106.

Foster, M., Fell, R. and Spannagle, M., 2000. The statistics of embankment dam failures and accidents. Canadian Geotechnical Journal, 37(5): 1000–1024 https://doi.org/10.1139%2Ft00-030.
Fox, G.A., Felice, R.G., Midgley, T.L., Wilson, G.V. and Al-Madhhachi, A.-S.T., 2013. Laboratory soil piping and internal erosion experiments: evaluation of a soil piping model for low-compacted soils. Earth Surface Processes and Landforms, 39(9): 1137–1145 https://doi.org/10.1002%2Fesp.3508.
Fread, D.L., 1984. DAMBRK: The NWS dam-break flood forecasting model, 4. Hydrologic Research Laboratory, National Weather Service, NOAA Silver Spring.
Fread, D.L., 1988. BREACH, an erosion model for earthen dam failures. Hydrologic Research Laboratory, National Weather Service, NOAA.
Fread, D.L., 1996. Dam-breach floods, Hydrology of disasters. Springer, pp. 85-126.
Fread, D.L., 2014. National Weather Service models to forecast dam-breach floods. Hydrology of disasters: 192-211.
Frieser, B.I., Vrijling, J.K. and Jonkman, S.N., 2005. Probabilistic evacuation decision model for river floods in the Netherlands.
Garambois, S., Sénéchal, P. and Perroud, H., 2002. On the use of combined geophysical methods to assess water content and water conductivity of near-surface formations. Journal of Hydrology, 259(1-4): 32–48.
García-García, F., Sánchez-Gómez, M., Navarro, V. and Pla, S., 2011. Formation, infill, and dissection of a latest-Pleistocene landslide-dammed reservoir (Betic Cordillera, Southern Spain): Upstream and downstream geomorphological and sedimentological evidence. Quaternary International, 233(1): 61–71 https://doi.org/10.1016%2Fj.quaint.2010.07.010.
Geertsema, M. and Clague, J.J., 2006. 1,000-year record of landslide dams at Halden Creek, northeastern British Columbia. Landslides, 3(3): 217-227.
Glancy, P.A. and Bell, J.W., 2000. Landslide-induced flooding at Ophir Creek, Washoe County, western Nevada, May 30, 1983. 2330-7102, US Geological Survey.
Görüm, T., 2019. Landslide recognition and mapping in a mixed forest environment from airborne LiDAR data. Engineering Geology, 258: 105155 https://doi.org/10.1016%2Fj.enggeo.2019.105155.
Graham, W.J., 1999. A procedure for estimating loss of life caused by dam failure. US Department of the Interior, Bureau of Reclamation.
Grandjean, G., Gourry, J.C., Sanchez, O., Bitri, A. and Garambois, S., 2011. Structural study of the Ballandaz landslide (French Alps) using geophysical imagery. Journal of Applied Geophysics, 75(3): 531–542 https://doi.org/10.1016%2Fj.jappgeo.2011.07.008.
Gregoretti, C., Maltauro, A. and Lanzoni, S., 2010. Laboratory Experiments on the Failure of Coarse Homogeneous Sediment Natural Dams on a Sloping Bed. Journal of Hydraulic Engineering, 136(11): 868–879 https://doi.org/10.1061%2F%28asce%29hy.1943-7900.0000259.
Griffiths, D.H. and Barker, R.D., 1993. Two-dimensional resistivity imaging and modelling in areas of complex geology. Journal of applied Geophysics, 29(3-4): 211–226.
Guerrero, J., Gutiérrez, F., García-Ruiz, J.M., Carbonel, D., Lucha, P. and Arnold, L.J., 2018. Landslide-dam paleolakes in the Central Pyrenees, Upper Gállego River Valley, NE Spain: timing and relationship with deglaciation. Landslides, 15(10): 1975–1989 https://doi.org/10.1007%2Fs10346-018-1018-9.
Guo, Y., Hansen, D. and Li, C., 2009. Probabilistic approach to estimating the effects of channel reaches on flood frequencies. Water resources research, 45(8).
Guzzetti, F., Mondini, A.C., Cardinali, M., Fiorucci, F., Santangelo, M. and Chang, K.-T., 2012. Landslide inventory maps: New tools for an old problem. Earth-Science Reviews, 112(1-2): 42-66.
Hamilton, W.L., 2014. Ancient lakes of Zion National Park. Geology of Utah's Far South: Utah Geological Association Publication, 43: 1–23.
Han-Qiu, X., 2005. A study on information extraction of water body with the modified normalized difference water index (MNDWI). Journal of remote sensing, 5: 589-595.

Hancox, G.T., McSaveney, M.J., Manville, V.R. and Davies, T.R., 2005. The October 1999 Mt Adams rock avalanche and subsequent landslide dam ‐ break flood and effects in Poerua River, Westland, New Zealand. New Zealand Journal of Geology and Geophysics, 48(4): 683-705.

Hanisch, J. and Söder, C.O., 2000. Geotechnical assessment of the Usoi landslide dam and the right bank of Lake Sarez. Usoi Landslide dam and lake Sarez. An assessment of hazard and risk in the Pamir mountains, Tajikistan. ISDR Prevention Series(1): 23-42.

Hanson, G.J., Cook, K.R. and Hunt, S.L., 2005. Physical modeling of ovetopping erosion and breach formaion of cohesive embankments. Transactions of the ASAE, 48(5): 1783–1794 https://doi.org/10.13031%2F2013.20012.

Hanson, G.J., Tejral, R.D., Hunt, S.L. and Temple, D.M., 2010. Internal erosion and impact of erosion resistance, Proceedings of the 30th US Society on dams annual meeting and conference, pp. 773–784.

Hartvich, F., 2008. A reconstruction of a former rockslide-dammed lake: the case of the Kokomeren River valley (Tien Shan, Kyrgyzstan), Poster presentation at the EGU conference, Vien, 2008.

Havenith, H.-B., Torgoev, I. and Ischuk, A., 2018. Integrated Geophysical-Geological 3D Model of the Right-Bank Slope Downstream from the Rogun Dam Construction Site, Tajikistan. International Journal of Geophysics, 2018: 1–16 https://doi.org/10.1155%2F2018%2F1641789.

Havenith, H.-B., Torgoev, I., Torgoev, A., Strom, A., Xu, Y. and Fernandez-Steeger, T., 2015. The Kambarata 2 blast-fill dam, Kyrgyz Republic:blast event, geophysical monitoring and dam structure modelling. Geoenvironmental Disasters, 2(1): 11.

Heim, A., 1932. Landslides and human lives (Bergsturz und Menschenleben). Bi-Tech Publishers, Vancouver, BC: 196.

Hermanns, R.L., Fauqué, L. and Wilson, C.G.J., 2015. 36Cl terrestrial cosmogenic nuclide dating suggests Late Pleistocene to Early Holocene mass movements on the south face of Aconcagua mountain and in the Las Cuevas–Horcones valleys, Central Andes, Argentina. Geological Society, London, Special Publications, 399(1): 345-368.

Hermanns, R.L., Folguera, A., Penna, I., Fauqué, L. and Niedermann, S., 2011a. Landslide dams in the Central Andes of Argentina (northern Patagonia and the Argentine northwest), Natural and artificial rockslide dams. Springer, pp. 147-176.

Hermanns, R.L., Hansen, L., Sletten, K., Böhme, M., Bunkholt, H., Dehls, J.F., Eilertsen, R., Fischer, L., Lheureux, J.S. and Høgaas, F., 2012. Systematic geological mapping for landslide understanding in the Norwegian context. Landslide and engineered slopes: protecting society through improved understanding. Taylor & Francis Group, London: 265-271.

Hermanns, R.L., Hewitt, K., Strom, A., Evans, S.G., Dunning, S.A. and Scarascia-Mugnozza, G., 2011b. The classification of rockslide dams, Natural and artificial rockslide dams. Springer, pp. 581-593.

Hermanns, R.L., L'Heureux, J.-S. and Blikra, L.H., 2013. Landslide triggered tsunami, displacement wave. Encyclopedia of Natural Hazards: 611-615.

Hermanns, R.L. and Niedermann, S., 2011. Late Pleistocene–early Holocene paleoseismicity deduced from lake sediment deformation and coeval landsliding in the Calchaquíes valleys, NW Argentina, Geological Criteria for Evaluating Seismicity Revisited: Forty Years of Paleoseismic Investigations and the Natural Record of Past Earthquakes. Geological Society of America https://doi.org/10.1130%2F2011.2479%2808%29.

Hermanns, R.L., Niedermann, S., Garcia, A.V., Gomez, J.S. and Strecker, M.R., 2001. Neotectonics and catastrophic failure of mountain fronts in the southern intra-Andean Puna Plateau, Argentina. Geology, 29(7): 619–622.

Hermanns, R.L., Niedermann, S., Ivy-Ochs, S. and Kubik, P.W., 2004. Rock avalanching into a landslide-dammed lake causing multiple dam failure in Las Conchas valley (NW Argentina)—evidence from surface exposure dating and stratigraphic analyses. Landslides, 1(2): 113–122.

Hermanns, R.L. and Schellenberger, A., 2008. Quaternary tephrochronology helps define conditioning factors and triggering mechanisms of rock avalanches in NW Argentina. Quaternary International, 178(1): 261–275.

1669 Hermanns, R.L., Schleier, M., Böhme, M., Blikra, L.H., Gosse, J., Ivy-Ochs, S. and Hilger, P.,
1670 2017. Rock-avalanche activity in W and S Norway peaks after the retreat of the Scandinavian
1671 Ice Sheet, Workshop on World Landslide Forum. Springer, pp. 331–338.
1672 Hewitt, K., 1982. Natural dams and outburst floods of the Karakoram Himalaya. IAHS, 138: 259-
1673 269.
1674 Hewitt, K., Clague, J.J. and Orwin, J.F., 2008. Legacies of catastrophic rock slope failures in
1675 mountain landscapes. Earth-Science Reviews, 87(1-2): 1-38.
1676 Hewitt, K., Gosse, J. and Clague, J.J., 2011. Rock avalanches and the pace of late Quaternary
1677 development of river valleys in the Karakoram Himalaya. Geological Society of America
1678 Bulletin, 123(9-10): 1836–1850 https://doi.org/10.1130%2Fb30341.1.
1679 Hilger, P., Gosse, J.C. and Hermanns, R.L., 2019. How significant is inheritance when dating
1680 rockslide boulders with terrestrial cosmogenic nuclide dating?—a case study of an historic
1681 event. Landslides, 16(4): 729–738 https://doi.org/10.1007%2Fs10346-018-01132-0.
1682 Hilger, P., Hermanns, R.L., Gosse, J.C., Jacobs, B., Etzelmüller, B. and Krautblatter, M., 2018.
1683 Multiple rock-slope failures from Mannen in Romsdal Valley, western Norway, revealed from
1684 Quaternary geological mapping and 10Be exposure dating. The Holocene, 28(12): 1841-1854.
1685 Hungr, O., 1995. A model for the runout analysis of rapid flow slides, debris flows, and
1686 avalanches. Canadian Geotechnical Journal, 32(4): 610-623.
1687 Hungr, O., 2006. Rock avalanche occurrence, process and modelling, Landslides from massive
1688 rock slope failure. Springer, pp. 243–266.
1689 Hungr, O., 2011. Prospects for prediction of landslide dam geometry using empirical and dynamic
1690 models, Natural and Artificial Rockslide Dams. Springer, pp. 463-477.
1691 Hungr, O., Leroueil, S. and Picarelli, L., 2014. The Varnes classification of landslide types, an
1692 update. Landslides, 11(2): 167-194.
1693 Hunt, S.L., Hanson, G.J., Cook, K.R. and Kadavy, K.C., 2005. Breach widening observations
1694 from earthen embankment tests. Transactions of the ASAE, 48(3): 1115–1120
1695 https://doi.org/10.13031%2F2013.18521.
1696 Hydro, B.C., 1993. Guidelines for consequence-based dam safety evaluations and improvements
1697 (Interim). BC Hydro, Burnaby, BC, Canada.
1698 Intrieri, E., Raspini, F., Fumagalli, A., Lu, P., Del Conte, S., Farina, P., Allievi, J., Ferretti, A. and
1699 Casagli, N., 2018. The Maoxian landslide as seen from space: detecting precursors of failure
1700 with Sentinel-1 data. Landslides, 15(1): 123–133.
1701 Ischuk, A.R., 2011. Usoi rockslide dam and lake Sarez, Pamir mountains, Tajikistan, Natural and
1702 Artificial Rockslide Dams. Springer, pp. 423-440.
1703 Ivy-Ochs, S., Poschinger, A.V., Synal, H.A. and Maisch, M., 2009. Surface exposure dating of
1704 the Flims landslide, Graubünden, Switzerland. Geomorphology, 103(1): 104-112.
1705 Ivy-Ochs, S., Martin, S., Campedel, P., Hippe, K., Alfimov, V., Vockenhuber, C., Andreotti, E.,
1706 Carugati, G., Pasqual, D., Rigo, M. and Viganò, A., 2017. Geomorphology and age of the
1707 Marocche di Dro rock avalanches (Trentino, Italy). Quaternary Science Reviews, 169: 188–
1708 205 https://doi.org/10.1016%2Fj.quascirev.2017.05.014.
1709 Jaboyedoff, M., Oppikofer, T., Abellán, A., Derron, M.-H., Loye, A., Metzger, R. and Pedrazzini,
1710 A., 2012. Use of LIDAR in landslide investigations: a review. Natural hazards, 61(1): 5-28.
1711 Jing, X., Chen, Y., Williams, D., Serna, M. and Zheng, H., 2019. Overtopping Failure of a
1712 Reinforced Tailings Dam: Laboratory Investigation and Forecasting Model of Dam Failure.
1713 Water, 11(2): 315 https://doi.org/10.3390%2Fw11020315.
1714 Johnson, H.P., 1978. Paleomagnetism of Igneous rock samples -DSDP LEG 45.
1715 Jongmans, D. and Garambois, S., 2007. Geophysical investigation of landslides: a review.
1716 Bulletin de la Société géologique de France, 178(2): 101-112.
1717 Jonkman, S.N., 2007. Loss of life estimation in Flood risk assessment. Theory and applications.
1718 PhD Thesis. Delft University of Technology.". Delft: Delft University.
1719 Kakinuma, T. and Shimizu, Y., 2014. Large-Scale Experiment and Numerical Modeling of a
1720 Riverine Levee Breach. Journal of Hydraulic Engineering, 140(9): 04014039
1721 https://doi.org/10.1061%2F%28asce%29hy.1943-7900.0000902.

Ke, L. and Takahashi, A., 2012a. Influence of internal erosion on deformation and strength of gap-graded non-cohesive soil, Proceedings of the Sixth International Conference on Scour and Erosion, Paris, pp. 847–854.
Ke, L. and Takahashi, A., 2012b. Strength reduction of cohesionless soil due to internal erosion induced by one-dimensional upward seepage flow. Soils and Foundations, 52(4): 698–711.
Khan, S., 2012. Vulnerability assessments and their planning implications: a case study of the Hutt Valley, New Zealand. Natural Hazards, 64(2): 1587–1607 https://doi.org/10.1007%2Fs11069-012-0327-x.
Kokusho, T. and Fujikura, Y., 2008. Effect of particle gradation on seepage failure in granular soils, Proceedings 4th International Conference on Scour and Erosion (ICSE-4). November 5-7, 2008, Tokyo, Japan, pp. 497–504.
Korchevskiy, V.F., Kolichko, A.V., Strom, A.L., Pernik, L.M. and Abdrakhmatov, K.E., 2011. Utilisation of data derived from large-scale experiments and study of natural blockages for blast-fill dam design, Natural and artificial rockslide dams. Springer, pp. 617-637.
Korup, O., 2002. Recent research on landslide dams-a literature review with special attention to New Zealand. Progress in Physical Geography, 26(2): 206-235.
Korup, O., 2005a. Geomorphic hazard assessment of landslide dams in South Westland, New Zealand: fundamental problems and approaches. Geomorphology, 66(1-4): 167-188.
Korup, O., 2005b. Geomorphic imprint of landslides on alpine river systems, southwest New Zealand. Earth Surface Processes and Landforms, 30(7): 783-800.
Korup, O. and Tweed, F., 2007. Ice, moraine, and landslide dams in mountainous terrain. Quaternary Science Reviews, 26(25-28): 3406-3422.
Kubik, P. W., Ivy-Ochs, S., Masarik, J., Frank, M. and Schlüchter, C., 1998. 10Be and 26Al production rates deduced from an instantaneous event within the dendro-calibration curve, the landslide of Köfels, Ötz Valley, Austria. Earth and Planetary Science Letters, 161(1-4): 231-241.
Lang, A., Moya, J., Corominas, J., Schrott, L. and Dikau, R., 1999. Classic and new dating methods for assessing the temporal occurrence of mass movements. Geomorphology, 30(1-2): 33–52 https://doi.org/10.1016%2Fs0169-555x%2899%2900043-4.
Leblanc, M., Favreau, G., Maley, J., Nazoumou, Y., Leduc, C., Stagnitti, F., Oevelen, P.J.v., Delclaux, F. and Lemoalle, J., 2006. Reconstruction of Megalake Chad using Shuttle Radar Topographic Mission data. Palaeogeography, Palaeoclimatology, Palaeoecology, 239(1-2): 16–27 https://doi.org/10.1016%2Fj.palaeo.2006.01.003.
Lee, C.F. and Dai, F.C., 2011. The 1786 Dadu River Landslide Dam, Sichuan, China, Natural and Artificial Rockslide Dams. Springer, pp. 369-388.
Liang, Y., Zeng, C., Wang, J.J., Liu, M.W., Yeh, T.C.J. and Zha, Y.Y., 2017. Constant Gradient Erosion Apparatus for Appraisal of Piping Behavior in Upward Seepage Flow. Geotechnical Testing Journal, 40(4): 20150282 https://doi.org/10.1520%2Fgtj20150282.
Liao, H.-m., Yang, X.-g., Xu, F.-g., Xu, H. and Zhou, J.-w., 2018. A fuzzy comprehensive method for the risk assessment of a landslide-dammed lake. Environmental Earth Sciences, 77(22) https://doi.org/10.1007%2Fs12665-018-7946-9.
Lindell, M.K., Prater, C.S. and Peacock, W.G., 2007. Organizational Communication and Decision Making for Hurricane Emergencies. Natural Hazards Review, 8(3): 50–60 https://doi.org/10.1061%2F%28asce%291527-6988%282007%298%3A3%2850%29.
Liu, N., Chen, Z., Zhang, J., Lin, W., Chen, W. and Xu, W., 2010. Draining the Tangjiashan Barrier Lake. Journal of Hydraulic Engineering, 136(11): 914–923 https://doi.org/10.1061%2F%28asce%29hy.1943-7900.0000241.
Liu, Y., 2009. An explicit risk-based approach for large-levee safety decisions.
Loke, M.H., Chambers, J.E., Rucker, D.F., Kuras, O. and Wilkinson, P.B., 2013. Recent developments in the direct-current geoelectrical imaging method. Journal of applied geophysics, 95: 135–156.
Lucieer, A., Jong, S.M.d. and Turner, D., 2014. Mapping landslide displacements using Structure from Motion (SfM) and image correlation of multi-temporal UAV photography. Progress in Physical Geography, 38(1): 97–116.
Macchione, F. and Sirangelo, B., 1988. Study of earth dam erosion due to overtopping.

Mansoor, A., Khan, N.M., Akbar, A., Abbas, Y. and Farooq, M.U., 2020. Quantification of Flood Hazards Due to Assumed Breaching of Attabad Landslide Dam, Pakistan, Recent Trends in Environmental Hydraulics. Springer International Publishing, pp. 181–195 https://doi.org/10.1007%2F978-3-030-37105-0_16.

Manville, V., 2001. Techniques for evaluating the size of potential dam-break floods from natural dams. Institute of Geological & Nuclear Sciences.

Marot, D., Rochim, A., Nguyen, H.-H., Bendahmane, F. and Sibille, L., 2016. Assessing the susceptibility of gap-graded soils to internal erosion: proposition of a new experimental methodology. Natural Hazards, 83(1): 365–388 https://doi.org/10.1007%2Fs11069-016-2319-8.

Massey, C.I., Townsend, D.B., Dellow, G.D., Lukovic, B., Rosser, B.J., Archibald, G.C., Villeneuve, M., Davidson, J., Jones, K.E., Morgenstern, R. and al, e., 2018. Kaikoura Earthquake Short-Term Project: landslide inventory and landslide dam assessments. GNS Science, Lower Hutt (NZ), pp. 45.

Massonnet, D. and Feigl, K.L., 1998. Radar interferometry and its application to changes in the Earth's surface. Reviews of geophysics, 36(4): 441–500.

McCann, D. and Forster, A., 1990. Reconnaissance geophysical methods in landslide investigations. Engineering Geology, 29(1): 59-78.

McClelland, D.M. and Bowles, D.S., 1999. Life-loss estimation: what can we learn from case histories, Proceedings of the Australian committee on large dams (ANCOLD) annual meeting. Jindabyne.

McFeeters, S.K., 1996. The use of the Normalized Difference Water Index (NDWI) in the delineation of open water features. International Journal of Remote Sensing, 17(7): 1425–1432 .

Meric, O., Garambois, S., Jongmans, D., Wathelet, M., Chatelain, J.-L. and Vengeon, J.M., 2005. Application of geophysical methods for the investigation of the large gravitational mass movement of Séchilienne, France. Canadian Geotechnical Journal, 42(4): 1105–1115.

Miller, B., Dufresne, A., Geertsema, M., Atkinson, N., Evensen, H. and Cruden, D., 2018. Longevity of dams from landslides with sub-channel rupture surfaces, Peace River region, Canada. Geoenvironmental Disasters, 5(1): 1.

Moffat, R. and Fannin, R.J., 2011. A hydromechanical relation governing internal stability of cohesionless soil. Canadian Geotechnical Journal, 48(3): 413–424.

Moffat, R., Fannin, R.J. and Garner, S.J., 2011. Spatial and temporal progression of internal erosion in cohesionless soil. Canadian Geotechnical Journal, 48(3): 399–412.

Morche, D. and Schmidt, K.H., 2012. Sediment transport in an alpine river before and after a dambreak flood event. Earth Surface Processes and Landforms, 37(3): 347-353.

Moreiras, S.M., Hermanns, R.L. and Fauqué, L., 2015. Cosmogenic dating of rock avalanches constraining Quaternary stratigraphy and regional neotectonics in the Argentine Central Andes (32 S). Quaternary Science Reviews, 112: 45-58.

Nadal-Romero, E., Verachtert, E., Maes, R. and Poesen, J., 2011. Quantitative assessment of the piping erosion susceptibility of loess-derived soil horizons using the pinhole test. Geomorphology, 135(1-2): 66–79 https://doi.org/10.1016%2Fj.geomorph.2011.07.026.

Nasiri, H., Yusof, M.J.M. and Ali, T.A.M., 2016. An overview to flood vulnerability assessment methods. Sustainable Water Resources Management, 2(3): 331–336 https://doi.org/10.1007%2Fs40899-016-0051-x.

Neshikhovskiy, R., 1988. Floods on rivers and lakes. Hydrometeoizdat, Leningrad (in Russian): 184.

Niazi, F.S., Habib ur, R. and Akram, T., 2010. Application of electrical resistivity for subsurface characterization of Hattian Bala landslide dam, GeoFlorida 2010: Advances in Analysis, Modeling & Design, pp. 480–489.

Nibigira, L., 2018. Formation, breaching and flood consequences of a landslide dam near Bujumbura, Burundi https://doi.org/10.5194%2Fnhess-2017-372-ac1.

Nicolussi, K., Spötl, C., Thurner, A. and Reimer, P.J., 2015. Precise radiocarbon dating of the giant Köfels landslide (Eastern Alps, Austria). Geomorphology, 243: 87–91 https://doi.org/10.1016%2Fj.geomorph.2015.05.001.

Nikonov, A.A. and Shebalina, T.Y., 1979. Lichenometry and earthquake age determination in central Asia. Nature, 280(5724): 675–677 https://doi.org/10.1038%2F280675a0.
Okada, H. and Suto, K., 2003. The microtremor survey method. Society of Exploration Geophysicists.
Okeke, A.C.-U. and Wang, F., 2016a. Critical hydraulic gradients for seepage-induced failure of landslide dams. Geoenvironmental Disasters, 3(1) https://doi.org/10.1186%2Fs40677-016-0043-z.
Okeke, A.C.-U. and Wang, F., 2016b. Hydromechanical constraints on piping failure of landslide dams: an experimental investigation. Geoenvironmental Disasters, 3(1) https://doi.org/10.1186%2Fs40677-016-0038-9.
Okeke, A.C.-U., Wang, F., Kuwada, Y. and Mitani, Y., 2017. Experimental Study of the Premonitory Factors for Internal Erosion and Piping Failure of Landslide Dams, Advancing Culture of Living with Landslides. Springer International Publishing, pp. 389–397 https://doi.org/10.1007%2F978-3-319-53498-5_45.
Olhoeft, G.R., 2002. Applications and frustrations in using ground penetrating radar. IEEE aerospace and electronic systems magazine, 17(2): 12–20.
Oppikofer, T., Hermanns, R. L., Roberts, N. J., and Böhme, M., 2019, SPLASH: semi-empirical prediction of landslide-generated displacement wave run-up heights. Geological Society, London, Special Publications 477(1):353-366.
Oppikofer, T., Hermanns, R. L., Sandøy, G., Böhme, M., Jaboyedoff, M., Horton, P., Roberts, N. J., and Fuchs, H., 2016, Quantification of casualties from potential rock-slope failures in Norway. Landslides and Engineered Slopes: Experience, Theory and Practice, p. 1537-1544.
Oppikofer, T., Hermanns, R. L., Jakobsen, V. U., Böhme, M., Nicolet, P., and Penna, I., 2020, Forecasting dam height and stability of dams formed by rock slope failures in Norway: Nat. Hazards Earth Syst. Sci. Discuss., v. 2020, p. 1-24.
Ostermann, M., Ivy‐Ochs, S., Sanders, D. and Prager, C., 2017. Multi‐method (14C, 36Cl, 234U/230Th) age bracketing of the Tschirgant rock avalanche (Eastern Alps): implications for absolute dating of catastrophic mass‐wasting. Earth Surface Processes and Landforms, 42(7): 1110-1118.
Ostermann, M. and Sanders, D., 2017. The Benner pass rock avalanche cluster suggests a close relation between long-term slope deformation (DSGSDs and translational rock slides) and catastrophic failure. Geomorphology, 289: 44-59.
Ouma, Y.O. and Tateishi, R., 2014. Urban flood vulnerability and risk mapping using integrated multi-parametric AHP and GIS: methodological overview and case study assessment. Water, 6(6): 1515-1545.
Pánek, T., 2015. Recent progress in landslide dating: a global overview. Progress in Physical Geography, 39(2): 168–198.
Pánek, T., Hradeckỳ, J., Minár, J., Hungr, O. and Dušek, R., 2009. Late Holocene catastrophic slope collapse affected by deep-seated gravitational deformation in flysch: Ropice Mountain, Czech Republic. Geomorphology, 103(3): 414–429.
Pánek, T., Hradeckỳ, J., Smolková, V., Šilhán, K., Minár, J. and Zernitskaya, V., 2010. The largest prehistoric landslide in northwestern Slovakia: Chronological constraints of the Kykula long-runout landslide and related dammed lakes. Geomorphology, 120(3-4): 233–247.
Pánek, T., Smolková, V., Hradeckỳ, J., Baroň, I. and Šilhán, K., 2013. Holocene reactivations of catastrophic complex flow-like landslides in the Flysch Carpathians (Czech Republic/Slovakia). Quaternary research, 80(1): 33–46.
Papyrin, L.P., 2001. Sarezskaya katastrofa: geofizichesky prognoz.(The Sarez catastrophe: geophysical forecast). Geofizika XXI Stoletiya: 183e194.
Park, C.B., Miller, R.D. and Xia, J., 1999. Multichannel analysis of surface waves. Geophysics, 64(3): 800-808.
Parvaiz, I., Champatiray, P.K., Bhat, F.A. and Dadhwal, V.K., 2012. Earthquake-induced landslide dam in the Kashmir Himalayas. International journal of remote sensing, 33(2): 655–660.
Patella, D., 1997. Self-potential global tomography including topographic effects. Geophysical Prospecting, 45(5): 843–863.

Patzelt, G., 2012. Die Bergstürze von Tschirgant und von Haiming, Oberinntal, Tirol–Begleitworte zur Kartenbeilage. Jahrbuch der Geologischen Bundesanstalt, 152(1-4): 13-24.
Peakall, J., Ashworth, P. and Best, J., 1996. Physical modelling in fluvial geomorphology: principles, applications and unresolved issues. The scientific nature of geomorphology: 221-253.
Peng, M. and Zhang, L., 2012a. Analysis of human risks due to dam-break floods—part 1: a new model based on Bayesian networks. Natural hazards, 64(1): 903-933.
Peng, M. and Zhang, L.M., 2012b. Analysis of human risks due to dam break floods—part 2: application to Tangjiashan landslide dam failure. Natural hazards, 64(2): 1899-1923.
Peng, M. and Zhang, L.M., 2012c. Breaching parameters of landslide dams. Landslides, 9(1): 13-31.
Peng, M. and Zhang, L.M., 2013a. Dynamic decision making for dam-break emergency management – Part 1: Theoretical framework. Natural Hazards and Earth System Sciences, 13(2): 425–437 https://doi.org/10.5194%2Fnhess-13-425-2013.
Peng, M. and Zhang, L.M., 2013b. Dynamic decision making for dam-break emergency management – Part 2: Application to Tangjiashan landslide dam failure. Natural Hazards and Earth System Sciences, 13(2): 439–454 https://doi.org/10.5194%2Fnhess-13-439-2013.
Peng, M., Zhang, L.M., Chang, D.S. and Shi, Z.M., 2014. Engineering risk mitigation measures for the landslide dams induced by the 2008 Wenchuan earthquake. Engineering Geology, 180: 68–84 https://doi.org/10.1016%2Fj.enggeo.2014.03.016.
Penna, I.M., Hermanns, R.L., Niedermann, S. and Folguera, A., 2011. Multiple slope failures associated with neotectonic activity in the Southern Central Andes (37 – 37 30′ S), Patagonia, Argentina. Bulletin, 123(9-10): 1880 – 1895.
Perrone, A., Lapenna, V. and Piscitelli, S., 2014. Electrical resistivity tomography technique for landslide investigation: a review. Earth-Science Reviews, 135: 65–82.
Pesci, A., Teza, G., Casula, G., Loddo, F., De Martino, P., Dolce, M., Obrizzo, F. and Pingue, F., 2011. Multitemporal laser scanner-based observation of the Mt. Vesuvius crater: Characterization of overall geometry and recognition of landslide events. ISPRS journal of photogrammetry and remote sensing, 66(3): 327–336.
Peternel, T., Kumelj, Š., Oštir, K. and Komac, M., 2017. Monitoring the Potoška planina landslide (NW Slovenia) using UAV photogrammetry and tachymetric measurements. Landslides, 14(1): 395–406.
Plaza, G., Zevallos, O. and Cadier, É., 2011. La Josefina Landslide Dam and Its Catastrophic Breaching in the Andean Region of Ecuador, Natural and artificial rockslide dams. Springer, pp. 389–406.
Prager, C., Ivy-Ochs, S., Ostermann, M., Synal, H.A. and Patzelt, G., 2009. Geology and radiometric 14C-, 36Cl-and Th-/U-dating of the Fernpass rockslide (Tyrol, Austria). Geomorphology, 103(1): 93–103.
Preusser, F., Degering, D., Fuchs, M., Hilgers, A., Kadereit, A., Klasen, N., Krbetschek, M., Richter, D. and Spencer, J.Q.G., 2008. Luminescence dating: basics, methods and applications. Eiszeitalter und Gegenwart - Quaternary Science Journal, 57(1/2): 95–149.
Ramsbottom, D. and others, 2003. Flood risks to people: Phase 1. London: DEFRA.
Raspini, F., Bardi, F., Bianchini, S., Ciampalini, A., Del Ventisette, C., Farina, P., Ferrigno, F., Solari, L. and Casagli, N., 2017. The contribution of satellite SAR-derived displacement measurements in landslide risk management practices. Natural hazards, 86(1): 327-351.
Redpath, B.B., 1973. Seismic refraction exploration for engineering site investigations. Army Engineer Waterways Experiment Station, Livermore, Calif.(USA ….
Regmi, R.K., Lee, G. and Jung, K., 2013. Analysis on failure of slope and landslide dam. KSCE Journal of Civil Engineering, 17(5): 1166-1178.
Regmi, R.K., Nakagawa, H., Kawaike, K., Baba, Y. and Zhang, H., 2010. Two and three dimensional slope stability analysis of landslide dam failure due to sliding.
Reneau, S.L. and Dethier, D.P., 1996. Late Pleistocene landslide-dammed lakes along the Rio Grande, White Rock Canyon, New Mexico. Geological Society of America Bulletin, 108(11): 1492-1507.

Richards, K.S. and Reddy, K.R., 2010. True triaxial piping test apparatus for evaluation of piping potential in earth structures. Geotechnical Testing Journal, 33(1): 83–95.
Rickenmann, D., 2005. Runout prediction methods, Debris-flow hazards and related phenomena. Springer, pp. 305-324.
Rifai, I., Erpicum, S., Archambeau, P., Violeau, D., Pirotton, M., Abderrezzak, K.E.K. and Dewals, B., 2017. Overtopping induced failure of noncohesive, homogeneous fluvial dikes. Water Resources Research, 53(4): 3373–3386 https://doi.org/10.1002%2F2016wr020053.
Risley, J.C., Walder, J.S. and Denlinger, R.P., 2006. Usoi dam wave overtopping and flood routing in the Bartang and Panj Rivers, Tajikistan. Natural Hazards, 38(3): 375-390.
Rochim, A., Marot, D., Sibille, L. and Le, V.T., 2017. Effects of Hydraulic Loading History on Suffusion Susceptibility of Cohesionless Soils. Journal of Geotechnical and Geoenvironmental Engineering, 143(7): 04017025 https://doi.org/10.1061%2F%28asce%29gt.1943-5606.0001673.
Rossi, G., Tanteri, L., Tofani, V., Vannocci, P., Moretti, S. and Casagli, N., 2018. Multitemporal UAV surveys for landslide mapping and characterization. Landslides, 15(5): 1045–1052.
Rott, H. and Siegel, A., 1999. Analysis of mass movements in alpine terrain by means of SAR interferometry, IEEE 1999 International Geoscience and Remote Sensing Symposium. IGARSS'99 (Cat. No. 99CH36293). IEEE, pp. 1933–1936.
Safran, E.B., O'Connor, J.E., Ely, L.L., House, P.K., Grant, G., Harrity, K., Croall, K. and Jones, E., 2015. Plugs or flood-makers? The unstable landslide dams of eastern Oregon. Geomorphology, 248: 237-251.
Sandrp, 2018. Landslide DAM on Tsangpo creates flood disaster risk for Siang.
Sanhueza-Pino, K., Korup, O., Hetzel, R., Munack, H., Weidinger, J.T., Dunning, S., Ormukov, C. and Kubik, P.W., 2011. Glacial advances constrained by 10 Be exposure dating of bedrock landslides, Kyrgyz Tien Shan. Quaternary Research, 76(3): 295-304.
Santamarina, J.C., Rinaldi, V.A., Fratta, D., Klein, K.A., Wang, Y.-H., Cho, G.C. and Cascante, G., 2005. A survey of elastic and electromagnetic properties of near-surface soils. Near-surface geophysics, 1: 71-87.
Sassa, K., 2010. Integrated landslide simulation model LS-RAPID operation manual. ICL, Godai Kaihatsu Corporation.
Sassa, K., Nagai, O., Solidum, R., Yamazaki, Y. and Ohta, H., 2010. An integrated model simulating the initiation and motion of earthquake and rain induced rapid landslides and its application to the 2006 Leyte landslide. Landslides, 7(3): 219-236.
Satofuka, Y., Mori, T., Mizuyama, T., Ogawa, K. and Yoshino, K., 2010. Prediction of floods caused by landslide dam collapse. Journal of disaster research, 5(3): 288-295.
Sattar, A. and Konagai, K., 2012. Recent landslide damming events and their hazard mitigation strategies. Advances in Geotechnical Earthquake Engineering–Soil Liquefaction and Seismic Safety of Dams and Monuments.
Scaioni, M., Longoni, L., Melillo, V. and Papini, M., 2014. Remote sensing for landslide investigations: an overview of recent achievements and perspectives. Remote Sensing, 6(10): 9600–9652.
Schleier, M., Hermanns, R.L., Gosse, J.C., Oppikofer, T., Rohn, J. and Tønnesen, J.F., 2017. Subaqueous rock-avalanche deposits exposed by post-glacial isostatic rebound, Innfjorddalen, Western Norway. Geomorphology, 289: 117-133.
Schleier, M., Hermanns, R.L., Rohn, J. and Gosse, J.C., 2015. Diagnostic characteristics and paleodynamics of supraglacial rock avalanches, Innerdalen, Western Norway. Geomorphology, 245: 23-39.
Smith, W.D., Dunning, S.A., Brough, S., Ross, N., Telling, J., 2020. GERALDINE (Google earth Engine supraglacial Debris Input dEtector) – a new tool for Identifying and monitoring supraglacial landslide inputs. Earth Surface Dynamcis. https://doi.org/10.5194/esurf-2020-40
Schmocker, L. and Hager, W.H., 2009. Modelling dike breaching due to overtopping. Journal of Hydraulic Research, 47(5): 585–597.
Schmocker, L. and Hager, W.H., 2012. Plane dike-breach due to overtopping: Effects of sediment, dike height and discharge. Journal of Hydraulic Research, 50(6): 576–586.
Schuster, R.L., 1986. Landslide dams: processes, risk, and mitigation. ASCE.

Schuster, R.L., 1995. Landslide dams—a worldwide phenomenon. J Jpn Landslide Soc, 31(4): 38–49.
Schuster, R.L. and Evans, S.G., 2011. Engineering measures for the hazard reduction of landslide dams, Natural and Artificial Rockslide Dams. Springer, pp. 77–100.
Schuster, R.L., Logan, R.L. and Pringle, P.T., 1992. Prehistoric rock avalanches in the Olympic Mountains, Washington. Science, 258(5088): 1620–1621.
Shen, D.Y., Shi, Z.M., Peng, M., Zhang, L.M., and Jiang, M.Z., 2020. Longevity analysis of landslide dams. Landslides, https://doi.org/10.1007/s10346-020-01386-7
Shi, Z.M., Guan, S.G., Peng, M., Zhang, L.M. Zhu, Y., and Cai, Q.P., 2015. Cascading breaching of the Tangjiashan landslide dam and two smaller downstream landslide dams. Engineering Geology, 193: 445–458.
Shi, Z.M., Xiong, X., Peng, M., Zhang, L.M., Xiong, Y.F., Chen, H.X. and Zhu, Y., 2017. Risk assessment and mitigation for the Hongshiyan landslide dam triggered by the 2014 Ludian earthquake in Yunnan, China. Landslides, 14(1): 269–285.
Shroder Jr, J.F. and Weihs, B.J., 2010. Geomorphology of the Lake Shewa landslide dam, Badakhshan, Afghanistan, using remote sensing data. Geografiska Annaler: Series A, Physical Geography, 92(4): 469-483.
Simmler, H. and Samet, L., 1982. Dam failure from overtopping studied on a hydraulic model, ICOLD, Fourteenth Congress, pp. 427–445.
Singh, V.P., 2013. Dam breach modeling technology, 17. Springer Science & Business Media.
Sivakumar Babu, G.L. and Vasudevan, A.K., 2008. Seepage velocity and piping resistance of coir fiber mixed soils. Journal of irrigation and drainage engineering, 134(4): 485–492.
Smith, P.J., Kojiri, T. and Sekii, K., 2006. Risk-based flood evacuation decision using a distributed rainfall-runoff model. Annu Rep Disaster Prev Res Inst Kyoto Univ, 49(B): 717–732.
Stokoe, K.H., Wright, S., Bay, J. and Roesset, J., 1994. Characterization of geotechical sites by SASW method. Unknown Journal: 15-25.
Strangway, D.W., 1983. Audiofrequency magnetotelluric (AMT) sounding. Developments in geophysical exploration methods, 5: 107.
Strangway, D.W., Swift, C.M. and Holmer, R.C., 1973. The application of audio-frequency magnetotellurics (AMT) to mineral exploration. Geophysics, 38(6): 1159–1175.
Strom, A.L., 1996. Some morphological types of long-runout rockslides: effect of the relief on their mechanism and on the rockslide deposits distribution. In: Senneset, K. (Ed.), Landslides. Proc. of the Seventh International Symposium on Landslides. Balkema, Trondheim, Norway, Rotterdam, pp. 1977-1982.
Strom, A., 2006. Morphology and internal structure of rockslides and rock avalanches: grounds and constraints for their modelling, Landslides from Massive Rock Slope Failure. Springer, pp. 305-326.
Strom, A., 2010. Landslide dams in Central Asia region. Journal of the Japan Landslide Society, 47(6): 309-324.
Strom, A., 2013. Geological prerequisites for landslide dams' disaster assessment and mitigation in Central Asia, Progress of Geo-Disaster Mitigation Technology in Asia. Springer, pp. 17–53.
Strom, A., 2014. Sarez lake problem: ensuring long-term safety, Landslide Science for a Safer Geoenvironment. Springer, pp. 633–639.
Strom, A.L. and Korup, O., 2006. Extremely large rockslides and rock avalanches in the Tien Shan Mountains, Kyrgyzstan. Landslides, 3(2): 125–136.
Strom, A. and Abdrakhmatov, K., 2018. Rockslides and rock avalanches of Central Asia: distribution, morphology, and internal structure. Elsevier.
Strom, A., Li, L. and Lan, H., 2019. Rock avalanche mobility: optimal characterization and the effects of confinement. Landslides: 1-16.
Sun, R., Wang, X., Zhou, Z., Ao, X., Sun, X. and Song, M., 2014. Study of the comprehensive risk analysis of dam-break flooding based on the numerical simulation of flood routing. Part I: model development. Natural hazards, 73(3): 1547-1568.
Tabata, S., 2001. Study on prediction of peak discharge in floods caused by landslide dam failures. Journal of Erosion Control Engineering, 54(4): 73-76.

2049 Tacconi Stefanelli, C., Catani, F. and Casagli, N., 2015. Geomorphological investigations on
2050 landslide dams. Geoenvironmental Disasters, 2(1): 21.
2051 Tacconi Stefanelli, C., Vilímek, V., Emmer, A. and Catani, F., 2018. Morphological analysis and
2052 features of the landslide dams in the Cordillera Blanca, Peru. Landslides, 15(3): 507-521.
2053 Tachikawa, T., Kaku, M. and Iwasaki, A., 2011. Aster GDEM version 2 validation report. Report
2054 to the ASTER GDEM Version, 2.
2055 Takahashi, T., 1988. Hydrograph prediction of debris flow due to failure of landslide dam. Annual
2056 Reports of Disaster Prevention Research Institute, Kyoto University, 31(2): 601-615.
2057 Tanoue, M., Hirabayashi, Y. and Ikeuchi, H., 2016. Global-scale river flood vulnerability in the last
2058 50 years. Scientific reports, 6: 36021.
2059 Tezkan, B., 1999. A review of environmental applications of quasi-stationary electromagnetic
2060 techniques. Surveys in Geophysics, 20(3-4): 279–308.
2061 Thouret, J.-C., Gunnell, Y., Jicha, B.R., Paquette, J.-L. and Braucher, R., 2017. Canyon incision
2062 chronology based on ignimbrite stratigraphy and cut-and-fill sediment sequences in SW Peru
2063 documents intermittent uplift of the western Central Andes. Geomorphology, 298: 1–19
2064 https://doi.org/10.1016%2Fj.geomorph.2017.09.013.
2065 Tofani, V., Catani, F. and Casagli, N., 2010. Weather Forecasting and Radar Technologies for
2066 Landslide Prediction and Mapping: Some Examples in Italy. na.
2067 Tomlinson, S.S. and Vaid, Y.P., 2000. Seepage forces and confining pressure effects on piping
2068 erosion. Canadian Geotechnical Journal, 37(1): 1–13 https://doi.org/10.1139%2Ft99-116.
2069 Torgoev, I., Havenith, H.-B. and Strom, A., 2013. Impact of 3000-t blast on unstable slopes near
2070 the Kambarata-2 HPP site, Kyrgyzstan, Landslide Science and Practice. Springer, pp. 37–42.
2071 Torgoev, I.A., Havenith, H.-B. and Torgoev, A.D., 2014. Geophysical Monitoring of Artificial
2072 Landslide Dam of Kambarata Hydro Power Plant-2 (Kyrgyzstan), Landslide Science for a Safer
2073 Geoenvironment. Springer, pp. 641–647.
2074 Trauth, M.H., Alonso, R.A., Haselton, K.R., Hermanns, R.L. and Strecker, M.R., 2000. Climate
2075 change and mass movements in the NW Argentine Andes. Earth and Planetary Science
2076 Letters, 179(2): 243-256.
2077 Trauth, M.H., Deino, A. and Strecker, M.R., 2001. Response of the East African climate to orbital
2078 forcing during the last interglacial (130–117 ka) and the early last glacial (117–60 ka). Geology,
2079 29(6): 499-502.
2080 Trauth, M.H. and Strecker, M.R., 1999. Formation of landslide-dammed lakes during a wet period
2081 between 40,000 and 25,000 yr B.P. in northwestern Argentina. Palaeogeography,
2082 Palaeoclimatology, Palaeoecology, 153(1-4): 277–287 https://doi.org/10.1016%2Fs0031-
2083 0182%2899%2900078-4.
2084 Urbina, E. and Wolshon, B., 2003. National review of hurricane evacuation plans and policies: a
2085 comparison and contrast of state practices. Transportation research part A: policy and
2086 practice, 37(3): 257–275.
2087 USBR, 2003. Guidelines for achieving public protection in dam safety decision making. US
2088 Department of the Interior.
2089 Van Asch, T.W.J., Tang, C., Alkema, D., Zhu, J. and Zhou, W., 2014. An integrated model to
2090 assess critical rainfall thresholds for run-out distances of debris flows. Natural hazards, 70(1):
2091 299-311.
2092 Van Der Knijff, J.M., Younis, J. and De Roo, A.P.J., 2010. LISFLOOD: a GIS ‐ based distributed
2093 model for river basin scale water balance and flood simulation. International Journal of
2094 Geographical Information Science, 24(2): 189-212.
2095 Van Tien, P., Sassa, K., Takara, K., Fukuoka, H., Dang, K., Shibasaki, T., Ha, N.D., Setiawan, H.
2096 and Loi, D.H., 2018. Formation process of two massive dams following rainfall-induced deep-
2097 seated rapid landslide failures in the Kii Peninsula of Japan. Landslides, 15(9): 1761-1778.
2098 Varnes, D.J., 1978. Slope movement types and processes. Special report, 176: 11-33.
2099 Wahl, T.L., 1997. Predicting embankment dam breach parameters-A needs assessment,
2100 Proceedings of the Congress-International Association for Hydraulic Research. Local
2101 organization committee of the XXV congress, pp. 48-53.
2102 Wahl, T.L., 2004. Uncertainty of predictions of embankment dam breach parameters. Journal of
2103 hydraulic engineering, 130(5): 389-397.

Walder, J.S., Iverson, R.M., Godt, J.W., Logan, M. and Solovitz, S.A., 2015. Controls on the breach geometry and flood hydrograph during overtopping of noncohesive earthen dams. Water Resources Research, 51(8): 6701–6724.
Walder, J.S. and O'Connor, J.E., 1997. Methods for predicting peak discharge of floods caused by failure of natural and constructed earthen dams. Water Resources Research, 33(10): 2337-2348.
Walker, M., 2005. Quaternary dating methods. John Wiley and Sons.
Wallace, L., Lucieer, A., Watson, C. and Turner, D., 2012. Development of a UAV-LiDAR system with application to forest inventory. Remote Sensing, 4(6): 1519–1543.
Walter, F., Amann, F., Kos, A., Kenner, R., Phillips, M., Preux, A.d., Huss, M., Tognacca, C., Clinton, J., Diehl, T. and Bonanomi, Y., 2020. Direct observations of a three million cubic meter rock-slope collapse with almost immediate initiation of ensuing debris flows. Geomorphology, 351: 106933 https://doi.org/10.1016%2Fj.geomorph.2019.106933.
Wan, C.F. and Fell, R., 2004. Laboratory tests on the rate of piping erosion of soils in embankment dams. Geotechnical testing journal, 27(3): 295–303.
Wang, F., Dai, Z., Okeke, C.A.U., Mitani, Y. and Yang, H., 2018a. Experimental study to identify premonitory factors of landslide dam failures. Engineering Geology, 232: 123–134.
Wang, F., Okeke, A.C.-U., Kogure, T., Sakai, T. and Hayashi, H., 2018b. Assessing the internal structure of landslide dams subject to possible piping erosion by means of microtremor chain array and self-potential surveys. Engineering Geology, 234: 11-26.
Wang, G., Furuya, G., Zhang, F., Doi, I., Watanabe, N., Wakai, A. and Marui, H., 2016a. Layered internal structure and breaching risk assessment of the Higashi-Takezawa landslide dam in Niigata, Japan. Geomorphology, 267: 48-58.
Wang, G., Huang, R., Kamai, T. and Zhang, F., 2013. The internal structure of a rockslide dam induced by the 2008 Wenchuan (Mw7. 9) earthquake, China. Engineering Geology, 156: 28-36.
Wang, G., Huang, R., Lourenço, S.D. and Kamai, T., 2014a. A large landslide triggered by the 2008 Wenchuan (M8. 0) earthquake in Donghekou area: Phenomena and mechanisms. Engineering geology, 182: 148-157.
Wang, L., Chen, Z., Wang, N., Sun, P., Yu, S., Li, S. and Du, X., 2016b. Modeling lateral enlargement in dam breaches using slope stability analysis based on circular slip mode. Engineering Geology, 209: 70–81.
Wang, S.-y. and Liu, J., 2013. Modeling the risk assessment of landslide-dammed lakes based on the emergency response measures in Wenchuan earthquake, 2008, China. Natural hazards, 67(2): 523–547.
Wang, S., Chen, J.-s., He, H.-q. and He, W.-z., 2016c. Experimental study on piping in sandy gravel foundations considering effect of overlying clay. Water Science and Engineering, 9(2): 165–171.
Wang, Y., Han, B., Wu, J., Chen, Y., Zhou, Y. and Jiang, F., 2014b. The evolution of the Zhanggu landslide. Project Planning and Project Success: The 25% Solution: 129.
Wang, Z., 2008. A thunder at the beginning of the 21st century—the giant Yigong landslide. Landslides and Engineered Slopes, 2: 2111–2118.
Ward, S.N. and Day, S., 2011. The 1963 landslide and flood at Vaiont Reservoir Italy. A tsunami ball simulation. Italian journal of geosciences, 130(1): 16-26.
Wasowski, J. and Bovenga, F., 2014. Investigating landslides and unstable slopes with satellite Multi Temporal Interferometry: Current issues and future perspectives. Engineering Geology, 174: 103–138.
Wassmer, P., Schneider, J.L., Pollet, N. and Schmitter-Voirin, C., 2004. Effects of the internal structure of a rock–avalanche dam on the drainage mechanism of its impoundment, Flims sturzstrom and Ilanz paleo-lake, Swiss Alps. Geomorphology, 61(1-2): 3–17.
Weidinger, J.T., 2011. Stability and life span of landslide dams in the Himalayas (India, Nepal) and the Qin Ling Mountains (China), Natural and Artificial Rockslide Dams. Springer, pp. 243-277.

Weidinger, J.T., Korup, O., Munack, H., Altenberger, U., Dunning, S.A., Tippelt, G. and Lottermoser, W., 2014. Giant rockslides from the inside. Earth and Planetary Science Letters, 389: 62-73.
Whiteley, J., Chambers, J., Uhlemann, S., Boyd, J., Cimpoiasu, M., Holmes, J., Inauen, C., Watlet, A., Hawley-Sibbett, L. and Sujitapan, C., 2020. Landslide monitoring using seismic refraction tomography–The importance of incorporating topographic variations. Engineering Geology, 268: 105525.
Whiteley, J., Chambers, J., Uhlemann, S., Wilkinson, P. and Kendall, J., 2019. Geophysical monitoring of moisture‐induced landslides: a review. Reviews of Geophysics, 57(1): 106-145.
Wong, H.N., Ho, K.K.S. and Chan, Y.C., 1997. Assessment of consequence of landslides. Landslide risk assessment. AA Balkema, Rotterdam: 111–149.
Woo, G., 2008. Probabilistic criteria for volcano evacuation decisions. Natural Hazards, 45(1): 87–97.
Xiong, X., Shi, Z.M., Guan, S.G. and Zhang, F., 2018. Failure mechanism of unsaturated landslide dam under seepage loading – Model tests and corresponding numerical simulations. Soils and Foundations, 58(5): 1133–1152 https://doi.org/10.1016%2Fj.sandf.2018.05.012.
Xu, F.-g., Yang, X.-g. and Zhou, J.-w., 2016. Dam-break flood risk assessment and mitigation measures for the Hongshiyan landslide-dammed lake triggered by the 2014 Ludian earthquake. Geomatics, Natural Hazards and Risk, 8(2): 803–821 https://doi.org/10.1080%2F19475705.2016.1269839.
Xu, F., Zhou, H., Zhou, J. and Yang, X., 2012. A mathematical model for forecasting the dam-break flood routing process of a landslide dam. Mathematical Problems in Engineering, 2012.
Xu, H., Jiang, H., Yu, S., Yang, H. and Chen, J., 2015. OSL and pollen concentrate 14C dating of dammed lake sediments at Maoxian, east Tibet, and implications for two historical earthquakes in AD 638 and 952. Quaternary International, 371: 290–299 https://doi.org/10.1016%2Fj.quaint.2014.09.045.
Xu, Q., Fan, X.-M., Huang, R.-Q. and Van Westen, C., 2009. Landslide dams triggered by the Wenchuan Earthquake, Sichuan Province, south west China. Bulletin of engineering geology and the environment, 68(3): 373-386.
Xu, Y. and Zhang, L.M., 2009. Breaching Parameters for Earth and Rockfill Dams. Journal of Geotechnical and Geoenvironmental Engineering, 135(12): 1957–1970 https://doi.org/10.1061%2F%28asce%29gt.1943-5606.0000162.
Yamada, R., Kariya, Y., Kimura, T., Sano, M., Li, Z. and Nakatsuka, T., 2018. Age determination on a catastrophic rock avalanche using tree-ring oxygen isotope ratios - the scar of a historical gigantic earthquake in the Southern Alps, central Japan. Quaternary Geochronology, 44: 47–54 https://doi.org/10.1016%2Fj.quageo.2017.12.004.
Yamazaki, D., Ikeshima, D., Neal, J.C., O'Loughlin, F., Sampson, C.C., Kanae, S. and Bates, P.D., 2017. MERIT DEM: A new high-accuracy global digital elevation model and its merit to global hydrodynamic modeling. AGUFM, 2017: H12C–04.
Yamazaki, F. and Matsuoka, M., 2007. Remote sensing technologies in post-disaster damage assessment. Journal of Earthquake and Tsunami, 1(03): 193-210.
Yan, J., Cao, Z.-x., Liu, H.-h. and Chen, L., 2009. Experimental study of landslide dam-break flood over erodible bed in open channels. Journal of Hydrodynamics, 21(1): 124-130.
Yang, K.-H. and Wang, J.-Y., 2017. Experiment and statistical assessment on piping failures in soils with different gradations. Marine Georesources & Geotechnology, 35(4): 512–527.
Yang, S.-H., Pan, Y.-W., Dong, J.-J., Yeh, K.-C. and Liao, J.-J., 2012. A systematic approach for the assessment of flooding hazard and risk associated with a landslide dam. Natural Hazards, 65(1): 41–62 https://doi.org/10.1007%2Fs11069-012-0344-9.
Yang, X., Zhou, H., Li, H., Yang, Z., Qiao, L. and Lin, Y., 2010. Safety Assessment of Quake Lakes, GeoFlorida 2010: Advances in Analysis, Modeling & Design, pp. 2002-2011.
Yarnold, J. and Lombard, J., 1989. Litho-kinematic facies model for large landslide deposits in arid settings. AAPG (Am. Assoc. Pet. Geol.) Bull.;(United States), 73(CONF-8905132-).
Yi, C., Zhu, L., Seong, Y.B., Owen, L.A. and Finkel, R.C., 2006. A lateglacial rock avalanche event, Tianchi Lake, Tien Shan, Xinjiang. Quaternary International, 154-155: 26–31 https://doi.org/10.1016%2Fj.quaint.2006.02.011.

Young, W.J. and Warburton, J., 1996. Principles and practice of hydraulic modelling of braided gravel-bed rivers. Journal of Hydrology (New Zealand): 175–198.
Yu, M.-h., Wei, H.-y., Liang, Y.-j. and Zhao, Y., 2013. Investigation of non-cohesive levee breach by overtopping flow. Journal of Hydrodynamics, 25(4): 572–579 https://doi.org/10.1016%2Fs1001-6058%2811%2960398-4.
Yunus, A.P., Avtar, R., Kraines, S., Yamamuro, M., Lindberg, F. and Grimmond, C., 2016. Uncertainties in tidally adjusted estimates of sea level rise flooding (bathtub model) for the Greater London. Remote Sensing, 8(5): 366.
Zachos, L.G., Swann, C.T., Altinakar, M.S., McGrath, M.Z. and Thomas, D., 2016. Flood vulnerability indices and emergency management planning in the Yazoo Basin, Mississippi. International Journal of Disaster Risk Reduction, 18: 89–99 https://doi.org/10.1016%2Fj.ijdrr.2016.03.012.
Zerkal, O.V., Makhinov, A.N., Strom, A.L., Kim, V.I., Kharitonov, M.E., Fomenko, I.K. (Editor), in press. Formation of the 2018 Bureya landslide, Far East of Russia. . Understanding and Reducing Landslide Disaster Risk. Springer.
Zhang, J., Li, Y., Xuan, G., Wang, X. and Li, J., 2009a. Overtopping breaching of cohesive homogeneous earth dam with different cohesive strength. Science in China Series E: Technological Sciences, 52(10): 3024–3029.
Zhang, L., Peng, M., Chang, D. and Xu, Y., 2016. Dam failure mechanisms and risk assessment. John Wiley & Sons.
Zhang, L.M., Xu, Y. and Jia, J.S., 2009b. Analysis of earth dam failures: A database approach. Georisk, 3(3): 184–189.
Zhang, Y., Huang, C.C., Shulmeister, J., Guo, Y., Liu, T., Kemp, J., Patton, N.R., Liu, L., Chen, Y., Zhou, Q. and others, 2019. Formation and evolution of the Holocene massive landslide-dammed lakes in the Jishixia Gorges along the upper Yellow River: No relation to China's Great Flood and the Xia Dynasty. Quaternary Science Reviews, 218: 267–280.
Zhu, J., Li, Y. and Hu, Y., 2012. A virtual geographic environment for simulation analysis of dam-break flood routing. Trans Tech Publ, pp. 926-931.
Zhu, Y., Visser, P.J., Vrijling, J.K. and Wang, G., 2011. Experimental investigation on breaching of embankments. Science China Technological Sciences, 54(1): 148–155.